MODELLING OF RESILIENT RUBBLE MOUND BREAKWATER AGAINST TSUNAMI

Thesis

Submitted in partial fulfilment of the requirements for the degree of

DOCTOR OF PHILOSOPHY

by

MANU K SAJAN

(197083CV010)

DEPARTMENT OF CIVIL ENGINEERING

NATIONAL INSTITUTE OF TECHNOLOGY KARNATAKA,

SURATHKAL, MANGALORE - 575 025

OCTOBER 2024

MODELLING OF RESILIENT RUBBLE MOUND BREAKWATER AGAINST TSUNAMI

Thesis

Submitted in fulfilment of the requirements for the degree of

DOCTOR OF PHILOSOPHY

by

MANU K SAJAN

Under the guidance of

Dr. BABLOO CHAUDHARY

DEPARTMENT OF CIVIL ENGINEERING

NATIONAL INSTITUTE OF TECHNOLOGY KARNATAKA,

SURATHKAL, MANGALORE - 575 025

OCTOBER 2024

DECLARATION

I hereby declare that the Research Thesis entitled "**Modelling of Resilient Rubble Mound Breakwater Against Tsunami"**, which is being submitted to the **National Institute of Technology Karnataka, Surathkal,** in partial fulfilment of the requirements for the award of the Degree of **Doctor of Philosophy** in **Civil Engineering** is a *bonafide report of the research work carried out by me*. The material contained in this thesis has not been submitted to any University or Institution for the award of any degree.

Place: NITK, SURATHKAL

Date: 01/10/2024

MANU K SAJAN

197083CV010

Department of Civil Engineering

CERTIFICATE

This is to certify that the Research Thesis entitled **"Modelling of Resilient Rubble Mound Breakwater Against Tsunami"** submitted by **MANU K SAJAN (**Register Number: **197083CV010)**, as the record of research work carried out by him, *is accepted as the Research Thesis submission* in partial fulfilment of the requirements for the award of the degree of **Doctor of Philosophy**.

Prof. Basavaraju Manu
HOD and Chairman - DRPC
Department of Civil Engineering

Dr. Babloo Chaudhary
Research Supervisor
Department of Civil Engineering

ACKNOWLEDGEMENT

I would like to take this opportunity to express my sincere gratitude and profound thanks to the individuals who have been instrumental in my academic journey and research work. First and foremost, I would like to express my heartfelt appreciation to my esteemed research advisor and mentor, **Dr Babloo Chaudhary**, Assistant Professor, Department of Civil Engineering, National Institute of Technology Karnataka, for his unwavering support, motivation, enthusiasm, and guidance throughout my research work. His invaluable insights and feedback have been a constant source of inspiration and motivation for me.

I am also thankful to RPAC Panel Members **Prof. Sitaram Nayak,** Professor, Department of Civil Engineering, National Institute of Technology Karnataka, and **Dr. Debabrata Karmakar**, Associate Professor, Department of Water Resources & Ocean Engineering, National Institute of Technology Karnataka for their valuable guidance and suggestion throughout my work.

I would also like to extend my sincere appreciation and respect to **Prof. B. M. Sunil, Dr Sreevalsa Kolathayar, and Dr G. Sridhar**, Department of Civil Engineering, National Institute of Technology Karnataka, for their invaluable guidance and support throughout my research work. I am very thankful to the Head of the Department, **Prof. Basavaraju Manu, and former HODs**, DRPC-Secretary **Dr Mithun Mohan**, and all the faculty members of the Department of Civil Engineering for their kind-hearted cooperation, encouragement, and support throughout my academic journey.

I express my profound gratitude to the Ministry of Ports, Shipping, and Waterways, Government of India and DST (Department of Science & Technology) / SERB (Science and Engineering Research Board) for their generous financial support. I want to acknowledge the invaluable contributions of my fellow lab mates Akarsh P K, Subodh Kumar, Babita Sah, and lab juniors, especially Sudhanshu Kumar, who have provided immense support and assistance during the experimental phase of my research work.

Lastly, I express my heartfelt gratitude to my family and friends for their constant encouragement, unwavering support, and timely help throughout my academic journey.

MANU K SAJAN

ABSTRACT

The Rubble Mound (RM) breakwater is the most common type of breakwater constructed near the seacoasts of many countries across the globe. Most of these countries have a higher population density concentrated near their coastal lines. Tsunamis are one of the most devastating natural hazards a breakwater could encounter during its life time. Unfortunately, many breakwaters were damaged or collapsed in several countries during past tsunamis, such as the 2004 Indian Ocean tsunami and the 2011 Great East Japan tsunami. Due to the collapse of these breakwaters, the tsunamis were not blocked, giving them direct and unfettered access into the coastal areas, leading to tremendous loss of life and property. This underscores the urgent need for comprehensive research and development of effective countermeasures to make tsunami-resilient RM breakwaters. However, the existing literature is limited in addressing the behaviour of RM breakwaters during tsunamis and developing mitigation strategies. The present study aims to address these gaps by (i) investigating the behaviour of RM breakwaters under tsunami and (ii) proposing novel countermeasure techniques to enhance their resilience. To the end, rigorous methodology involving physical model tests, analytical studies, profile mapping and numerical simulations were performed on conventional and proposed reinforced breakwater models. The Northern breakwater at the Ennore Port, India, was chosen as the prototype for being the longest breakwater in the country to be impacted by the 2001 Indian Ocean tsunami. The small-scale model of the prototype breakwater was tested in the lab and revealed the failure mechanisms in conventional breakwaters during tsunami events, laying the groundwork for the development of innovative countermeasures. Novel techniques incorporating gabions, geobags, geogrids, sheet piles, and crown walls with shear key were devised and evaluated using tsunami overflow tests, analytical studies, profile mapping, and numerical simulations. As far as the author knows, it is the first time that gabions and geosynthetics have been employed in RM breakwaters to make a tsunami-resilient model. In the physical model tests, particular attention was given to critical scenarios observed in the past, such as the overflow of the Kamaishi breakwater during the 2011 Great East Japan Tsunami. This event is significant because the Kamaishi breakwater, which was considered tsunami-resistant, experienced severe damage due to the overflow of the tsunami that exceeded its design height. To address such crucial scenarios where tsunamis exceed the design height of breakwaters, the tsunami was allowed to overflow the breakwater in the physical model tests. This meticulous consideration of real-world scenarios in the testing phase ensured that the developed solutions were robust and adaptive to extreme events, enhancing the reliability

and applicability of the research findings. In order to evaluate the effectiveness of the developed reinforced models, comparative analyses were conducted between reinforced and conventional (unreinforced) RM breakwaters in terms of settlement, horizontal displacement, pore water pressure, scouring, and seepage. The emerged portion of conventional RM above the mean sea level (MSL) was observed to be scoured entirely during the tsunami overflow. On the contrary, the reinforced models remained intact even after the tsunami overflow. It was observed during the tests that the reinforced models reduced settlement of the crest by more than 90.2% and lateral displacement by more than 94.6%. Additionally, the placement of sheet piles in the seabed soils at either end of the breakwater in the reinforced models reduced the incremental pore water pressure in the seabed during the tsunami by 54.2%. The quantification of damages on RM breakwaters by profile mapping revealed that 4.5×10^{-3} m^3 of the conventional breakwater volume was scoured by tsunami overflow, which was prevented entirely in the reinforced models. Numerical analyses and analytical studies were also performed, which underscored the stability enhancement of the reinforced models and the effectiveness of sheet piles in arresting seepage through the seabed. The stability of the reinforced models was observed to be 2.2 times higher than the stability of conventional models. Further parametric studies analysing the influence of tsunami height, depth of shear key, and number of shear keys were also performed in the validated numerical model. The results of the numerical analysis revealed that the developed techniques are very successful in mitigating the damages on RM breakwaters caused by tsunamis.

Keywords: Rubble Mound Breakwaters; Tsunami; Tsunami Overflow Tests; Damage Analysis; Profile Mapping; Numerical Analysis; Tsunami Resilience

TABLE OF CONTENTS

LIST OF FIGURES

LIST OF TABLES

NOMENCLATURE

RM	Rubble Mound
GBRM	Geobag Reinforced Rubble Mound breakwater
GRM	Gabion Reinforced Rubble Mound breakwater
GGRM	Geogrid Reinforced Rubble Mound breakwater
WGRM	Wrap-Faced Geogrid-Reinforced Rubble Mound breakwater
IPWP	Incremental Pore Water Pressure
R_d	Relative Displacement
S	Relative Eroded Area
DIC	Digital Image Correlation
MSL	Mean Sea Level
ΣM_{sf}	Factor of safety at a particular stage

CHAPTER 1
INTRODUCTION

1.1 BACKGROUND

Coastlines are the interfaces between land and sea where most of the world's population resides. Coastal regions are subjected to dynamic interaction with frequent sea waves, wind waves, tides, cyclones, and tsunamis. An offshore barrier is often constructed to arrest the water waves and create a tranquil sea area near a port or harbour. This tranquil area is primarily created to aid various activities, including, but not limited to, the anchoring of ships, docking of vessels, and conducting recreational activities. These offshore structures are called breakwaters.

The primary function of breakwaters is to protect against invasive sea waves on the coastline. In addition, breakwaters can function as a barrier to divert currents, protect against shoaling, and provide dock or quay facilities. Breakwaters can be broadly classified into the Fixed type and Floating type. Fixed breakwaters are built on the seabed, whereas the floating type is built to float over the water's surface. Based on the material used in the construction, the fixed-type breakwaters can be further classified into RM breakwaters, caisson-type breakwaters and composite breakwaters. RM breakwaters are made of quarry rocks placed over the seabed, and caisson breakwaters are made of filled caissons placed over the bedding layer on the seabed. Composite breakwaters consist of caissons placed on top of an RM.

RM breakwaters are widely constructed across the coastline of many countries, as shown in Figure 1.1. An RM breakwater, as the name indicates, is constructed by placing large volumes of heavier quarry rock blocks at desired offshore locations. The construction of RM breakwaters is advantageous over other methods mainly due to its cost and ease of construction. Further, the repair and maintenance of these breakwaters are comparatively more straightforward. Also, RM breakwaters have fewer environmental impacts than other breakwaters.

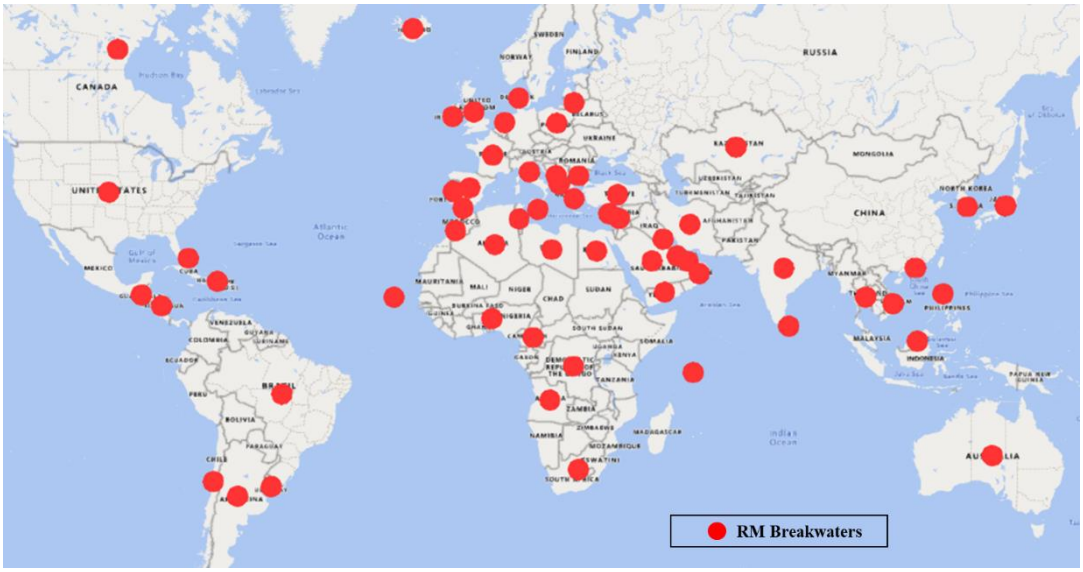

Figure 1.1 Countries with RM breakwaters (Source: International Breakwater Directory)

Tsunamis are sea waves of longer wavelengths, usually up to hundreds of kilometres in scale and periods of frequencies ranging from a few minutes to several hours. Tsunamis are caused by a sudden vertical displacement of a large volume of water due to significant seismic events such as an earthquake occurring at the seabed, landslides into water bodies, nuclear explosions and meteoroid impacts. Tsunamis behave as shallow waves since the water depth and wavelength ratio are often tiny. Tsunamis tend to lose very little energy during their propagation since the rate at which a wave loses its energy is inversely related to its wavelength. Shallow-water waves move at a speed that is equal to the square root of the product of the acceleration of gravity and the water depth. Therefore, tsunamis travel at considerably higher speeds when the water depth is more significant. However, the speed of these waves reduces as they approach the shore. Therefore, the height of the wave increases to conserve the total energy. This results in the shoaling phenomenon, where the distances between individual waves decrease.

The tsunami hazard map depicted in Figure 1.2 highlights that many countries are susceptible to tsunamis (2 m to 10 m). In most countries, RM breakwaters are used to protect their coastal areas. However, RM breakwaters are vulnerable to tsunamis.

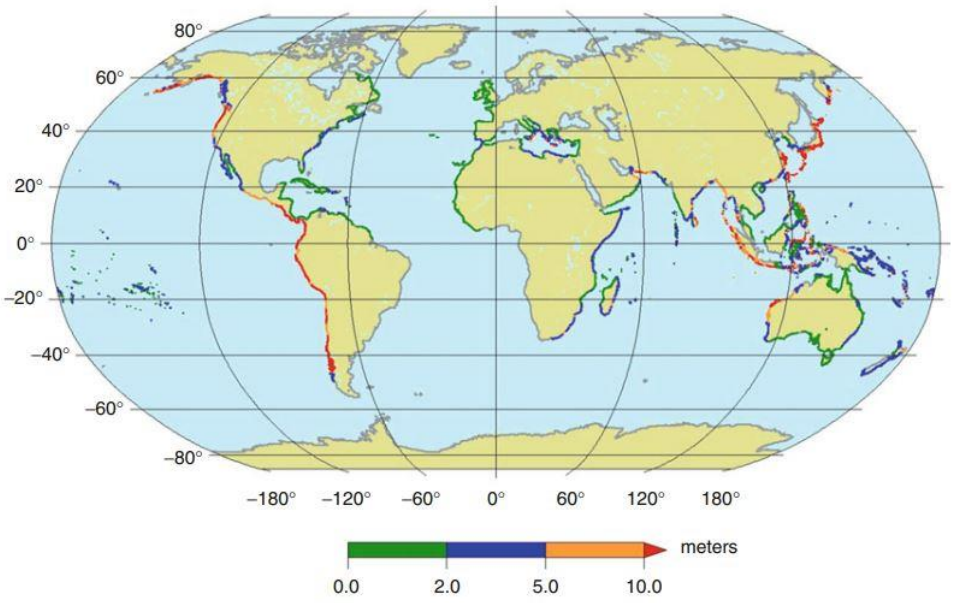

Figure 1.2 Tsunami hazard map with run-up heights for a mean return period of 500 years (after Løvholt et al., 2016)

Tsunamis damaged many RM Breakwaters in the past. For example, several RM breakwaters were partially damaged or collapsed by the 2004 Indian Ocean Earthquake and Tsunami. Similarly, several breakwaters were damaged during the 2011 Great East Japan Earthquake and Tsunami. The damages that occurred to RM breakwaters by past tsunamis are illustrated in Figure 1.3. According to post-tsunami field studies by Bricker et al. (2012) and Kato et al. (2012), the primary mechanism behind the failure of breakwater under tsunami overflow was the scouring at the harbourside of coastal structures. During a tsunami, the pore water pressure in the seabed soils increases, weakening the foundation. The submergence of RM breakwater during tsunami overflow reduces the effective weight of rubbles due to buoyancy. During this process, the breakwater loses its stability and eventually fails. Therefore, it is essential to develop countermeasures that make RM breakwaters resilient against tsunamis. Consequently, existing RM breakwaters must also be converted into tsunami-resilient structures.

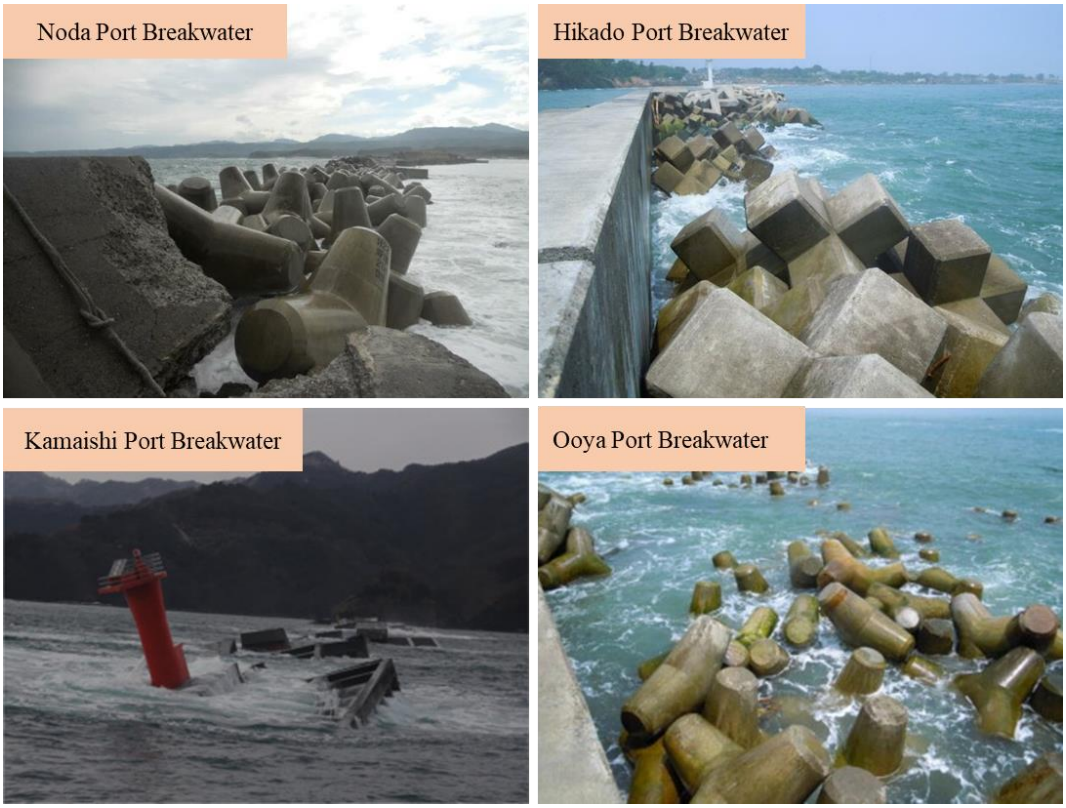

Figure 1.3 Extend of damages on breakwaters during the 2011 Great East Japan tsunami (after Esteban et al., 2014)

1.2 TSUNAMI-INDUCED DAMAGES ON BREAKWATERS

Even though breakwaters are continuously subjected to dynamic sea wave interactions, the most critical loading condition in the design life of breakwaters could occur during a tsunami impact. This critical loading condition was observed in the damage of several RM breakwaters by the tsunami impacts. For example, several RM breakwaters in Indonesia, Sri Lanka, Maldives, Japan and India were damaged and even collapsed by the 2004 Indian Ocean Tsunami and the 2011 Great East Japan Tsunami. The details of some damaged breakwaters are detailed in Figure 1.4. The failure of breakwaters results in the inundation of tsunamis into the land, causing enormous destruction to coastal life and properties. Therefore, it is essential to develop countermeasures to make the RM breakwaters resilient against tsunamis.

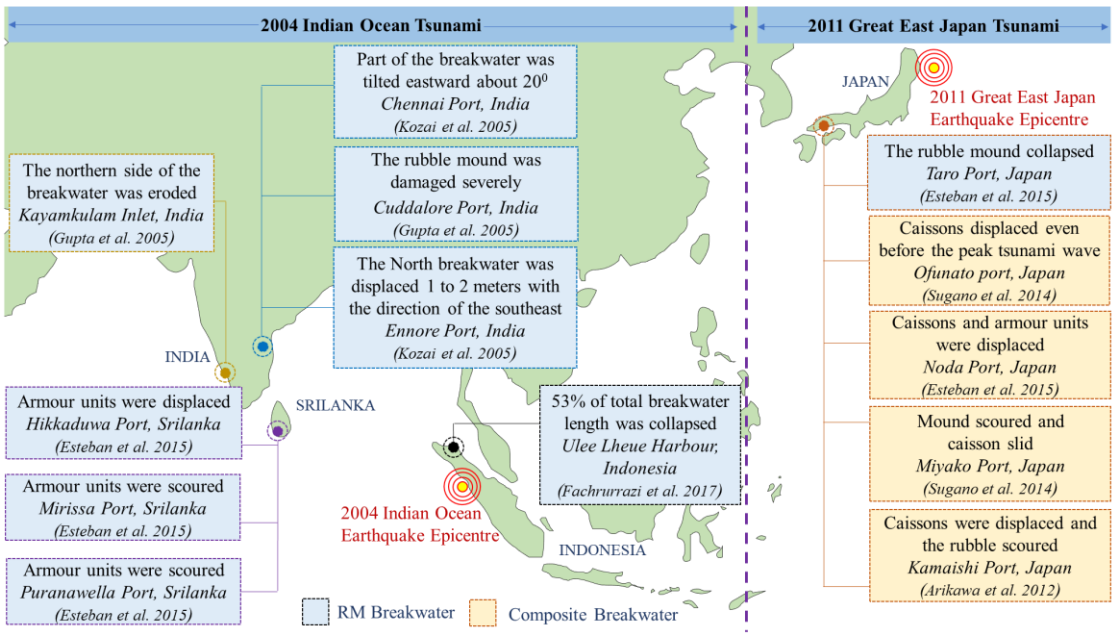

Figure 1.4 Breakwater damages during the past tsunamis

1.3 CRITICAL CONDITIONS DURING TSUNAMI

The foundation soil of an RM breakwater is usually subjected to large hydrostatic loads under normal conditions and increased loads during the devastating impact of a high-head tsunami. In addition, the breaking of waves around the breakwater structure can lead to the seabed scouring near the breakwater. This type of scouring was explored in detail by conducting comprehensive numerical analyses as well as complete experimental works in wave basins (Bricker et al., 2012; Fredsoe and Sumer, 1997; Hur et al., 2007; Mulders et al., 2015; Rajaratnam, 1981; Sumer and Fredsoe, 2000). Since tsunami loading is a much more intense phenomenon, the scouring failure of RM breakwaters primarily due to wave breakings at the harbourside slope becomes highly obvious. The additional action of water currents can also aid the impact force of these waves. Zhao et al. (2018) recently addressed and studied this scenario in detail through numerical simulations.

The study of the structural behaviour of an RM breakwater is as crucial as the foundation responses while reimagining a resilient design. Hence, protective measures must be incorporated into the structure and foundation for an RM breakwater to be resilient against a tsunami attack. The RM will be primarily subjected to overtopping of water under a tsunami impact (Contestabile et al., 2017; Franco et al., 2009; Losada

et al., 2008; Romano et al., 2015; Vicinanza et al., 2014). Overtopping water over breakwater can exert tremendous pressure on the crown walls (Aniel-Quiroga et al., 2019; Norgaard et al., 2013). Further, the overtopping waves can break on the harbour side slope of the RM, leading to the dislocation of rubbles as well as the scouring of the seabed (Chaudhary et al. 2017a, 2019). The drawdown condition of tsunamis can also cause additional drag forces on the seaside-sloping sides. Thus, the overtopping and drawdown cases are the two critical conditions that contribute to altering the stability of the RM. In addition to these, the permeability of the RM is also responsible for the infiltration of incident waves. The infiltration may lead to the exertion of additional hydraulic pressure from inside the structure (Muttray and Oumeraci, 2005; Recio and Oumeraci, 2008).

The design and maintenance of RM breakwaters is a field that has seen extensive research. However, the concept of tsunami loading on RM breakwaters is an area that has only recently entered the scientific discourse. Limited research and literature on this subject and the impact of behaviour have not yet been fully explained. The main objective of this study is to analyse and evaluate the behaviour of tsunami loading on RM breakwater and develop competent techniques to redesign the existing prototype to be resilient against tsunami-induced damage.

1.4 FAILURE MECHANISMS

The impact of tsunamis destabilises the RM breakwater due to several mechanisms that could eventually lead to the failure of the breakwater. Seepage forces induced by the head difference between sea levels at either side of the breakwater are one of the crucial failure mechanisms. The higher seepage of water through the body of the RM breakwater induces drag forces on rubbles (Fujisawa et al. 2012; Fujisawa and Murakami 2014). During a tsunami impact, these drag forces would be high enough to displace the rubbles, thereby destabilising the breakwater.

Moreover, the breaking of overflowing tsunamis on the harbourside slopes of the mound causes the scouring of rubble. The excess force imparted by the breaking wavefront can dislodge armour units on the harbour side (Suzuki et al. 2018). The drag forces and impact on the seabed result in scouring of seabed soils. Such scouring of the seabed eventually reduces the performance of the breakwater (Temel and Dogan 2021).

According to post-tsunami field studies by Bricker et al. (2012) and Kato et al. (2012), the primary mechanism behind the failure of breakwater under tsunami overflow was the scouring at the harbourside of coastal structures. During a tsunami, the pore water pressure in the seabed soils increases, weakening the foundation. The submergence of RM breakwater during tsunami overflow reduces the effective weight of rubbles due to buoyancy. During this process, the breakwater loses its stability and eventually fails. In order to make the breakwater resilient against tsunami damage, it is crucial to implement countermeasures.

1.5 RESEARCH GAP

Despite being a sizeably large construction and an essential part of many coastlines, study on RM breakwaters (susceptible to tsunami) has only lately started to garner interest from scientists, particularly in the wake of the 2004 Indian Ocean Tsunami. Little attention has been paid around the world in the past to developing a tsunami-resilient breakwater. This research area became popular among researchers, especially after the tsunami caused by the 2004 Indian Ocean Earthquake and the 2011 Great East Japan Earthquake. Since Japan is one of the most affected countries by tsunamis, most of the research in this area has been done (or is ongoing) in Japan.

Furthermore, most of the breakwaters in Japan are composite breakwaters. It is the main reason most of the available research works relate to composite breakwaters. Some studies have investigated the effectiveness of countermeasures for making tsunami-resilient composite breakwaters (Chaudhary et al. 2017b, 2018b, a; c, 2019; Chaudhary and Hazarika 2018; Hazarika et al. 2015). However, the behaviour of RM breakwaters is entirely different from that of composite breakwaters. Therefore, developing new countermeasures techniques for RM breakwaters is imperative to protect them against tsunami hazards. One main difference between the two types of breakwaters is how they interact with waves. An RM breakwater absorbs the energy of incoming waves, while a composite breakwater deflects waves and reduces their energy. This difference in wave interaction can affect the performance and effectiveness of the two types of breakwaters in different situations.

Limited research has been done on analysing the behaviour of RM breakwaters under tsunami impact. Some available studies did not consider the presence of the seabed beneath breakwaters under tsunami impact, which does not reflect real-world scenarios and highlights insufficiency in data on the exact behaviour of RM breakwaters under tsunami loading. The outcomes of a joint research project conducted by European (e.g. NGI, DEU, METU, TU-BS, LWI) and Japanese research organizations (e.g. PARI and NIMPAT) found a lack of information regarding the behaviour of RM breakwaters subjected to tsunamis (Harbitz et al. 2016). This project called RAPSODI (Risk Assessment and Design of Prevention Structures for Enhanced Tsunami Disaster Resilience), was carried out after the 2011 Great East Japan Earthquake and Tsunami. In addition, there were limited attempts to develop any feasible countermeasure to make tsunami-resilient RM breakwater.

The Indian Peninsula is surrounded by more than seventy RM breakwaters distributed across over 200 major ports and harbours. Among these, one of the longest breakwaters is located at the Northern side of Kamarajar Port Ltd. in Tamil Nadu and spans 3 km. This breakwater in the Bay of Bengal was struck by the devastating Indian Ocean tsunami of 2004. Following this, a post-tsunami field survey and geographic information system (GIS) mapping conducted by Kozai et al. (2005) found that the Ennore breakwater has moved about 1 to 2 meters in the southeast direction. When the Indian Ocean tsunami struck in 2004, the Ennore port was in its infancy. The coastal area was comprised mainly of barren land, and the port acted as a satellite port to divert traffic from the busier Chennai port. However, the Ennore port has since been significantly expanded, and the Government of India has recently declared it the 12th major port in the nation. The importance of this port highlights the dire necessity of converting the existing breakwater at Ennore port into a tsunami-resilient one. Similarly, during the 2004 Indian Ocean tsunami, the western coasts of Kerala and Karnataka were also severely hit by the refracted tsunamis, resulting in widespread destruction (Gupta and Murthy, 2005; Synolakis and Kong, 2006).

The current unavailability of research on a resilient RM breakwater against tsunamis and the necessity of transforming the global majority of breakwaters to be resilient against these disastrous tsunamis have been found to be critical gap areas that require

competent and urgent resolution. This research effectively tries to fill this gap by developing new countermeasure techniques for the breakwater at Ennore port. The effectiveness of these countermeasures will be examined through physical model tests, analytical studies and numerical simulations. Therefore, the present study proposes several reinforced models of RM breakwater by adopting different countermeasure techniques using reinforcing elements such as gabions, geogrids, geobags, crown walls (with shear key), and sheet piles.

Some tsunami-resilient breakwaters failed in the past. For example, the tsunami breakwater at Kamaishi (Japan) collapsed during the 2011 Great East Japan Earthquake and Tsunami. The tsunami-resilient breakwater was designed to resist tsunamis of the 1896 Meiji-Sanriku Earthquake. However, the breakwater still failed because the 2011 tsunami was even higher, significantly exceeding the design tsunami height. Based on this ground fact, the novel technique is developed in such a way that if a future tsunami exceeds its design height, then also the reinforced breakwater can retain its resiliency against tsunami. The effectiveness of this technique is examined by allowing the tsunamis to overflow the breakwater.

1.6 OBJECTIVES OF THE STUDY

The present study aims to conduct simulated experiments in a laboratory setting and evaluate the effects of tsunamis on the modelled breakwater. These observations shall then be factored in while adopting suitable countermeasures to design a resilient breakwater. The individual performances of these countermeasures will be evaluated by performing several physical model tests, analytical studies and rigorous numerical simulations. The main objectives of the present study are as follows.

1. To determine the failure reasons and mechanisms of RM breakwater subjected to tsunami by conducting physical model tests, analytical studies and numerical simulations.
2. To develop new countermeasure techniques in order to make the RM breakwater resilient against tsunami-induced damage.
3. To conduct physical model tests to evaluate the effectiveness of the new techniques.
4. To carry out analytical studies to determine the extent to which the new techniques can mitigate damages caused by tsunamis.
5. To perform numerical simulations in order to elucidate the mechanisms of effectiveness of the developed techniques.

1.7 SCOPE OF THE STUDY

The main scope of this study is to experimentally and numerically evaluate the performance of the new countermeasure techniques, which can make RM breakwaters resilient against tsunami impact. The main scopes of the study are listed below.

1. To determine the behaviour of RM breakwaters by examining the causes and mechanisms of failure when a tsunami impacts it.

2. To develop countermeasures for the RM breakwater to make it resilient against tsunamis, so that the breakwater prevents or reduces the impact of tsunamis on coastal areas.

3. To develop countermeasures for the existing breakwater since the resources and expenses for the construction of a new tsunami-resilient breakwater after demolishing an existing conventional breakwater are unreasonable. In addition,

some countermeasures are developed with intended application in greenfield projects.

4. The Northern breakwater at Ennore Port, Chennai (the longest RM breakwater in India) was chosen as the prototype for the study. The experimental investigations were carried out in the laboratory for a physical breakwater model by conducting tsunami overflow tests.

5. The effectiveness of the countermeasures (resilient breakwater) is judged through physical model tests, analytical studies, profile mapping and numerical simulations.

1.8 ORGANISATION OF THE REPORT

This study comprehensively evaluates the performance of geosynthetic-reinforced RM breakwaters under tsunami overflow. The research was conducted through physical modelling and numerical analysis to determine the effectiveness of countermeasures such as gabions, geobags, geogrids, crown walls (with shear key) and sheet piles for mitigating tsunami-induced damages on RM breakwaters. The report is formulated under different chapters, which are detailed below.

CHAPTER 2 LITERATURE REVIEW:

The chapter details the application of geosynthetics to coastal structures. The review section has been formulated in such a way that the essential aspects of the effect of tsunami impact on breakwaters have been comprehensively discussed. Thereafter, a comprehensive review of literature on the topic of response studies of seabed near breakwaters has been detailed. A detailed review of the failure of the RM breakwater by scouring is reported after that. The provision of berms and toe structures as a mitigation measure has been addressed in the subsequent section. Then, the uncertainties that occur when scaling down a prototype breakwater and ocean environment to a laboratory flume using Froude's scaling method are addressed. Following this, the development of resilient measures in composite breakwaters against tsunamis has been comprehensively detailed. Further, the various types of geosynthetics and their effectiveness in enhancing the stability and durability of coastal

structures are discussed. The chapter also discusses deformation analysis on RM breakwaters and summarizes the key findings of previous studies on this subject.

CHAPTER 3 METHODOLOGY:

This chapter outlines the research methodology used in the study. The section provides details of the physical model test setup, procedures for conducting tsunami overflow tests, and instrumentation. The chapter also explains the significance of the prototype breakwater. It provides details on the preparation of seabed and breakwater in the tsunami flume. The section also includes damage analysis techniques by using analytical methods and profile mapping. Moreover, the section also details the different RM breakwater models developed for the physical model tests.

CHAPTER 5 GABION-REINFORCED RM BREAKWATER:

This chapter evaluates the performance of Gabion-reinforced RM breakwater (GRM) under tsunami overflow. The section discusses the results obtained from (i) physical model tests, (ii) analytical study, (iii) profile mapping and (iv) numerical simulations. In the physical model tests, the comparison of conventional and reinforced models was made in terms of settlement, lateral displacement, incremental pore water pressure (IPWP), deformations, damage parameters and quantification of scouring by profile mapping. The chapter also includes a validation study of the developed numerical model in PLAXIS 3D and a detailed overview of the effects of seepage through the seabed by using the results from numerical analysis.

CHAPTER 4 GEOBAG-REINFORCED RM BREAKWATER:

This chapter evaluates the performance of Geobag-reinforced RM breakwater (GBRM) under tsunami overflow. The section discusses the effectiveness of GBRM models in terms of the reduction in settlement, lateral displacement, IPWP, deformation, mechanism of deformation, damage assessment, profile mapping, and numerical study.

CHAPTER 6 GEOGRID-REINFORCED RM BREAKWATER:

This chapter evaluates the performance of Geogrid-reinforced RM breakwaters under tsunami overflow. The section discusses average settlement, average lateral displacement, IPWP, deformation analysis, damage analysis (relative displacement and relative eroded area), profile comparison, and numerical analyses.

CHAPTER 9 CONCLUSIONS:

This chapter summarizes the key findings of the study. It provides an assessment of the performance of reinforced RM breakwaters when subjected to tsunami overflow. The section highlights the critical observations in the behaviour of conventional breakwaters under tsunami overflow. It provides a comprehensive comparison between the conventional and reinforced models. This chapter also outlines possible avenues for future research on the subject of modelling resilient RM breakwaters against tsunamis. The section provides details of the remaining research work to be done to cover the complete objective of the thesis.

In conclusion, this study provides a comprehensive evaluation of the performance of reinforced RM breakwaters under tsunami overflow. The study highlights the effectiveness of novel countermeasure techniques using geosynthetics in enhancing the stability and durability of RM breakwaters under a tsunami. Additionally, the effects of the crown wall (with shear key) on top of the RM and sheet piles on the seabed are discussed.

1.9 SUMMARY

The design and maintenance of RM breakwaters is a field that has seen extensive research. However, the concept of tsunami loading on RM breakwaters is an area that has only recently entered scientific discourse, especially after the 2011 Great East Japan Earthquake and Tsunami. Limited research and literature exist regarding this subject, and the failure mechanisms of RM breakwaters under tsunami loadings have not yet been fully explained. The behaviour of RM breakwaters under continuous tsunami overflow cannot be extrapolated from its responses to solitary waves since most of the failure mechanisms on breakwaters under tsunami attack were observed to be a result of prolonged overtopping tsunamis (Esteban et al. 2015). As far as the author knows, limited articles are available for developing countermeasure techniques for the RM breakwater to make it resilient against tsunamis. The main objective of this study is to analyse and evaluate the behaviour of RM breakwater under prolonged tsunami overtopping and develop competent and new techniques to make it resilient against tsunami-induced damage.

Furthermore, some attempts have been made there to develop countermeasures, but all of them are for composite breakwaters not for (Chaudhary et al. 2017b, d; c, 2018a, 2019; Chaudhary and Hazarika 2018; Kikuchi et al. 2015; Kishida et al. 2013; Mitsui et al. 2013; Takahashi et al. 2014a; Tsujio et al. 2013), because most of the breakwater in Japan are composite breakwater. During the tsunami, the behaviour of the RM breakwater is quite different from that of the composite breakwater. Moreover, most of the breakwaters in the world are RM breakwaters. Hence, countermeasures for the RM breakwater against tsunami are essential and need to be addressed immediately. The present study thus incorporates a variety of resilient measures that may be adopted during the design phase of RM breakwaters to withstand the impact of a tsunami.

CHAPTER 2
LITERATURE REVIEW

2.1 INTRODUCTION

Limited research has been done regarding the Impacts of tsunamis on RM breakwater and countermeasure development. Despite it being a massive structure with regards to scale, as well as a crucial component of several coastlines, the research on RM breakwaters (subjected to tsunami) only recently began to attract attention from researchers, especially after the 2004 Indian Ocean tsunami. This literature survey aims to compile every vital article that was recently referred to on the scenario of an RM subjected to the tsunami.

The post-tsunami research project RAPSODI (Risk Assessment and Design of Prevention Structures for Enhanced Tsunami Disaster Resilience) conducted by European (e.g. NGI, DEU, METU, TU-BS, LWI) and Japanese (e.g. PARI and NIMPAT) research organizations, after 2011 Great East Japan Earthquake and Tsunami, stated that there is lack of information regarding the behaviour of RM breakwater subjected to tsunami (Harbitz et al. 2016). The available studies in this domain were focused majorly on the post-tsunami field surveys (Bricker et al. 2012, 2015; Jayaratne et al. 2016; Kazama and Noda 2012; Kozai et al. 2005; Sheth et al. 2006) and analysis of breakwater stability under tsunami (Aniel-Quiroga et al. 2018, 2019; Guler et al. 2018). An attempt to make tsunami-resilient RM breakwater was found to be very limited. Further, a comprehensive analysis of the effects of scouring and seepage occurring through the body of the RM breakwater as well as foundation seabed soils during the tsunami was not performed in earlier studies.

Even though it is an essential coastal protection and strategic and lifesaving structure, the development of tsunami countermeasures for RM breakwaters is an almost untouched topic for researchers. Since Japan is one of the most affected countries by tsunamis, most of the research work in the areas has been done there (Arikawa et al. 2012; Kasama et al. 2020; Kato et al. 2012; Kazama and Noda 2012; Sassa et al. 2016; Sugano et al. 2014; Takahashi et al. 2014b). Furthermore, some attempts have been made there to develop countermeasures, but all of them are for composite breakwaters

(Chaudhary et al. 2017b, d; c, 2018a, 2019; Chaudhary and Hazarika 2018; Kikuchi et al. 2015; Kishida et al. 2013; Mitsui et al. 2013; Takahashi et al. 2014a; Tsujio et al. 2013), because most of the breakwater in Japan are composite breakwater. On the other hand, the majority of breakwaters in the world are RM-type. Several RM breakwaters were damaged during past tsunamis (e.g., the 2004 Indian Ocean Tsunami). The behaviour of the RM breakwater is much different from that of the composite breakwater. Tsunami countermeasures developed for composite breakwater are not applicable to RM breakwater. Therefore, it is of utmost importance to develop countermeasures for RM breakwaters against tsunamis.

2.2 BEHAVIOUR OF RM BREAKWATERS UNDER TSUNAMI

The studies on responses of RM breakwaters under tsunami impact are limited. This particular area of research got attention among researchers mainly after the 2004 Indian Ocean earthquake and tsunami (and the 2011 Great East Japan earthquake and tsunami). The studies conducted by Guler et al. (2015) investigated the effect of tsunamis on RM breakwaters. The experiments were conducted on a model of an RM breakwater located at Haydarpasa Port, Turkey. The model breakwater was subjected to tsunami loading in a wave flume of length 105 m. The effect of tsunamis on the breakwater was modelled by studying the effects of a solitary wave impact and the effect of overflow over the breakwater separately. The experimental results proved that the existing breakwater under study could not withstand even moderate tsunami attacks.

Therefore, the suggestion of increasing the width of the breakwater at the harbour side was put forward. The overflow over the breakwater was maintained for a duration until damage was observed in the breakwater. The height of tsunamis was determined using numerical modelling by triggering earthquakes at various possible locations and evaluating the corresponding height of tsunamis at the shore. The height of solitary waves was scaled down using the same scale factor used for the model. A notable finding in the experiments conducted in wave flume showed that the stones at the bottom portion of the RM breakwater in the seaside were not moved by the highest tested tsunami.

In comparison, the stones on the top side and the crown wall were displaced. This trend confirmed that the toe of the breakwater was not affected by a tsunami of considerable height. However, the effect of scouring due to other phenomena can occur near the toe, as discussed in the previous paragraphs. The experimental observations also highlighted that the failure of the crown wall under overtopping water also depends on the random arrangement and interlocking between the rubbles. This is a factor that cannot be replicated as precisely as in the field.

The article published by Aniel-Quiroga et al. (2018) had details of experimental results when an RM breakwater was subjected to tsunami impact. The breakwaters were modelled for the existing breakwaters on the Mediterranean coast of Spain. The model was prepared in the laboratory flume of 52 m long. The behaviour of the breakwater with and without a crown wall was investigated. The waves were generated in compliance with the scaling laws adopted for modelling the breakwater. The authors investigated the cumulative damage of the breakwater under repeated five numbers of the impact of the tsunamis. After each set of wave heights, the flume was drained to evaluate the displacements and damages clearly. The displacement of armour units was visually counted using camera and laser profiling method. The authors suggested that the results of both the methods were almost same, so visual counting was sufficient. It was pointed out in the experiments that the damage to the seaside of the breakwater due to drawdown was more significant in the case of the model with the crown wall. It was also notable that the breakwater without a crown wall had shown lesser damage at a higher wave height. This was justified by the stability response of RM armour units that might have occurred during wave action. The results highlighted that during a tsunami event, an RM breakwater with a crown wall has much resistance when compared with a geometrically similar breakwater without a crown wall. Another important finding of the article is that the presence of a crown wall, even though it prevented the failure on the harbour side, caused the seaside slopes to be damaged due to the rigorous drawdown of water through these slopes. Thus, the choice of the weight of quarry stone required in the harbour side of the RM breakwater should be strictly determined considering the tsunami effect. This research has suggested a curve-fitting equation from the graphically plotted experimental data to determine the same. As detailed by the authors,

the effect of the geometry of the breakwater under tsunami impact is a vital topic of research which was not considered in this study. The damages that occurred under a tsunami impact were found to be more rigorous over a short period. Therefore, tsunami loading on an RM breakwater should also consider the fast evolution from minor damage to severe in a short span.

The study conducted by Aniel-Quiroga et al. (2019) recently attempted to incorporate tsunami loading into the design of the crown wall on the RM breakwaters. The study modelled the fishing harbour on the Spanish Mediterranean coast on a 1:20 scale. The article was an extension of the previous literature by the same authors that detailed the experimental analysis (Aniel-Quiroga et al., 2018). The authors clarified the method to overcome the difficulty in scaling down actual tsunamis to a laboratory setup. A salient point to be noted in this study is that the authors connected the crown wall with the top RM layer, which replicates the real-world scenario. In most of the other literature, the crown wall was kept without any connection to the RM. The wall was fixed in this literature to study the pressure distribution on the crown wall under wave topping. An anchorage was provided to the crown wall. The conventional method adopted in the article was to split the effect of tsunamis into two different waves. The impact of the first wave was simulated separately, and the overflow of the tsunami was simulated later by using currents with the aid of a pump. The experiments took only the impact of the first wave into consideration. Twelve pressure gauges were placed at various points inside the breakwater and near the crown wall. In the graphical representations the authors have converted the pressure to a non-dimensional factor for the clear depiction of results. The forces and moments acting on the crown wall were determined to estimate the stability of the crown wall. It was highlighted that the pressure due to overtopping of waves were not considered as the effect of these pressures is adding more stability against sliding or overturning of the crown wall. However, since the forces were integrated from pressure sensor data, it was found that the estimated moments were not incrementing linearly with higher tsunamis, which was justified by the effect of overtopping action of waves. In the experimental analysis it was found out that higher waves did not caused damage on the harbour slope as these waves had collapsed at a farther distance towards the harbour side.

Tsunamis have longer wavelengths, which are difficult to scale down to a wave flume, as mentioned previously. The widely used method of studying a tsunami impact by considering the effect of a solitary wave hitting an offshore structure was suggested to be the least accurate in the research work by Goseberg et al. (2013). The article put forward the idea of using pumps with proportional-integral-derivative controllers in a closed-circuit flume system, where the volume of water in the storage reservoir is used to form the volume of water in the wave crest generated in the flume. Even though the conservation of volume assumption was not that practical, the authors were successful in generating long waves of wave profiles resembling actual tsunamis. The generated waves are long waves which otherwise cannot be generated in the usual flume dimensions. The authors also highlighted some critical aspects of this type of wave generation. The 180^0 bend in the circuit flume will cause spiral flows and secondary flows when the generated waves travel through the flume. These additional flows could cause energy loss to the generated long waves. The study is thus limited to the possibility of generation of the long waves. The impact of these waves on the model beach and the uncertainties in assuming a unit reflection coefficient to the beach model were not evaluated.

On the contrary, the increase in the volume of water due to the reflection of waves has been evaluated using pressure sensors. Correspondingly, the pump systems were adjusted based on algorithms so that the desired long waves were persistent in the wave flume. Although the article has its limitations in the usage of a circuit flume system for wave propagation, the method of wave generation suggested was innovative in recreating long tsunamis at a laboratory scale without consuming large spaces.

The studies of Bricker et al. (2012) proved that tsunamis overtopping can result in damage to the foundation of breakwater. In the handbook of coastal disaster mitigation for engineers and planners (Bricker et al. 2015), it was clearly mentioned that the geotechnical failure of a breakwater by punching could not be prevented along with the typical scour prevention measures. The jet of water that was overtopping was observed to eventually drift away from the breakwater as the height of the tsunami increased. The observations were made on the numerically modelled Kamaishi breakwater in Japan under the impact of the Great East Japan tsunami of March 11, 2011. The study also

highlighted the failure of the harbour side of the breakwater was higher due to the gap provided between the caissons resting on top of the RM. These findings clearly stated that the harbour side of a RM breakwater is prone to severe damages during the waver overtopping and the degree of such damage would be larger in the absence of a crown wall or caisson.

The permeability of the core in an RM breakwater is an important parameter that determines the amount of water that will be permeated through the structure under a tsunami attack, thereby imparting uplift pressures that could develop beneath the crown wall along with some rearrangement in core materials due to hydraulic pressure. In the study conducted by Recio and Oumeraci (2008), the determination of the permeability of the core by laboratory experiments based on Darcy's law has been detailed. The amount of water that will be transmitted through breakwater also depends on the period and amplitude of the impacting waves. Thus, as quoted in the article by Oumeraci and Kortenhaus (2011), longer waves have a higher potential to transfer water through the permeable core of the breakwater. The study suggested that the wave transmission by overtopping and through the breakwater should be summated to determine the transmission coefficient of the breakwater.

The decay of a wave when it passes through the RM breakwater is a complicated process to evaluate in the study conducted by Muttray and Oumeraci (2005). The authors discussed the phenomenon of wave overtopping inside an RM breakwater. When a wave propagates through the core, the water level within the core increases and may reach up to the crest level, causing internal overtopping of the waves. This phenomenon increases with the increase in wave height, which clearly states that under the impact of tsunami loading, internal wave overtopping would occur. The internal wave height and the changes in pore water pressure are interrelated. Thus, to determine the damping effect of a breakwater core, these two parameters need to be evaluated. An extensive experimental study was conducted in which the RM model was subjected to both regular and irregular waves, and the overtopping of waves was not allowed. Therefore, the infiltration of the wave from the crest of RM was not considered in the study, which is a limitation. The research put forward modified equations that successfully predict the attenuation of waves passing through the breakwater by taking

into consideration the turbulent losses. The study also highlighted that the hydraulic resistance involved in the wave infiltration can be approximated by linear polynomial or quadratic methods of estimating the resistance.

In the numerical analysis by Dentale et al. (2018), an essential method of evaluating wave impregnation through armour units was adopted. The method used the Flow Within the Armour Units (FWAU) model, in which the interaction of turbulent flow through the armour blocks can be analysed. In contrast, in most of the other literature, the armour layer was defined as a porous medium. Hence, the field conditions were not appropriately simulated. The analysis used FLOW -3D® software, which works on Reynolds Averaged Navier-Stokes (RANS) equations based on the Volume of Fluid (VOF) method. The method of adding armour units as individual 3D elements drawn in CAD software helped in modelling the breakwater with more resemblance to field conditions. The results of the analysis proved that the proposed numerical method predicted the wave run-up, overtopping, and reflection coefficients of waves with higher accuracy than the existing formulae.

The wave overtopping reduction under oblique waves was studied by van Gent and van der Werf (2019). The study was conducted by modelling an RM breakwater in a wave basin with two types of crown walls. The crown walls with and without shear key were subjected to the impact of waves at different angles. Since the study was focused on crown wall behaviour, the armour blocks were kept more stable by using wire mesh and heavier blocks. An overtopping chute connected to a tank was kept calculating the quantity of water collected. The study thus suggested reduction factors for determining vertical and horizontal forces on the crown wall.

Further, the provision of a key on the wall tends to reduce the uplift forces considerably and increase the horizontal forces. Also, a reduction factor was coined to calculate the overtopping discharge by oblique waves. The authors suggested designing crown walls by considering the oblique wave loads so that the designed size of the structure could be reduced.

2.3 BEHAVIOUR OF FOUNDATION SEABED OF THE RM BREAKWATER

The research work by Jeng and Ye (2012) innovatively introduced the concept of the initial consolidation of foundation seabed soil under self-weight of RM and prevailing hydrostatic pressures. The authors determined the time required for the dissipation of excess pore pressure developed in the seabed due to the construction of RM by adopting Terzaghi's theory of one-dimensional consolidation. Different parameters were varied, and the authors numerically analysed the response of the system by using a modified version of the FEM model called PORO-WSSI III. A three-dimensional FEM analysis was performed with 27 node brick elements were chosen for discretisation. The analysis pointed out that Young's modulus of the seabed is the most sensitive parameter that decides the consolidation settlement of RM. It was inferred that the seabed beneath the breakwater was subjected to considerable values of effective normal stresses and shear stresses. The shear stresses were found to develop higher towards the toe of RM. The shear failure of soil near the toe resulted in the uplifting phenomenon. It was also found that tensile stresses were developed beneath the breakwater due to the deformation of the seabed. The study thus concluded that stiffer seabed soils could effectively reduce the consolidation settlement and shear stress concentrations near the toe of RM. The authors suggested experimentally verifying the results on a laboratory scale for further clarification of the observed responses of the seabed.

Liquefaction of seabed near RM under dynamic wave impacts was studied by Ulker et al. (2018) by using finite element modelling considering the seabed as a porous elastic medium. The article discussed different key parameters, including saturation and permeability of the seabed, wave period and inertial forces that influence the liquefaction of the seabed under wave load. The total effective mean stresses under various scenarios were graphically depicted to highlight the areas of liquefaction where effective stresses were found to be zero. The seabed was analysed in three phases: initial hydrostatic pressure, consolidation, and loading from standing waves. After the analysis, liquefaction was observed along some areas on the seaside slope of the breakwater, which the authors explained as the dislocation or scouring of material on the mound. The analysis of two types of RM with and without a core layer has shown that the presence of a core layer with stiffness different from that of the outer layer

caused more liquefaction along the seaside. This was explained as the effect of phase difference in the response of the core and outer layer. It was also inferred that the core of the RM takes the most stress.

In the real sea environment, the seabed is subjected not only to wave breaking but also to water currents. The coupled effect of waves and currents was studied by Zhao et al. (2018). The authors used VARANS equations to model the fluid and Biot's equations to model the poro-elastic seabed. The seawater was modelled in OpenFOAM, and the seabed was modelled in DIANA SWANDYNE-II. Thus, an FVM (Finite Volume Method)-FEM (Finite Element Method) coupled modelling has been adopted in this study. To validate the accuracy of developed models, the authors compared the model-predicted values with that of three previous studies. The results show that the developed model accurately predicts experimental outcomes.

Further, the model considered a co-current and counter-current effect, in which the latter tends to increase wavelength and later tends to reduce it. It was also observed that the wave height was amplified with counter-currents rather than with co-currents. It was thus evident that the water currents caused a significant effect on wave profiles. The effective stresses and pore pressure developed on the seabed depicted that those co-currents induce larger stress magnitudes. Shear stress was concentrated near both toes of RM. Even though the RM was modelled as a porous structure, a discontinuity was observed in pore pressure below the structure, which may be due to the difference in material stiffness between the mound and seabed. By using the Mohr-Coulomb theory, the stress angles were determined. Under the assumed criterion of angles above 35^0 caused shear failure, corresponding locations were plotted. It was found that stress was concentrated near both toes of RM even before wave loading. The development of shear stresses along the seaside slope was higher with co-currents, and along the harbour slope was higher with counter-currents. The instantaneous liquefaction of the seabed was observed along the upper layers under wave troughs.

In contrast, no such phenomenon was observed beneath the structure. However, the authors refer to previous studies where residual liquefaction was observed beneath the mound. The co-current waves were inducing a liquefaction phenomenon, and it occurred mainly on the front side of the mound. It was inferred from the study that the

seabed parameters, such as degree of saturation, permeability, and shear modulus, influence liquefaction potential. Further, the higher wave height, like that of a tsunami, could impart immense energy to the structure and seabed, which can increase the liquefaction potential of the seabed. It is worth noting that the developed shear stresses on RM under the combined action of wave and current were observed to be distributed asymmetrically, which can cause toppling on either side.

The liquefaction of the seabed beneath the breakwater was examined using shake table tests, as in the studies conducted by Najma and Ghalandarzadeh (2019). A composite breakwater with caisson on top of an RM was modelled with two layers of sand beneath. The experimental analysis showed that the seabed soil was laterally moved during seismic loading accompanied by the widening of RM. Further, the breakwater settled vertically downward, and the heaving of the seabed was observed at either side of the breakwater. The research concluded that embanking the existing liquefiable seabed with denser sand has not only prevented the liquefaction-induced damage but also mitigated the penetration of RM into the seabed under seismic loading.

The influence of berms in liquefaction of seabed was studied by Celli et al. (2019). The study pointed out that the length of the berm had a more significant influence than its height in preventing liquefaction of the seabed. The soil model was developed as poro-elastic anisotropic material with one-way coupled boundary conditions in OpenFOAM software. SWASH software was used to evaluate the properties of waves. The soil anisotropy was defined for permeability alone, and Young's modulus and Poisson's ratios were assumed to be constant. The vital step adopted in numerical analysis was the modelling of the RM seabed boundary without a bedding layer. In detail, the boundary between the mound and the seabed was modelled as rubbles resting on a flat seabed. This replicated the real-world scenario in which there will be portions of the seabed left without contact between the bottommost layer of rubbles. The dynamic pressure developed in the seabed had a positive relation with the porosity of the armour layer. The consolidation due to the weight of the breakwater was simulated using Biot's equations in the beginning. The vertical displacements of soil beneath the RM were found to have negative values. The authors justified this as the compression and upward movement of soil particles. This value depended on the magnitude of load acting on top

of the seabed soil. The same was observed for vertical effective stresses. The authors also highlighted that the changes in liquefaction of the seabed during the consolidation stage are much higher. Under the influence of wave actions, it was noted that the direction of seepage flow changed with wave crests and troughs. The direction of seepage flow was observed to be downwards with wave crests and the opposite with troughs. This upward seepage flow is critical as it could cause momentary liquefaction when it exceeds the vertical effective stress acting downward. The study did not evaluate the effect of shear stresses developed. The study concluded that the provision of the berm of more extended widths could shift the occurrence of momentary liquefaction from the seabed beneath the core to the seabed beneath the outer layers.

The response of the seabed under hydraulic and seismic loading was numerically evaluated by Zhao et al. (2020). A novel boundary condition called accurate absorbing boundary (ABC) was mathematically derived and applied. Even if the boundary were provided at short distances from the structure, it could represent the infinite boundary properties of the poroelastic seabed. When the infinite boundaries are trimmed to shorter boundaries, corresponding loading must be assigned on the ABC. The RM was modelled to be resting on a porous soil medium, which was laid on a solid, impermeable bedrock. The interfaces between the RM and seabed were designed to have continuity in displacement vectors of pore water.

In contrast, the interfaces between soil and bedrock were designed such that the relative displacement of pore water was zero. The pressure of the designed seawater had equilibrium continuity with the pore pressure. The top of seawater was modelled as a free surface, and the bottom of bedrock was designed to displace in accordance with the input wave force. The developed model was found to be accurate in assessing the seismic response of the seabed. Some significant findings of the study include the effect of water depth, inclination of RM and permeability of seabed on the seismic response of breakwater. It was found that the higher water depths above the seabed help dampen the seismic wave and, hence, reduce the response of breakwater.

In comparison, an increase in the inclination of side slopes of RM has increased the response of the structure. The effect was considerable for horizontal motion of seismic waves and insignificant for vertical movements. Further, the shear modulus of the

seabed was found to have a more significant influence on the response of the breakwater when compared with the permeability of the seabed. The toe of the mound was found to be most vulnerable to liquefaction under seismic loading. The horizontal seismic motion had a positive relationship with the liquified area, whereas vertical motion caused an opposite trend.

2.4 SCOUR FAILURE OF RM BREAKWATERS

The scour failure occurs when areas of the seabed soil in the vicinity of a breakwater erode to form holes due to different types of sea wave actions. A considerable number of studies have been conducted in this field since earlier days. A well-detailed experimental study was conducted by Fredsoe and Sumer (1997), where the authors pointed out that the reflection coefficient of RM breakwaters has a considerable effect on the scour depth. They concluded that as the reflection coefficient decreases, the scour depth decreases. The different mechanisms that trigger the scouring were clearly detailed in the article. The vital mechanism among these was streaming. Streaming can be defined as the movement of water over an area during a period. This water movement from the seaside of breakwater to different directions can carry seabed soil along with it. The experiments in this article thus showed that streaming caused the formation of a scour hole in front of the breakwater and upheaval of the soil at nearby vicinities of the breakwater head. Apart from streaming action, the plunging breakers also resulted in the formation of scour holes at the harbourside. A plunging breaker is a type of sea wave in which the crest of the wave rises and falls like a surfer wave. Some of the preventive measures suggested by the article state that reducing the side slope of the breakwater had reduced the scouring. When the roughness of the breakwater surface increases, the formation of a plunging breaker is suppressed and hence reduces the scouring. The construction of a protection layer around the RM was found to be very effective in avoiding scour formations. However, the experimental tests showed a scour on the protection layer itself, which was not investigated further. The protection layer provided was a layer of rubble. The protection layer prevented the scour formation completely when the width of the layer was extended all over the possible failure areas of the seabed.

A two-dimensional analysis of the scour has been done by Sumer and Fredsoe (2000) in which the failure mechanism of the protective layer was also studied. The article establishes that the width of the protection layer must be at least the width of the scour formed without the layer. Further, as the number of layers of the protective apron increased, the scour depth decreased. However, the apron was made of rounded boulders to study the failure profile more clearly. Therefore, the effect of irregular rocks as a protection layer was not considered. The article also pointed out that irregular waves have a lesser effect on scouring formation compared to steady waves. When waves are combined with ocean currents, the effect of scouring would be considerably more significant. The study did not consider the transfer of sediments by suspension. The effect of such suspended sediment movements was less than that of the scouring due to the movement of sediments over the seabed.

In the studies to evaluate the sand suction mechanisms conducted by Hur et al. (2007), both experimental and numerical analyses were conducted. Two types of RM breakwaters were modelled, one with inclined sides and another with vertical sides. The numerical study adopted a numerical wave tank for simulating waves. The model was resting on an impermeable layer with reclaimed sand on the onshore side. The experiment was conducted by generating regular waves using a wave paddle for 30 minutes. The scouring that occurred on the reclaimed sand was then visually evaluated using a video recorded by a camera. The experimental analysis was successful in replicating the so-called suction on the reclaimed sand. The term suction was used to refer to the formation of pits on the surface of reclaimed sand due to the initial formation of cave-like borrows inside the reclaimed sand near the breakwater boundary. The study concluded that breakwater width plays a vital role in dissipating the incident wave energy such that the suction phenomenon can be prevented by increasing the width of RM. Furthermore, the use of a filer layer between the reclaimed sand and breakwater was suggested to effectively reduce the formation of borrow-like caves inside the reclaimed sand.

In the overview of the article by Bricker et al. (2012), the scour formation in the seabed near the heel of a breakwater was evident in the investigations of coastal structures after tsunami impact. Several previous studies on the topic were summarized in the article. The plunging action of the wave jets was observed to be the primary reason behind the

scour formation at the harbour side of coastal structures. The long scouring formations observed behind seawalls, in some cases, might be due to the water currents moving parallel to the structure. This parallel movement has increased the dimension of a formed scour hole.

Further, the hydraulic action caused by the drawdown of tsunamis along the seaside of coastal structures had also aided in scouring and erosion. The literature compared different existing methods of determination of scour depth with actual scour depth data collected from the field. It concluded that only a few methods are compatible with scour depth evaluation by the tsunami. However, these methods were found to give conservative results since they were not developed considering the long waves, like tsunamis. In all of the cases studied, the method used by Rajaratnam (1981) was found to give higher values than actual despite the various parameters that have changed. Hence, this method can be adopted to estimate the scour depth induced by the jet plunging action of tsunamis.

An innovative method of estimating the damage level of armour units was put forward by Puente et al. (2014). The study used a Light Detection and Ranging (LiDAR) technology-based system called Terrestrial LiDAR. The method estimates the number of displaced armour units from MATLAB programming, which analyses the images from the scanner mounted near the wave basin. The results from the experimental analysis have proven that the proposed innovative methodology was highly accurate in determining the damage. The analysis was limited to the estimation of damages that occurred above the water level since the scanner was unable to detect the profile beneath the water. However, the authors suggested that this could be easily achieved with additional equipment.

The study by Mulders et al. (2015) addressed a relevant yet less attended issue of scouring of core materials during the construction phase. A detailed experimental study was conducted in the wave basin with different wave incident angles and materials grading. It was observed that the rubbles were rearranged to a stable ‘S'-shaped profile under the wave attack. A comparison of the prevailing equations to determine the number of transported stones under wave attack has shown that the equations either

underestimated or overestimated the displaced number. Therefore, the authors introduced a modification factor after analysing various results from different literature. Similarly, the existing equations for estimating various geometric parameters of reshaped profiles were compared with experimental results. It was also found that the total change in the volume of the breakwater was negligible even after being subjected to 3500 wave trains in every test. The research thus laid a solid base for the damage estimation of the core that could assist the contractor in making decisions when a heavy storm is forecasted while constructing an RM. It was concluded from the studies that higher wave load impact on widely graded cores resulted in more significant deformations. This points towards the necessity of evaluating the stability of breakwaters under the impact of tsunami load. The literature also highlighted the influence of the gradation of the core in the response to wave impact.

2.5 INFLUENCE OF TOE AND BERM ON RM BREAKWATERS

The research of van Gent (2013) put forward an equation to determine the size of rocks in rubble when a berm was provided. The experimental studies concluded that the provision of a berm reduced the size of rock in the RM. The upper and lower portion of the seaside slope of RM was studied separately by keeping the portion under study fixed using wire mesh. The width of the berm was also varied during the different sets of experiments. The experiments with the position of the berm at higher and lower heights highlighted that the higher berms had a more stabilizing effect as they prevented the run-down wave from reaching the area below. It was also found that the damages are concentrated in the transition portion of the lower slope and berm. The authors suggest providing smooth corners at this transition area to prevent such damage. However, the effect of such modification was not studied. The position and width of the berm, steepness of the wave, slope of the seaside, and surf-similarity parameters were found to be the main factors influencing the size of the rock on the top side of the berm. The authors suggested determining the recession of a berm, which is the distance between the outer end of the berm and the harbour side where damage has not occurred or is considerably low. The recession of a berm determination could aid in providing small-sized rubbles from the recession distance.

The toe structure can be described as a berm of shorter height in the armour layer. The primary function of a toe is the prevention of scour formation. In the research by van Gent and van der Werf (2014), the effect of this toe structure was studied. The experiments were conducted in a wave flume where the thickness of the toe was modelled to be less than 0.3 times the depth of water. A total of 192 tests with 1000 wave repetitions for each test were performed. The essential findings of this research include the considerable influence of low wave steepness in comparison with that of high-steepened waves. The factors influencing the toe stability were suggested to be the height and period of the wave, the depth of water at the toe, and the width and thickness of the berm. The results of experiments highlighted that the damage to the toe increases with wave height and decreases with an increase in water depth at the toe.

Similarly, an unconventional result was obtained for the thickness and width of the toe structure. As the thickness and width increased, more damage was found. Therefore, under a tsunami attack, where the wave height will be of higher magnitudes, the stability of the toe structure would be on the verge of critical condition or even failure. As a remedial measure, the size of the rock in the toe layer could be increased. The required size of the rock can be estimated from the equation suggested by the authors.

The performance of berms with comparatively small thicknesses was studied by Celli et al. (2018). Numerical analysis backed up by experimental studies had been conducted to determine the effect of low berms. The article suggested a new formula for estimating the stability number of RM by considering the effect of low berm. The numerical modelling was done using SWASH software. It was observed that the numerical model did not precisely predict the results of the model experiments. Hence, prototype measurements were used to model numerically. Thus, the article successfully introduced correction factors to the existing equation of stability calculation based on the relative height of the wave at the toe. The developed equation was applicable to both shallow and deep-water cases.

2.6 EFFECTS OF SCALING ON WAVE OVERTOPPING

Franco et al. (2009) conducted extensive research by comparing the actual prototype data with the model data to determine the effect of scaling in wave run-up and

overtopping on an RM breakwater. The breakwater at Ostia, Italy, was modelled in a wave flume as well as a wave basin for analysis under both 2D and 3D conditions. The studies were conducted in different sets. The initial set of experiments was conducted on the model of prototype breakwater. The other sets of experiments were conducted by modifying the seaside slope, permeability, and offshore distance. The results of these experiments concluded that the models failed to create wave overtopping under the scaled-down actual storm data. To find the reason behind this, the authors have modified several parameters of breakwater to incorporate the filed dimensions and conditions. Despite the efforts, it was found that all those parameters had a negligible effect on wave overtopping. Therefore, the article suggested that the breaking of waves at a longer offshore distance before reaching the breakwater could result in higher turbulent water that could not be accurately modelled on the laboratory scale. The factors such as curvature in the breakwater alignment, wind speed, etc, could not be quantified and modelled. These factors may result in the inaccurate overtopping of waves in the flume and basin. Whereas the authors pointed out that, in the case of RM with steeper slopes on either side, the overtopping of waves can be modelled with higher accuracy. The authors also extended the study by determining the roughness coefficient of the breakwater with reference to a smooth breakwater slope. A value of 0.4 as roughness coefficient was found to be reasonable for the RM under breaking and non-breaking wave impacts.

The research by Lykke Andersen et al. (2011) also backed up the relevance of scaling down the effect on small wave overtopping in RM breakwaters. As the majority of RM breakwaters are designed for small wave overtopping heights, the inefficiency of scaling down the wave could seriously impact the model's experimental results. The authors compared the effect on small and large-scale models. The large-scale model was four times larger than the small-scale model. The authors highlighted the scale-down effect on Reynold’s number as one of the reasons that could cause the small overtopping in the model. The scaling down of a prototype also resulted in changing the type of flow through the RM from turbulent to laminar.

Another important aspect highlighted in the article was the entrapped air in water used in the flume or basin. Generally, fresh water is used in studying the model, which will

have fewer air-entrapped bubbles compared to saline water. However, even if the model was subjected to saline water, the relative size of entrapped air bubbles was considerably more significant than that of actual sea water near the prototype. Also, the volume of air entrapped will be lesser in the model than in the prototype. Therefore, it was pointed out that the average mass of water that runs up the slope of RM in the prototype will be less than that of the model. This would obviously result in higher overtopping in the prototype and lower overtopping in the model. The experiments concluded that the top geometry of the RM has a significant influence on the overtopping of waves. Scaling effects were found to be lesser for RM with a wider top width.

2.7 DEVELOPMENT OF RESILIENT BREAKWATERS AGAINST TSUNAMI

In the studies conducted by Chaudhary et al. (2018b), Chaudhary et al. (2017a), the mitigation measures for composite breakwater (caisson type) were proposed under the impact of a strong earthquake and tsunami. This condition was suggested to be a critical condition by the authors, who quoted that the excess pore water pressure that has developed due to a seismic event might not be entirely dissipated when succeeded by a tsunami. The composite breakwater was made of caisson at the top of RM, resting on a sandy soil foundation. It was experimentally proved that this condition causes excessive vertical settlement and considerable lateral displacement of breakwater. Therefore, the foundation of the breakwater was reinforced by using a geogrid layer, gabions, and sheet piles. The experimental analysis showed that the provision of sheet piles and gabions could reduce the lateral movement of foundation soil and mound, respectively, under the abovementioned critical loading conditions. The primary function of sheet piles was to prevent the seepage of water through the foundation soil. The higher-level difference in water profile between the seaside and harbour side during a tsunami event could trigger the seepage of water through the foundation soil and, thereby, settlement of breakwater. A particular type of gabion was designed to reduce the impregnation of water through the mound from the seaside. These gabions had a metallic sheet placed on one face of the gabion, which represented an impermeable membrane. The study had made the breakwater strong enough to withstand the loadings since the failure of the foundation was solely the point of interest. The accelerogram data collected after

conducting shake table tests under 0.1g and 0.3g as foreshock and mainshock, respectively, proved that the presence of sheet pile walls had reduced the amplification of seismic waves. The settlement of the caisson was found to be less for breakwater with a reinforced foundation. This was evident from the lower values read from pore water pressure gauges in the foundation soil. The lower degree of settlement of RM due to the presence of a geogrid membrane resulted in a lower value of excess pore pressure. Similar were the results obtained for lateral displacement. The lateral displacement of the breakwater was resisted by the additional weight and frictional resistance imparted by gabions.

In comparison, the sheet piles had reduced the lateral movement of foundation soil. Thus, it was concluded in the article that reinforced breakwaters withstand earthquake and tsunami loads more effectively than unreinforced types. The displacement of the sheet pile wall was observed after a seismic event. The authors suggested anchoring the sheet piles with a geogrid membrane to prevent such displacement. Further, the gabions provided were not connected in the experiments. Therefore, the authors have suggested that connecting the gabions also anchoring it to sheet piles and caisson, could provide more resilience to the structure. The article thus put forward a novel method of implementing geosynthetics in breakwater foundations and improving them to make breakwater resilient to earthquake and tsunami loadings.

2.8 APPLICATION OF GEOSYNTHETICS ON COASTAL STRUCTURES

In the study conducted by Yu et al. (2005), the action mechanism of the geotextile-reinforced cushion under breakwater was investigated in the context of the Huanghua Port Project, which is located in Hebei Province, China. Various measures were used to systematically study the effects of the strata characterization and the reinforcement condition on the stability of the breakwater-ground system. These measures included material experiments, centrifuge modelling tests, and FEM numerical analyses. The study found that the geotextile-reinforced cushion under the breakwater constrains the lateral displacement of both the breakwater and the ground, which helps to control deformation and enhance the stability of the breakwater-ground system. The reinforcement also suppresses the range of high-stress levels in the system, which can help avoid the concatenation of the failure area in the embankment and the ground and

restrain the global slip surface from occurring or developing in the system. The study also found that the effectiveness of the reinforcement increases as the modulus of the geotextile increases and as the geotextile becomes wider.

Additionally, the weaker the ground is, the greater the lateral displacement becomes and the more noticeable the reinforcement effect is, significantly when a more robust layer underlies the weak layer. The distribution of the tensile force in the geotextile was found to be non-uniform, with greater force in the range of the central part of the breakwater. The Huanghua Port Project itself includes four 35-thousand-ton berths with an annual transporting capacity of 30 million tons. The breakwater is composed of two parts, the south breakwater and the north breakwater, which are 5030 and 4082 m in length, respectively, and have a typical depth of 6.3–7.7 m. The breakwater was built on soft clay strata about 12 m in thickness. A typical section of the breakwater includes a layer of geotextile sandwiched beneath the layer of sand 50 cm in thickness and an upper layer of gravel 50 cm in thickness. A shed covers the surface of the breakwater. Overall, this study provides valuable insights into the action mechanism of the geotextile-reinforced cushion under breakwater and the effects of strata characterization and reinforcement conditions on the stability of the breakwater-ground system. These findings can be helpful for future coastal engineering projects that use similar reinforcement methods.

The study by Shin and Oh (2007) discusses the changing materials used in hydraulic and coastal structures due to the increasing cost of conventional rubble and concrete systems. Geotextile tube technology is presented as an alternative material for constructing shore protection structures. The paper focuses on the issues related to the geotextile tube construction for erosion prevention at Young-Jin Beach on the east coast of Korea. The authors describe the construction procedure and present the results of in-situ measurements, including effective height, vertical stress at the bottom of the geotextile tube, shoreline variation, and water depth of the nearshore area. A total of eight geotextile tubes were installed at the Young-Jin Cove, with four double-lined geotextile tubes installed from south to north, spaced at 20.0 m intervals. The authors observed that the filling process occurred very fast, with settling and drainage taking place quickly. One geotextile tube was constructed in less than an hour, and the desired

final height was achieved after only four dredging and filling steps. The authors highlight that the expeditious construction is the most evident advantage of this innovative shore protection technology. However, the favourable economic aspect should not be overlooked. After a year of use, seaweed inhabited the surface of the submerged tube, and the authors concluded that the polymer material used in their manufacture was unlikely to have an adverse effect on marine life.

Moreover, it can be environmentally sustainable to the adjacent ecology. However, the long-term effectiveness of the installations cannot be judged until more time has passed. The test sites have been exposed to a number of severe storms common to the east coast of Korea, which makes it challenging to evaluate the structure's performance as a form of innovative shore protection. Over the short period of observations, the shoreline extended into the sea for three months due to the short-term effectiveness of wave adsorption and decrement of sea bed soil migration. After three months, however, the shoreline was re-eroded by tidal waves and geometrical reasons. The magnitude of re-erosion was relatively small compared to the extension of the shoreline. The water depth in the near shore area decreased with elapsed time, and the sand gradually accumulated around areas covered by the geotextile tube.

The research work by Alvarez et al. (2007) describes the erosion process of the beaches on the Northern coast of Yucatan, Mexico and the need for coastline stabilization due to human action and the risk of destruction from hurricanes. Geotextile tubes were used as low-crested structures to control beach erosion along a 4 km area of the beach. The study shows that geotextile tubes are effective and environmentally friendly for shore stabilization. However, future designing techniques require the development of predicting models for wave energy transmission, tube geometry, and relative submergence. There are also concerns about the behaviour of geotextile tubes in the mid-long term, such as durability against unpredictable UV exposition periods and behaviour against direct interaction with stresses generated by continuous wave action and sediment motion.

The studies of Koffler et al. (2008) discuss the potential of geosynthetic products in providing safe and cost-effective solutions to various engineering challenges and construction requirements. These products serve as alternatives to natural materials.

They can be used for a range of functions, including filtration, drainage, separation, and reinforcement requirements. The paper emphasizes that with the use of geosynthetics, the design lifetime of most geotechnical structures can be dramatically increased, and new modern design approaches can be explored. The development and challenge of the use of geosynthetics in geotechnical, hydraulic, coastal, and off-shore engineering is of particular interest due to the strong development of various industries worldwide. The research work provides some examples of successful geosynthetic projects. In the Amwaj Islands Project in Bahrain, geotubes were used to build 30 km of coastal dykes to prevent the settlement of artificial islands. The project was carried out in two stages and involved the hydraulic filling of sand behind the geotubes. In Sea Isle City, New Jersey, USA, geotubes were used to internally reinforce a frontal dune to protect the coastal road and properties from flooding during heavy storms. Geocontainers were used to build submerged containment dykes to reconstruct a failed underwater slope in Zoutkamp, Netherlands. The project involved several tiers of geocontainer dykes with sand used as fill material. The lowest tier was found 20 m below water surface level. The project was cost-effective and successful in stabilizing the slope and protecting the adjacent gas pipeline. The research also highlights the evolution of geotextiles from a limited application to a widely used and efficient means for fighting erosion and protecting marine and hydraulic constructions. Its application in concrete sites has also proved to be effective in terms of ease of use, cost-effectiveness, rapidity, and durability. Overall, the research highlights the potential of geosynthetic products in providing safe and cost-effective solutions to various coastal engineering challenges and construction requirements and provides examples of successful projects in different parts of the world.

The research by Yan and Chu (2010) presented a study that focused on the use of clay slurry-filled geotextile mats for the construction of dikes for land reclamation at Tianjin Port, China. The study aimed to assess the feasibility of using this innovative method and to propose a preliminary design for the dike. The researchers conducted laboratory tests to determine the suitable soil to fill the geotextile mats with and concluded that low-plasticity clay was the best material. They also proposed a simple method to estimate the required tensile strength and height of the geotextile mat. To verify the

proposed design and assess the stability of the dike, numerical analysis and centrifuge model tests were conducted. The results of the tests demonstrated that the dike built using the geotextile mats could remain stable, even under high acceleration. The foundation soil mainly controlled the ground settlement. After the verification process, a field trial was carried out to test the stability of the dike. The results showed that the dike was stable, and the maximum ground settlement and compressibility of the dike were within the expected limits.

Additionally, the use of a grouted geotextile mattress as a cover for the dike after the consolidation of the geotextile mats was suitable. Small cracks occurred on the surface of the mattress, but they did not cause significant damage to the overall structure. Overall, the study concluded that the use of clay slurry-filled geotextile mats for the construction of dikes is feasible and can provide stable structures for land reclamation. The proposed design, which was verified through various tests and a field trial, showed promising results and could be considered for future land reclamation projects.

The research work by Lee and Douglas (2012) discusses the problem of severe erosion of the shoreline in Malaysia caused by high-energy waves, which has led to the loss of valuable land and deterioration of the quality of the beach. The measures implemented in the past to mitigate these adverse effects have mostly been complex solutions. To address this issue, a pilot project utilizing geotextile tubes installed as submerged dikes was undertaken in 2006 at Teluk Kalong, Kemaman, Terengganu, which experienced severe erosion during the northeast monsoon period. The geotextile tubes were comprised of high-strength woven geotextile filled with sand slurry, and the project was successful in arresting further erosion of the shoreline and improving its condition. Encouraged by the success of the pilot project, a similar shoreline protection project was implemented in 2008 at Pantai Batu Buruk, which protected a 5 km stretch of beach. The project involved the installation of 3.5 m diameter geotextile tubes as submerged dikes approximately 150 m offshore. The geotextile fabric allowed consolidation of the sand to create a long sausage-like gravity structure. Post-installation surveys carried out indicated that the shoreline has improved with a much wider foreshore area, and significant sand deposition was recorded on the foreshore area. This contributed to the long-term shoreline management and promoting

sustainable protection of the shoreline. The article discusses the concept of shoreline management using geotextile tubes as submerged dikes, the details of these two projects, and the outcome of the projects. The success of the projects was evident from the significant accumulation of sand, which widened the shoreline and reduced the depth of seawater near the shore, thereby reducing erosion. The use of geotextile tubes as submerged dikes provided an environmentally friendly alternative to complex solutions for shoreline stabilization and management.

The research work by Bayesteh and Mansouriboroujeni (2020) investigates the behaviour of an RM breakwater constructed on soft soil, with a focus on settlement caused by submersion of rockfill particles into the seabed. Geosynthetics are commonly used as reinforcement in RM breakwater construction. However, numerical methods based on continuum mechanics cannot provide insight into settlement because they cannot approximate the individual movement of particles. A full-scale case study of a geosynthetic-reinforced RM breakwater on soft soil is presented. Monitoring results show that two mechanisms of settlement were likely to affect the unreinforced RM: submersion of individual particles of rockfill into seabed resulting from the discontinuous nature of the rockfill and elastic continuum settlement caused by the use of a geogrid as a separator and reinforcement. The results show that the settlement caused by the submersion of the particles was more significant than the classic elastic or consolidation settlement. The use of a geosynthetic as a reinforcing system before construction caused an interlock between the rockfill and geogrid mesh, prevented particle submersion, and created a continuum media. Thus, elastic and consolidation settlement are the main mechanisms that control the behaviour. The mechanism of settlement of the RM breakwater was investigated using discrete element simulation, and the results showed that this method was able to simulate the submersion of particles into the seabed. A series of simulations were conducted to evaluate the effect of geogrid length, number of reinforcement layers, and geogrid tensile strength on the performance of the reinforced breakwater. The results showed that increasing the length of the geogrid and the number of geogrid layers decreased settlement while increasing geogrid tensile strength decreased settlement up to a certain point. Over-reinforcement should be considered to prevent settlement.

According to the research by Ghazi et al. (2022), the construction of rubble-mound breakwaters on soft sea beds is challenging but necessary in many coastal areas. The main issues faced during construction include the loss of material due to the penetration of rock particles into the soft clayey bed, significant deformation during and after construction, and instability. The basal reinforcement method, which uses both separation and reinforcement, has been proposed as an effective solution. Previous researchers have focused on the role of reinforcement. However, less attention has been paid to the combination of reinforcement and separation. To address this gap, physical model tests were conducted to compare the action mechanisms of the basal reinforcement method and the gravity replacement method. The experimental results showed that the use of a geotextile for basal reinforcement reduced lateral deformation by up to 42% but had no significant effect on settlement. The combined reinforcement and separation mechanisms also reduced material loss by up to 44%. The study investigated the effect of basal reinforcement on controlling the deformation of a rubble-mound breakwater on a soft seabed and the prevention of rubble sinking into the soft bed using physical modelling tests. In the experiments with gravity replacement as a commonly used method, the total material wastage and the role of each effective sector (settlement and penetration) were investigated. Then, the basal reinforcement technique using a geotextile as a reinforcing layer in tests similar to those without reinforcement was carried out to study the improvement mechanisms. Results of the experiments using the gravity replacement method showed that the portions of deformation and penetration mechanisms in the extra material volume required during the breakwater construction are almost equal. In the tests without geotextile, the portion of penetration in the extra material required was up to 57%, indicating the importance of penetration in the rock material wastage. The use of geotextiles eliminated the loss of material caused by penetration due to the separation action. In the tests with geotextile, a decrease in the lateral deformations was evident in the results. Reinforcement caused a decrease of up to 29% in the lateral deformation at the breakwater toe. This effect decreased as the undrained shear strength of the bed increased. Measurement of lateral displacement outside of the breakwater toe showed that the reinforced breakwaters affected a smaller surrounding zone. The savings in

material consumption can be substantial when considering the combination role of separation and reinforcement of the geotextile.

2.9 DEFORMATION ANALYSIS OF RM BREAKWATERS

Digital image correlation (DIC) is a non-contacting optical full-field deformation measurement approach that was developed by Sutton et al. (1983) and Bruck et al. (1989). The solid mechanics community widely adopts it to measure strain fields. DIC is a powerful technique that can be used to conduct experiments on a wide range of scales, from microscopic to macroscopic. The technique is applicable in both 2D and 3D modes, with 3D volumetric digital image correlation measurements (VDIC) being used to capture full-field deformations in three dimensions. The basis of the DIC technique is to consider a set of points in the reference image and obtain the corresponding set in the distorted image. The numerical form (digital form) of images is a large matrix in which each component represents the status of a single unit, known as the pixel, in the image. After processing the image, the displacement field and movement of all existing units in the image can be achieved. In this technique, the information of the adjacent regions is also used to measure the displacement field of the desired area, so the computational cost is too high. A higher-order interpolation can be used to increase the accuracy of the DIC technique. In order to perform DIC, an area of interest (AOI) is manually specified and divided into an evenly spaced virtual grid. The displacements are computed at each point of the virtual grids to obtain full-field deformation. Two parameters influencing the accuracy of the captured images in the DIC technique are the numerical range of a pixel (grey-level resolution) and the number of pixels. The more extensive numerical range of a pixel would lead to better identification of the difference between different light intensities and colours, increasing the image's accuracy. Also, more pixels in one image increase the accuracy of the image. Overall, DIC is an effective technique for measuring deformation and strain fields and has been widely applied in various fields such as geotechnical engineering, solid mechanics, and materials science.

The research work by Takano et al. (2015) aims to investigate the deformation and failure of soil under triaxial compression using in situ X-ray computed tomography (CT) and digital image correlation (DIC). The focus is characterizing internal strains

and strain localisation patterning in wide-grained sand under different triaxial compression conditions using Three-dimensional (3D) volumetric DIC. The CT images are analysed using 3D volumetric DIC to obtain the total, incremental displacement and strain field for each loading step. The accuracy of the DIC results is validated by comparing them with the results obtained from integrating the number of voxels inside the boundary of the specimen. While the DIC results underestimate the volumetric strain at the final stage of the triaxial loading, both results show good agreement. The study concludes that the combination of X-ray CT and 3D-VDIC effectively characterises the strain localization process in soil under triaxial compression. The authors suggest that smaller axial strain acquisition during CT scans can improve the accuracy of DIC results. Overall, this research emphasizes the importance of understanding the mechanisms of deformation and failure of soils in geotechnical engineering and the role of the DIC technique in investigating localized deformation in laboratory mechanical testing.

2.10 SUMMARY

Comprehensive studies on the behaviour of RM breakwaters when subjected to tsunami loading, are limited. Even the studies conducted by Bricker et al. (2015b); Guler et al. (2015); Kasama et al. (2020); and Takahashi et al. (2014) have solely focused on the behaviour of the RM breakwater under tsunami impact rather than their effects on the seabed. Hence, the exact behaviour of RM breakwater under tsunami loading is unknown. A method for doubling the width of the armour layer was proposed by Guler et al. (2015) for counteracting tsunami impact. Further, the effect of the provision of shear keys beneath the crown walls was found to be an appreciable strategy for withstanding wave loadings by van Gent and van der Werf, (2019). However, their study on crown wall units failed to consider the effects of tsunami loading. Therefore, these methods have not been a suitable solution for making the breakwater resilient against failure when it comes to seepage and scouring. These moderate preventive measures will prove insufficient to overcome any tsunami impact (Bricker et al., 2012), where the height of the incident wave could reach up to 30 meters. Therefore, a dire need exists to design a competent RM breakwater and modify the existing ones into resilient structures. The implementation of three primary methods of inserting sheet

piles into the sea bed, providing a geogrid separation layer between RM and seabed, and providing gabions along the slope has been proven by Chaudhary et al. (2018b) to improve the resilience of composite breakwaters effectively. However, the behaviour of an RM breakwater is entirely different from that of composite breakwaters. Considering these factors, it is clear that there is an urgent need to develop suitable countermeasures for making RM breakwaters resilient against tsunami attacks.

CHAPTER 3
METHODOLOGY

3.1 INTRODUCTION

A series of physical model tests were conducted to determine the behaviour of conventional RM breakwater subjected to tsunami overflow. Further, the tests were conducted on the reinforced RM breakwater with proposed countermeasures to examine its performance when subjected to tsunamis. Since the wavelength of a tsunami is very long, the simulation of a tsunami cannot be approximated to a solitary wave generated in a hydraulic flume (Bricker et al. 2015). Generally, the wavelength of a tsunami varies from 20 km to 300 km, resulting in longer overflow duration over breakwaters. Therefore, an experimental setup has been developed in the Geo-Disaster Prevention Laboratory at the National Institute of Technology Karnataka that can simulate a continuous overflow of tsunamis for a prolonged duration. For the physical model tests, the RM breakwater (length =3080 m) at Ennore Port, India, has been chosen as a prototype. Detailed instrumentation was done in the physical model tests to ascertain the displacements in the crown wall, deformations in the mound and pore water pressure variation in breakwater and seabed soils. Later, complex numerical simulations were performed to understand the failure mechanisms. The numerical analysis detailed the effects of seepage on the stability of the conventional and reinforced RM breakwaters during a tsunami overflow.

3.2 NEWLY DEVELOPED RESILIENT MODELS

Novel reinforcing techniques were developed to make tsunami-resilient RM breakwaters. One of the novelties of the present study is the adoption of gabions and geosynthetics such as geobags and geogrids in the armour layers in RM breakwater to make it resilient against tsunamis. As far as the author knows, it is the first time that geosynthetics have been used in RM breakwater to mitigate tsunami-induced damage. The geobag armour layer offers better resistance to scouring under tsunami overflow as the geobags are heavier than the conventional armour units made of rubble. Similarly, each gabion is considerably heavier when compared to an armour unit. Therefore, gabions improve breakwater stability when used as a replacement for armour layers.

Consequently, the new armour layer protects the core layer of the RM breakwater by keeping the breakwater intact under tsunami overflow. Significant lateral thrust imparted by tsunamis on RM breakwater can result in the dislocation of armour units. The higher mass of gabions and geobags when compared with rubbles and the placement of geogrid layers on either side of the mound can resist the destabilising lateral forces caused by the tsunami.

Moreover, the crest of an RM breakwater is prone to scouring under overtopping tsunamis. The provision of crown walls ensures the protection of the crest region. Shear key are provided beneath the crown wall to improve its resistance against lateral tsunami forces. Since the physical model tests accounted for the tsunami overflow alone, shear key was attached to the seaside of the crown wall. However, if the drawdown of the tsunami—which was not considered in this study—is taken into account, a shear key should also be provided on the harbour side of the crown wall. For a resilient RM breakwater, reinforcing the body of the breakwater will not be sufficient to counteract the extensive seepage that might occur through foundation seabed soils. Therefore, two rows of sheet piles were provided on the seabed at the seaside and the harbour side ends of the breakwater. The provision of sheet piles was efficient in blocking seepage beneath composite breakwaters (Chaudhary et al. 2017c; d, 2018b, 2019). Sheet piles were provided at a depth of 250 mm with 50 mm embedded into the dense sand layer. A similar embedment was suggested in studies by Chaudhary et al. (2017a) and Kikuchi et al. (2015). The proposed countermeasures, such as geobag and geogrid armour layers, the crown wall with shear key and sheet piles, practically apply to existing and new RM breakwater construction projects.

The main focus of this study is to develop novel countermeasure techniques to mitigate the tsunami-induced damage to RM breakwaters. A comparative study is conducted to analyse the performance of the proposed reinforced breakwater models compared to the conventional model. The reinforced models proposed in the study are a combination of reinforcing elements such as gabions, geobags, geogrids, crown wall (with shear key) and sheet piles. Figure 3.1 details the models of RM breakwater utilized in the present study.

(a) Gabion-Reinforced Model

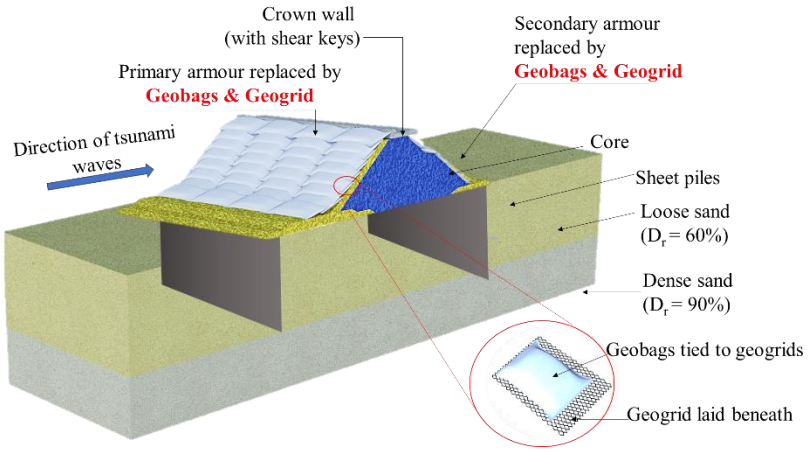

(b) Geobag-Reinforced Model

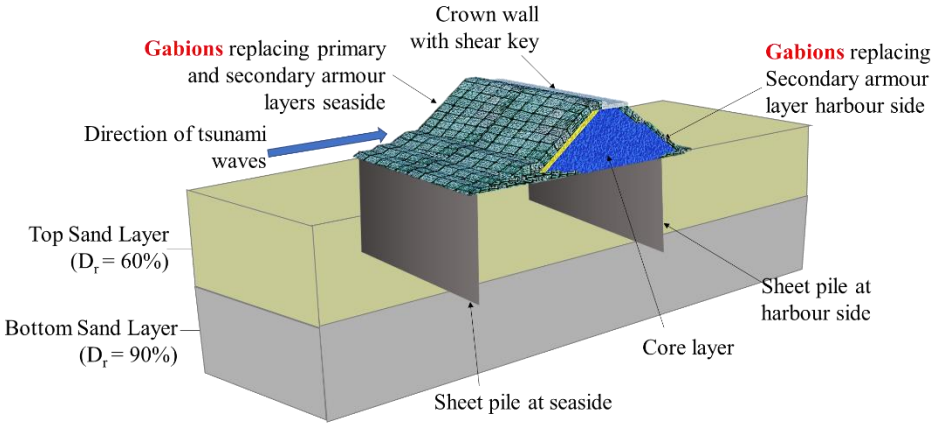

(c) Geogrid-Reinforced Model

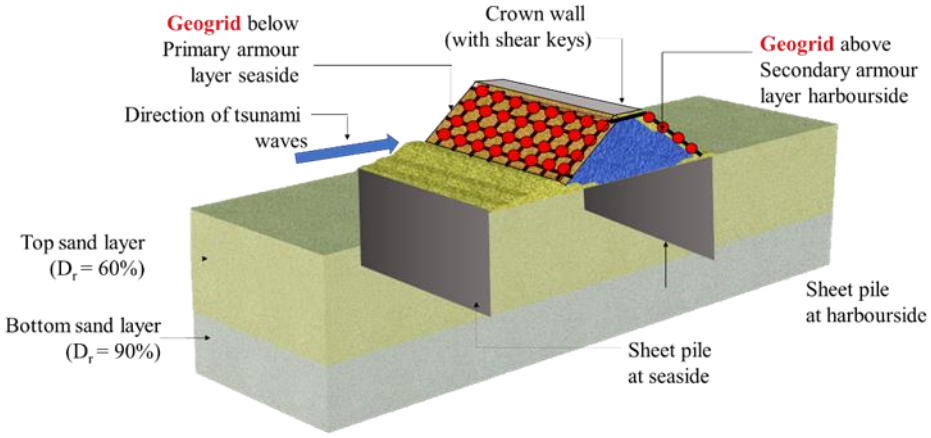

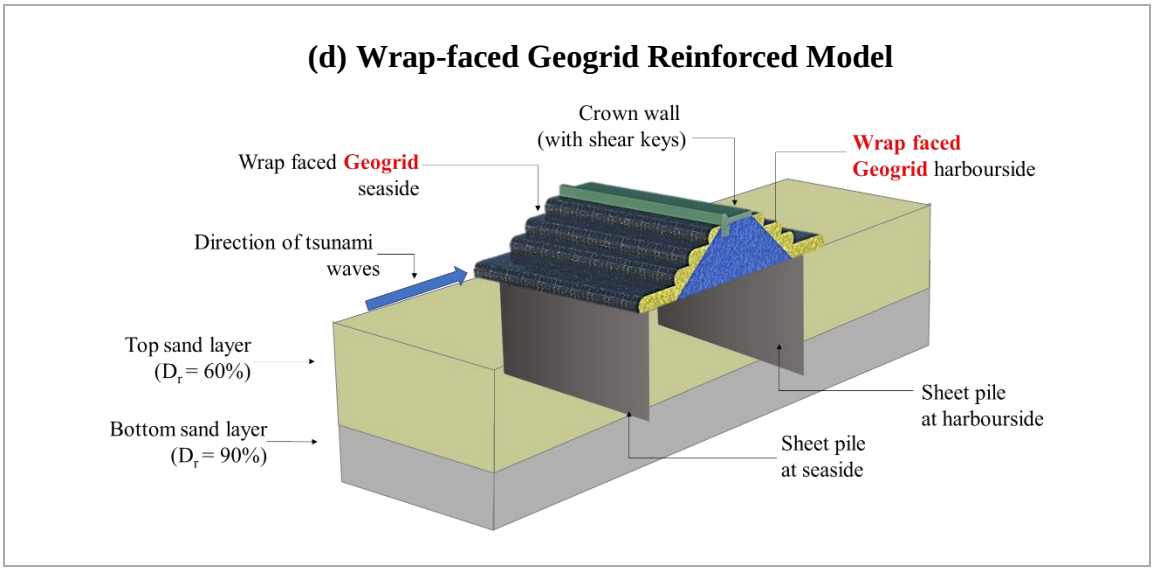

Figure 3.1 Novel reinforcing techniques to make tsunami-resilient RM breakwater

3.2.1 Geobag-Reinforced Model

One of the novelties of the present study is the adoption of a combined geobag-geogrid armour layer for RM breakwater to make it resilient against tsunamis. As far as the author knows, it is the first time that geosynthetics have been used in RM breakwater to mitigate tsunami-induced damage. The geobag armour layer offers better resistance to scouring under tsunami overflow as the geobags are heavier than the conventional armour units made of rubble. Consequently, the new armour layer protects the core layer of the RM breakwater by keeping the breakwater intact under tsunami overflow. Significant lateral thrust imparted by tsunamis on RM breakwater can result in the dislocation of armour units. The higher mass of geobags when compared with rubbles and the placement of geogrid layers on either side of the mound can resist the destabilising lateral forces caused by the tsunami.

Moreover, the crest of an RM breakwater is prone to scouring under overtopping tsunamis. The provision of crown walls ensures the protection of the crest region. Shear key are provided beneath the crown wall to improve its resistance against lateral tsunami forces. For a resilient RM breakwater, reinforcing the body of the breakwater will not be sufficient to counteract the considerable seepage that might occur through foundation seabed soils. Therefore, two rows of sheet piles were provided on the seabed at the seaside and the harbour side ends of the breakwater. The provision of sheet piles

was found to be efficient in blocking seepage beneath composite breakwaters (Chaudhary et al. 2017d; c, 2018b, 2019). Sheet piles were provided at a depth of 250 mm with 50 mm embedded into the dense sand layer. A similar embedment was suggested in studies by Chaudhary et al. (2017a) and Kikuchi et al. (2015). The proposed countermeasures, such as geobag and geogrid armour layers, the crown wall with shear key and sheet piles, are practically applicable to both existing and new RM breakwater construction projects. Figure 3.1 (b) details the proposed countermeasures to make RM breakwater resilient against tsunamis.

3.2.2 Gabion-Reinforced Model

Different reinforcing elements such as gabions, sheet piles and crown walls with shear key were incorporated in the conventional RM breakwater, as shown in Figure 3.1 (a). Each gabion is considerably heavier when compared to an armour unit. Therefore, gabions improve the stability of the breakwater when used as a replacement for armour layers. In the harbour side of the breakwater, gabions can offer better resistance against scouring due to overtopping tsunamis. Whereas, on the seaside of the breakwater, gabions can resist the higher lateral forces of the tsunamis. During a tsunami overflow, the head difference between the harbour and sea sides of the breakwater would be significant enough to cause seepage through the mound and seabed. The seepage through the seabed reduces the shear strength and hence causes a large settlement of breakwater. To avoid this, two rows of sheet piles are inserted into the seabed on either side of the breakwater. These sheet piles can act as cut-off walls that prevent seepage through the seabed. In the physical model tests on conventional RM breakwaters, it was observed that the crest was scoured during tsunami overflow. In the present study, the crown wall with a shear key is proposed that could offer better resistance to the tsunami. The crown wall can protect the crest from being scoured, and the embedment of the shear key into the body of the breakwater can resist the increased lateral forces during tsunami overflow.

3.2.3 Geogrid-Reinforced Model

The present study proposes a new reinforcing technique to strengthen RM breakwaters against tsunami-induced damages. The new techniques include using geogrid, sheet piles, and crown walls with shear key as reinforcing elements. Geogrid layers were

placed along the slopes on either side of the RM. The mesh opening size of the geogrids was smaller than the dimensions of the rubbles in the mound. Geogrids were strong enough to withstand the impact of tsunamis while still allowing water to pass through the body of the breakwater. During a tsunami event, the significant difference in water levels between the seaside and harbour sides results in excess seepage through the body of the breakwater. This may lead to the displacement or movement of the rubbles within the core and armour layer. However, providing geogrid layers can reduce the dislocation of armour rubbles from the breakwater. Geogrid, with its smaller mesh aperture size, can prevent the movement of the rubble along the slopes of the mound through an interlocking mechanism. The geogrid enhances the structural integrity of the breakwater, reducing the likelihood of damage during a tsunami and promoting long-term stability.

Geogrid placement plays a crucial role in the stability of a reinforced RM breakwater. Therefore, placing geogrids over the armour layer and placing geogrids above and below the armour layer was attempted in the present study. Additionally, the effect of extending geogrid beneath the heel of the mound was also considered. As illustrated in Figure 3.1 (c), two rows of sheet piles were positioned at both ends of the RM. These sheet piles serve as cut-off walls and prevent seawater from seeping through seabed soils beneath the mound during a tsunami. Reducing seepage can prevent a reduction in the shear strength of the foundation seabed soils caused by seepage. The placement of crown walls protects the crest of RM from scouring. Moreover, the shear key provided beneath these crown wall can resist the lateral forces from tsunamis and thereby improve the stability of crown walls.

3.2.4 Wrap-faced Geogrid Reinforced Model

Wrap-faced geogrid layers are used as reinforcing countermeasures for the RM breakwater to enhance its stability during a tsunami. The polypropylene biaxial geogrid wrapping provides excellent confinement to the RM, preventing the rubbles from dislocating during tsunami overflow and reducing the deformations on the breakwater. Thus, they can protect the mound against scouring and erosion during a tsunami. Lateral movements of the crown wall may occur during a tsunami. Tsunami-induced lateral forces may also cause lateral displacements of the rubbles from the body of the

breakwater. The wrap-faced geogrid layers can resist such lateral movement owing to their interlocking mechanism between the geogrid layers and rubbles. The primary functionality of RM breakwater is the dissipation of wave energy by transmitting it through the body. Owing to the seawater level difference between the seaside and harbour side of the breakwater during a tsunami, seepage may occur through the RM beneath the breakwater from the seaside to the harbourside. The geogrid layer will not reduce the permeability of the RM and, at the same time, provide extra stability to withstand a large volume of seepage. The wrapping of geogrid along the slopes of the RM prevents any dislocation of armour units due to the breaking of the tsunami front.

Moreover, the wrap-faced model can reduce the thickness of the armour layer and thereby offer a more cost-effective solution for making tsunami-resilient RM breakwater. In addition to these wraps facing geogrid layers, two rows of sheet piles are installed near both edges of the mound. Tsunami-induced seepage through the seabed soil beneath the breakwater is also responsible for breakwater failures. The sheet piles can act as cut-off walls and reduce such seepage through the seabed soils during tsunamis. Further, the provision of the crown walls with shear key can prevent the scouring of rubbles from the crest of the RM. Overall, these multifunctional countermeasures can prevent the failure of the RM breakwaters caused by tsunamis.

3.3 PROTOTYPE BREAKWATER

RM breakwaters are widely used across the coastal belt of the Indian Peninsula. In India, the majority of these RM breakwaters serve as fishing harbours. The longest RM breakwater in the country is situated in Tamil Nadu, in the Tiruvallur district, and is widely known as Ennore breakwater. It is located at a port owned by Kamarajar Port Ltd. and is the only corporatized major port. The port, which is located 18 km north of Chennai port, was built as a satellite port to divert the traffic from the latter.

The Ennore port is located at 13° 15’ 40” N latitude and 80° 20’ 15” E longitude, about 18 km north of the Chennai port along the Coromandel Coast. The Northern breakwater, as depicted in Figure 3.2, has been modelled for this research. The port is located at the seismic zone Zone III (Moderate Damage Risk Zone), according to the seismic zone map of India. The seawater-current velocity varies from 0.15 to 0.2 m/s (Asian

Consulting Engineers Private Limited, 2014). The direction of currents changes with the onset of the monsoon season. During the South East monsoon, the currents flow from the South towards the North; during the North East monsoon, the currents flow in the opposite direction.

The Ennore port was built with two breakwaters; the Northern breakwater is 3070 m long, and the South breakwater is 1040 m in length. The Northern breakwater has been chosen for this study since it is the longest breakwater in the country, and its orientation is parallel to the coastal line. This orientation was the primary reason for its exposure to the direct impact waves of the Indian Ocean tsunami of 2004.

Figure 3.2 The location of the Northern breakwater at Ennore port in the Indian sub-continent (Source: map data © 2022 Google)

The Indian Ocean tsunami resulted from the subduction of the Indian tectonic plate beneath the Burma plate, causing a release of enormous amounts of energy from the seabed near the Sumatra Islands in Indonesia. This caused an earthquake that registered 9.3 on the Moment Magnitude Scale and is widely regarded as one of the biggest natural disasters of the century. The run-up height of the waves reached up to 5 m on the Ennore coast and inundated 300 meters inland (Gupta and Murthy, 2005). Tsunamis reached the Ennore coastal line 2 hours and 40 minutes after the earthquake, which originated around 1300 m below sea level. The wavelength of the tsunami was 430 km, with a period of 40 minutes (Synolakis and Kong, 2006).

The greatest known natural calamity encountered during the design life of the prototype breakwater was the 2004 Indian Ocean tsunami. It is estimated that the Ennore breakwater moved around 1 to 2 meters in the southeast direction following the tsunami's impact (Kozai et al., 2005). The breakwater movement was mainly during the drawdown of the tsunami, which carried all the debris and mud from the inland during its withdrawal towards the sea. Witnesses also reported the phenomenon of mudflow inside the breakwater-enclosed tranquil zone (Kozai et al., 2005). However, the Ennore port faced lesser damage than the Chennai port since the Ennore coastal regions were primarily barren land.

However, in the following years, Ennore port was transformed from a simple satellite port to one of the major ports in the country, overseeing a higher count of traffic in both port and inland sections coupled with large volumes of cargo movements. Therefore, there is a pressing need for the Ennore breakwater to be made resilient against future tsunami attacks.

3.4 PHYSICAL MODEL TEST

A new apparatus was developed in the Geo Disaster Prevention laboratory at the National Institute of Technology Karnataka, Surathkal, India, that can be used to generate tsunami overflow through continuous recirculation. The apparatus has dimensions of 2400 mm (L) x 500 mm (W) x 1000 mm (H) and is comprised of acrylic plates and steel frames, as shown in Figure 3.3. An 1800 mm (L) x 500 mm (W) x 1000 mm (H) portion was separated as a chamber and utilized to create the physical models. Water is stored in the tank and circulated to simulate an overflowing tsunami in the flume. Continuous water flow is necessary for creating tsunamis since isolated waves cannot accurately convey the effects of the tsunami (Guler et al. 2015). During a tsunami impact, the height of tsunamis could exceed the designed wave height of RM breakwaters, which leads to an overflow of tsunamis over the RM breakwater. This critical condition is simulated in the physical model tests by employing submersible pumps that can ensure continuous overflow and recirculation of water. Continuous recirculation also ensures that the overflowing water to the harbour side is not reflected.

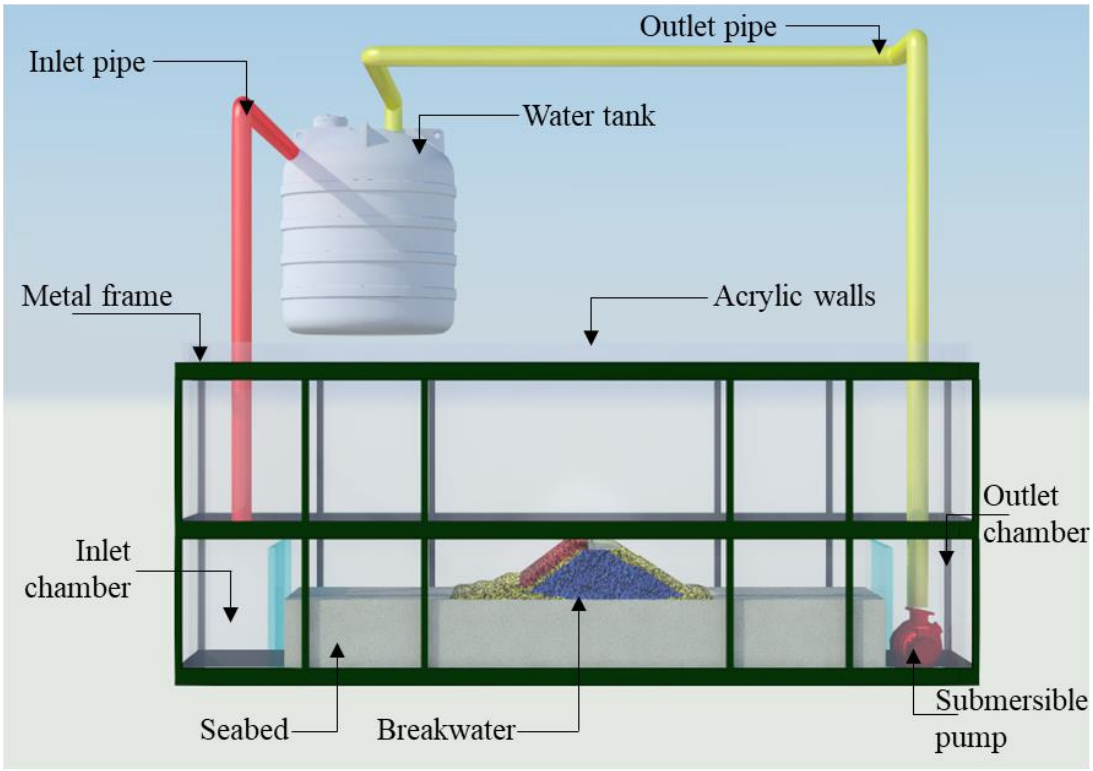

Figure 3.3 Experimental setup for physical model tests

3.4.1 Tsunami Overflow Test

During a tsunami impact, the height of tsunamis could exceed the designed wave height of RM breakwaters, which leads to an overflow of tsunamis over the RM breakwater. This critical condition is simulated in the physical model tests by continuous overflow and recirculation of water. The seawater level is maintained during the test using water pumps on both the sea and harbour sides of the breakwater. The tsunami's height is 0.15 m above the seawater level on the seaside. The seawater levels on both sides of the breakwater are carefully controlled. The water level is maintained at mean sea level (MSL) above the seabed before the tsunami overflow test begins. The data collected from these tests are used to study the impact of tsunamis on RM breakwaters and to develop more effective mitigation strategies. The information will help improve our understanding of the behaviour of RM breakwaters under tsunamis. Thereby adopting new countermeasures to make the breakwater resilient to protect the coastal communities and infrastructures from the impacts of devastating tsunamis. Table 3.1 provides the seawater levels during the tsunami overflow tests. Here, the water was

stored at a height of 0.6 m in the inlet chamber and then suddenly released by raising the gate in front of the tank.

It is important to note that the experimental setup used in this study has a limitation in simulating the tsunami drawdown condition. Although the drawdown effect, which is critical for understanding the full scope of tsunami-induced damage on the seaside of breakwaters, could not be directly modelled due to the constraints of the experimental apparatus, efforts were made to approximate the conditions. Specifically, the water level was deliberately set to a drawdown sea level before the initiation of the overflow experiment. While the scaling ratio of the study suggests a mean sea level of 0.12 m, the experiments were conducted at a reduced mean sea level of 0.05 m, mimicking the drawdown sea level prior to the tsunami overflow. This approach is consistent with methodologies employed in previous research, such as the study by Xu et al. (2020), and provides a reasonable approximation of the drawdown condition, despite the inherent limitations.

Table 3.1 Seawater levels during the tsunami overflow tests

Items	**Values**	
	Model (mm)	**Prototype (m)**
Before Tsunami		
Initial sea water level	50	5
During Tsunami		
Height of tsunami	150	15
Seawater level on the seaside	200	20
Seawater level on the harbourside	60	6

3.4.2 Preparation of Seabed

The prototype breakwater at Ennore port near Chennai, India, was used to conduct tsunami overflow tests. Figure 3.4 details the cross-section of the Northern breakwater at the Ennore port (Khattar 2001). The physical model of the prototype was prepared without a crown wall and is referred to as a conventional RM breakwater. The

breakwater consists of separate layers of quarry stones of various diameters. Each layer was modelled using the geometric details of the prototype breakwater. Crushed aggregates of scaled-down sizes were used to model the breakwater.

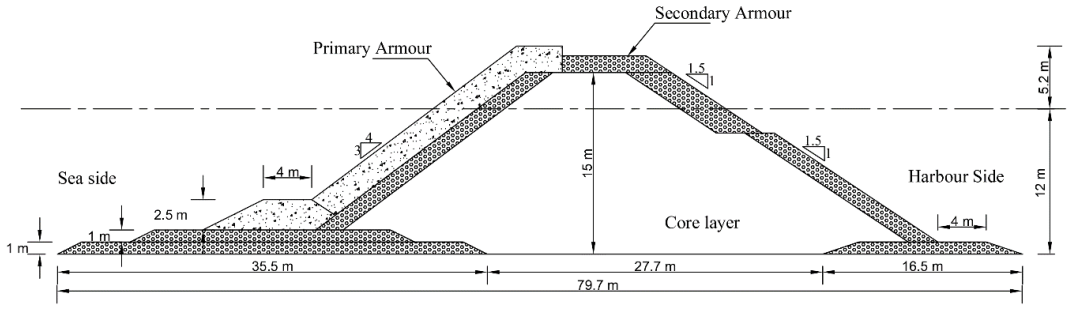

Figure 3.4 Northern breakwater at Ennore port, Chennai, India

The seabed was modelled in the tsunami flume as two layers, with the top layer in a loose state confining to a relative density of 60% and the bottom layer in a dense state confining to a relative density of 90%. The total depth of the seabed was 350 mm, in which the dense layer constituted 150 mm and the loose layer 200 mm. The top sand layer was filled in the tsunami flume at the required relative density by adopting the pluviation technique. The pluviation method cannot be used to obtain higher relative densities. Therefore, the dense layer was compacted to the required density using tamping plates. The physical properties of the sand used in the physical model tests are mentioned in Table 3.2. The friction angles were measured using direct shear tests, with specimens prepared under drained conditions. These tests were performed to analyse the behaviour of the material under effective stress conditions, providing realistic values for the friction angle that are critical for analysing the stability of the foundation seabed supporting the breakwater.

Table 3.2 Physical properties of seabed sands

Properties	Value
Specific gravity, G	2.66
Maximum dry density, γ_{dmax}	16.3 kN/m^3
Minimum dry density, γ_{dmin}	13.8 kN/m^3
Co-efficient of Permeability for loose sand, k_1	0.00308 cm/s
Co-efficient of Permeability for dense sand, k_2	0.00273 cm/s
Mean grain size, D_{50}	0.7 mm
Shear parameters for loose sand	C_1=0, ϕ_1 = 36°
Shear parameters for dense sand	C_2=0, ϕ_2 = 42°
Young's modulus for loose sand, E_1	20 x 10^3 kN/m^2
Young's modulus for dense sand, E_2	37 x 10^3 kN/m^2
Poisson's ratio, ν	0.3

Pluviation Method

The Air Pluviation method was adopted to prepare homogeneous, repeatable sand bed specimens of required relative density instead of simply pouring a particular weight of sand into a soil box. A portable travelling air pluviator system has been designed and developed at the Geo-Disaster Prevention Lab of NITK Surathkal (see Figure 3.5); the same has been used for this study. Among the two layers of river sand used to prepare the seabed, the upper seabed layer with relative densities (D_r) of 60% is prepared using the pluviation method. In the pluviation method, sand is spread by the raining method from a predetermined falling height in order to achieve the desired relative density (Passalacqua 1991).

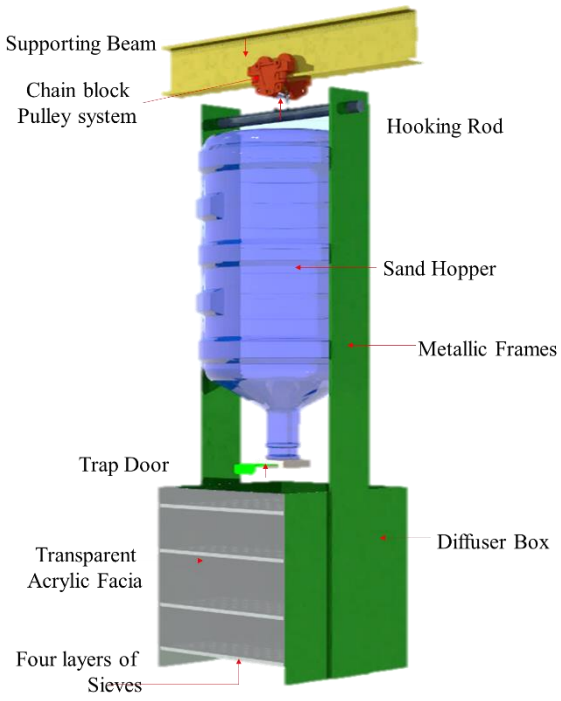

Figure 3.5 Schematic representation of the pluviation setup

In the method of air pluviation, the three major factors that are to be considered include the height of fall, deposition intensity and relative diffuser ratio (Knodel et al. 1992). The required height of fall can be adjusted by attaching the sand hopper to a chain block pulley system that is attached to a roller system. The roller system can run through a rail fixed on a lateral rod placed along the length of the tsunami flume. Calibration charts determine the required height of fall explicitly prepared for the sand used in this experiment (Vaid and Negussey 1984). It is inferred from the calibration chart that a height of fall of 57.5 cm (see Figure 3.6) is sufficient to achieve a relative density of 60%. The trap door beneath the sand hopper can be adjusted to maintain a constant deposition intensity.

The deposition intensity defines the total weight of the soil fallen from the hopper in unit time over a unit area (Dave and Murty 2012). The deposition intensity is fixed such that for a particular height of fall, the sand will not be retained on any of the sieves in the diffuser box. In the study, for a particular deposition intensity and height of fall (57.5 cm), a relative density of 60% will be achieved, and it is to be maintained for loose sand conditions. The pluviation box will be continuously moved throughout the soil box, and adjustment in height will be achieved by pulling the chain to achieve the

required density. Care should be taken against the accumulation of sand in diffuser sieves and uninterrupted sand deposition. Hence, by adjusting the height with two or more diffuser sieves, it is possible to achieve reliable relative density values.

The relative diffuser ratio is another key determining factor for the uniform distribution of the seabed layer. It is calculated as the ratio of the aperture size of the topmost sieve to the nominal diameter of the sand particle (D_{n50}). To facilitate an even distribution of sand as it passes through the diffuser box, evenly spaced holes with a relative diffuser ratio of 4.23 will be used. Four of such sieves are kept equidistant inside the diffuser box. The height of the fall will always be measured from the bottom of the lowest sieve plate to the top of the seabed.

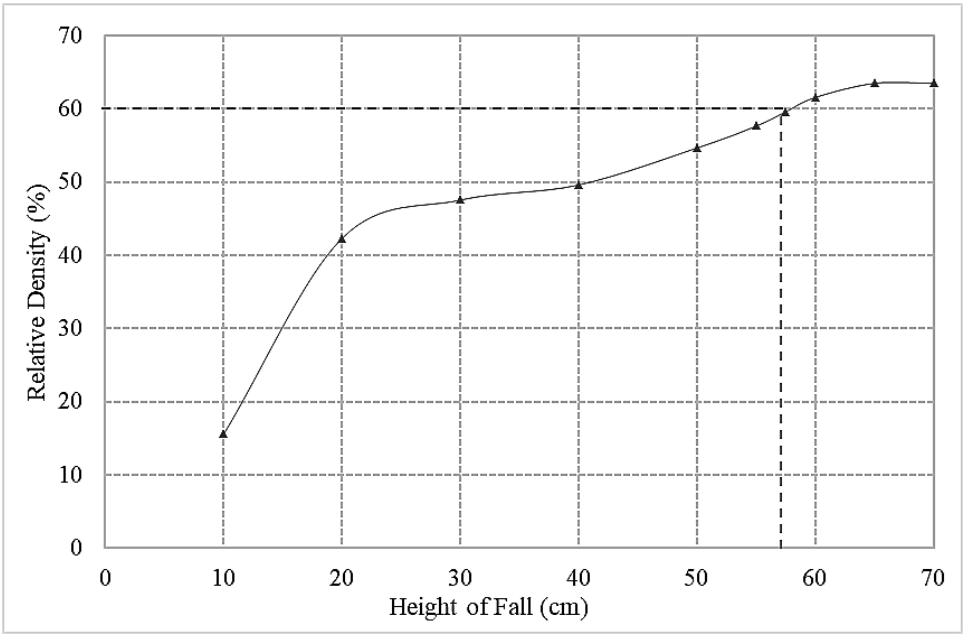

Figure 3.6 Calibration chart for estimating the height of fall for pluviation

3.4.3 Preparation of Breakwater

The breakwater was modelled on the seabed surface with rubbles of pre-determined size. The geometrical dimensions and sizes of rubbles were scaled down from the details of the prototype breakwater. A prototype-to-model scaling ratio of 1:100 was adopted for the physical modelling of the breakwater. The sizes of rubbles used for each layer in the breakwater were determined by scaling the weight of each layer, considering the stability of armour units (Guler et al. 2015). The similarity rules detailed by Takahashi et al. (2014), which consider the seepage effects through rubbles, were

adopted to model the breakwater as detailed in Table 3.3 Similarity relations used in the physical model tests.

Table 3.3 Similarity relations used in the physical model tests

Properties	**Prototype/Model**	**Scale Factor**
General dimensions	N	100
Time of seepage, t	$N^{1/2}$	10
Hydraulic gradient, i	1	1
Water Pressure, σ	N	100
Mean flow velocity, ν_m	$N^{1/2}$	10
Reynolds number, R_e	$N^{3/2}$	1000
Dynamic viscosity, ν	1	1
Weight of rubble, λ_w	0.95 N^{-3}	$9.5*10^{-7}$

The scaled rubbles were then coloured to distinguish their displacements under tsunamis. The physical properties of each type of rubble are tabulated in Table 3.4. The breakwater core layer was coloured blue with 6 mm rubbles, the secondary armour layer was prepared with yellow coloured 10 mm and the primary armour units with 20 mm red coloured rubbles.

Table 3.4 Properties of rubbles used for modelling of the breakwater

Properties	**6 mm**	**10 mm**	**20 mm**
Specific Gravity, G_s	2.74	2.76	2.79
Minimum Void ratio e_{min}	0.61	0.58	0.58
Maximum Void ratio e_{max}	0.96	0.92	0.88
Minimum Density $\Upsilon_{d\,min}$ (kN/m^3)	14.5	14.9	15.3
Maximum Density $\Upsilon_{d\,max}$ (kN/m^3)	17.6	18.1	18.3
Young's modulus, E (kN/m^2)	110 x 10^3	130 x 10^3	170 x 10^3
Poisson's ratio, ν	0.2	0.2	0.2

Various techniques were implemented to strengthen the breakwater, including geogrid, sheet piles, and a crown wall (with a shear key). Different breakwater models were developed; the first model represented a conventional RM breakwater, and the others incorporated countermeasures to form a reinforced RM breakwater. The proposed countermeasures include gabions, geobags, geogrids, the crown wall with shear key and sheet piles. The geogrid used in the study was a polyethene sheet biaxial geogrid placed along either side of the RM. The aperture size of geogrid was selected to be smaller than the core rubble size. Geogrids in a real-world setting can be used to improve the bearing capacity of the foundation ground beneath the breakwater, which has been demonstrated to be effective at Huanghua Port in China (Yu et al. 2005). The properties of geogrid and geotextile used for making geobags are given in Table 3.5.

Table 3.5 Properties of geosynthetic materials

Properties	Range
Geotextile	
Mass per unit area (GSM)	250
Colour	white
Polymer	polypropylene
Tensile strength (kN/m)	20
Permeability (m/s)	0.02
Geogrid	
Mass per unit area (GSM)	850
Polymer	polyethene
Colour	Black
Tensile strength (kN/m)	50
Aperture size (mm)	3

The crushed stones used for physical modelling were coloured to distinguish the different layers in RM breakwater. The conventional model was prepared with crushed stones of different sizes for the physical model tests. The reinforced models were modelled with different combinations of reinforcing elements such as geogrid layers, geobags, gabions, and crown walls (with a shear key). In addition, the seabed beneath

the breakwater was reinforced with steel sheet piles. Figure 3.7 displays the materials utilized to model different types of RM breakwaters in the physical model tests.

Figure 3.7 Materials used for physical modelling tests

3.4.4 Instrumentation

The instrumentation used in the experiments is illustrated in Figure 3.8. Lateral displacement and vertical settlements of the RM crest were monitored by the use of displacement transducers (LVDTs) located at two different positions (V1 and V2) and two additional positions (H1 and H2), respectively. Four pore water pressure transducers (P1 to P4) were deployed to determine the pore water pressures within the seabed soils and the breakwater. The data from sensors were continuously recorded throughout the physical model tests at a sampling rate of 1 per second. Detailed data about the performance of the different breakwaters under various conditions was collected using these instrumentation techniques. All the transducers were connected to a dynamic amplifier and a data acquisition system, which allowed for real-time collection and recording of the data. The data obtained from the transducers was used to assess the behaviour of the RM under tsunami overflow conditions and to evaluate its overall performance and stability.

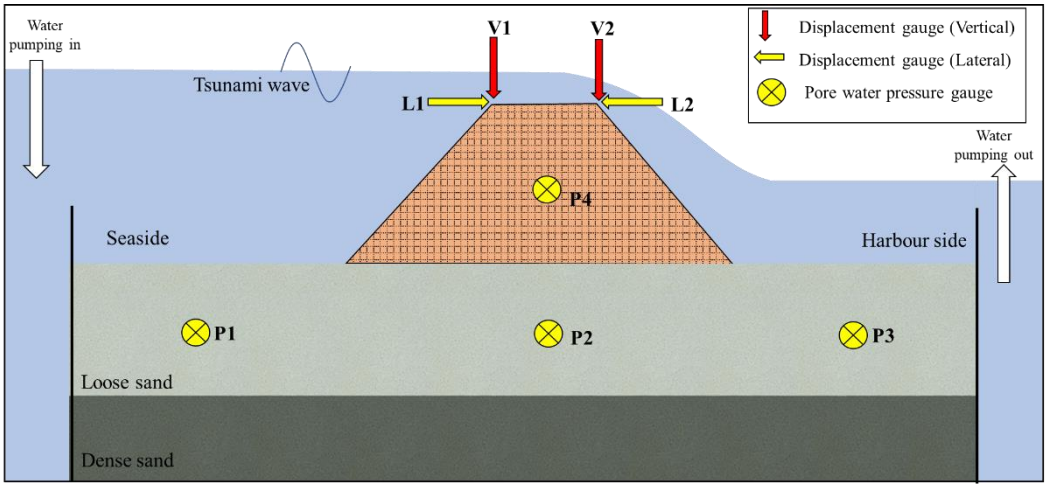

Figure 3.8 Instrumentation for physical model test

3.5 ANALYTICAL STUDY

Even though the real-time data on the pore water pressure and crown wall displacements can be recorded by adopting the instrumentation above, the proper assessment of damages on an RM breakwater is cumbersome. The initiation of damage on the armour units and its propagation under dynamically interacting tsunami trains cannot be fully comprehended through analytical solutions (Campos et al. 2020a). Most of the analytical approaches have been developed through empirical equations. Some of the conventional analytical methods used to quantify the damages on RM breakwaters have been adopted in the study. These equations were preliminarily developed for solitary wave conditions. However, they can be extended to the case of a tsunami interaction (Xu et al. 2020).

3.5.1 Relative Displacement

The relative displacement proposed by Hudson (1959) is one of the most straightforward parameters that can effectively communicate the intensity of damage on armour layers. The relative displacement is defined as the ratio between the displaced armour units and the total number of units, which can be determined using the equation (3.1).

$$R_d = \frac{N_{displaced}}{N_{total}} \times 100\% \qquad (3.1)$$

3.5.2 Relative Eroded Area

Another parameter proposed by Broderick (1984) is the Relative eroded area (S). This can be used to determine the amount of scouring that occurred on the mound under the wave action and can be calculated using equation (3.2).

$$S = \frac{A_e}{D_{n50}^2} \tag{3.2}$$

The limitations in the determination of average eroded area A_e using direct measurements were resolved through the equation (3.3) proposed by Vidal et al. (2004).

$$A_e = {N_d D_{n50}^3}\Big/{(1-n)B} \tag{3.3}$$

Thus, the average area of the mound eroded can be estimated by knowing the number of eroded armour units N_d, the nominal diameter of the armour stone D_{n50} and its bulk porosity n. The grain sizes used for D_{n50} in the analysis was 20 mm, since majority of the scouring was observed in the primary armour layer. Therefore, the relative eroded area was estimated considering the displacement of the primary armour units. The width of the model cross-section, B, which was considered as 0.4 m for the study, also has significance in the average eroded area. Based on the range of values obtained for S, for breakwater slope (cot α) varying from 1.5 to 4, the damages that occurred on the RM can be categorised as per Table 3.6 (Campos et al. 2020b).

Table 3.6 Damage thresholds for various values of S and R_d

Thresholds	**S**	**R_d**
Initiation of Damage	1.5 - 3	0 - 0.05
Iribarren's Damage	2.5 - 4	-
Initiation of destruction	6.5 - 11	.05 - 0.10
Destruction	12 – 18 and above	>0.2

3.6 PROFILE MAPPING

Even though the semi-empirical equations could depict the degree of damage to the RM structure, a more precise damage assessment can be obtained by comparing the 3D profile of the RM before and after tsunami impact using non-contact distance measuring gauges and sophisticated computation tools. The device uses non-contact distance measuring gauges and advanced computational tools to compare the 3D profile of the RM before and after the impact of the tsunami. This is a significant improvement over the conventional semi-empirical equations that are used to estimate the damage, as the mapping device provides a much more precise evaluation.

The device has two units that are capable of moving in both the X and Y planes, and each unit is fitted with motorized wheels for forward and backward movement, as shown in Figure 3.9. The base unit is positioned on top of a tsunami flume, and it moves along the support frames to complete the scanning process. The sensor mount unit, on the other hand, is placed on top of the base unit and is equipped with laser displacement and ultrasound distance-measuring sensors. The scanning process involves moving the base unit along the length of the RM and then shifting the sensor mount unit one grid length along the width of the RM. To ensure accurate measurements, the movement of the base unit is calibrated at a fixed speed, and the position coordinates of the sensors are calculated with precision.

The data obtained is then exported in real-time through wireless communication and processed using 3D point cloud processing open-source software, CloudCompare. The use of this mapping device provides a more accurate assessment of the damage caused to the RM by the tsunami, as it takes into account the changes in the 3D profile of the RM before and after the impact. The device is an automated and programmable profile mapping device, making it a powerful tool for engineers and scientists to use in evaluating the damage caused by tsunamis. The results obtained from the use of this device are more precise and reliable. They can be used to inform decision-making and guide future research and development in this field.

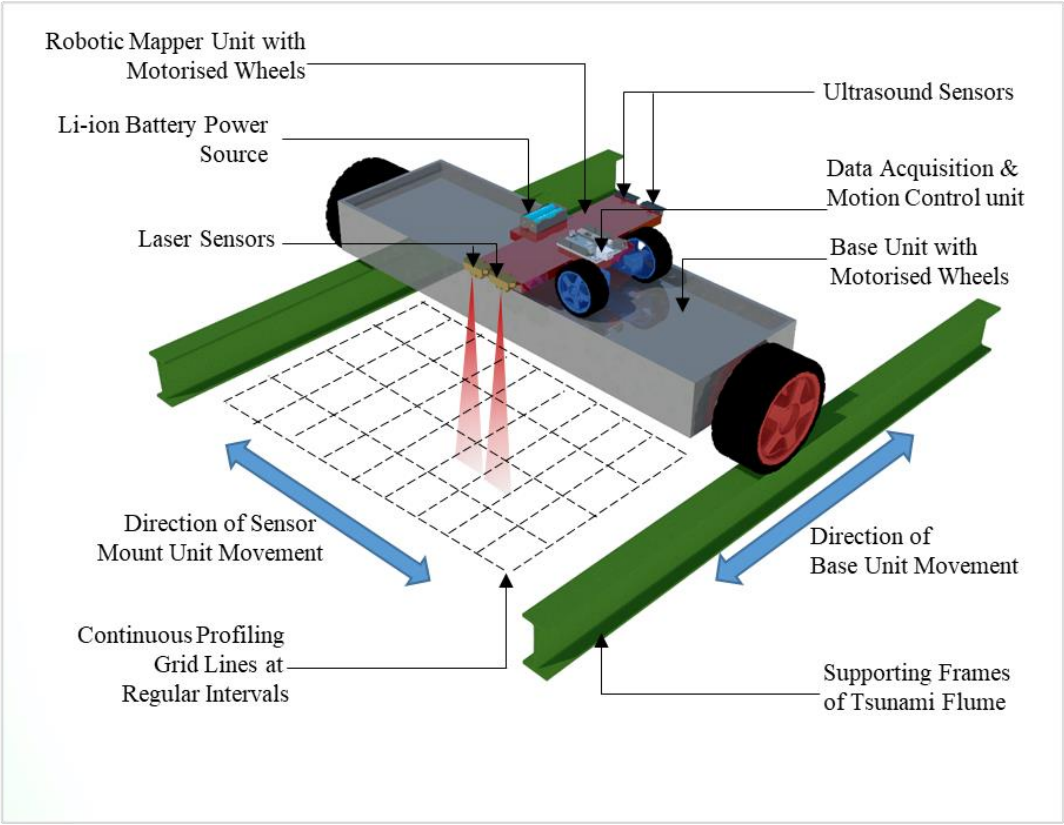

Figure 3.9 Schematic representation of profile mapper

3.7 NUMERICAL SIMULATION

The numerical modelling of tsunamis, RM, and seabed is done by using FEM-based software, PLAXIS 3D, to evaluate the fluid-solid interactions during a tsunami impact. Precise modelling of the hydraulic conditions is simulated to evaluate seepage effects through the body of the breakwater and seabed soils. The modelled breakwater on the seabed layer is then evaluated for defined tsunami overflow. The numerical simulation is validated with experimental observations. Further, the conventional and reinforced RM breakwater models are subjected to seepage and stability analyses. Each of the reinforcing elements is prepared as a separate geometric entity to simulate the proper interaction between them. For example, the geobag armour layer used in the geobag-reinforced models is created as each bag for replicating a real-world interaction, as shown in Figure 3.10.

On the other hand, geogrids are modelled using the predefined geogrid elements. Dynamic hydraulic conditions during a tsunami overflow are simulated using

predefined flow multipliers. A fully coupled flow deformation analysis is performed, where the deformations corresponding to the flow of water can be determined precisely.

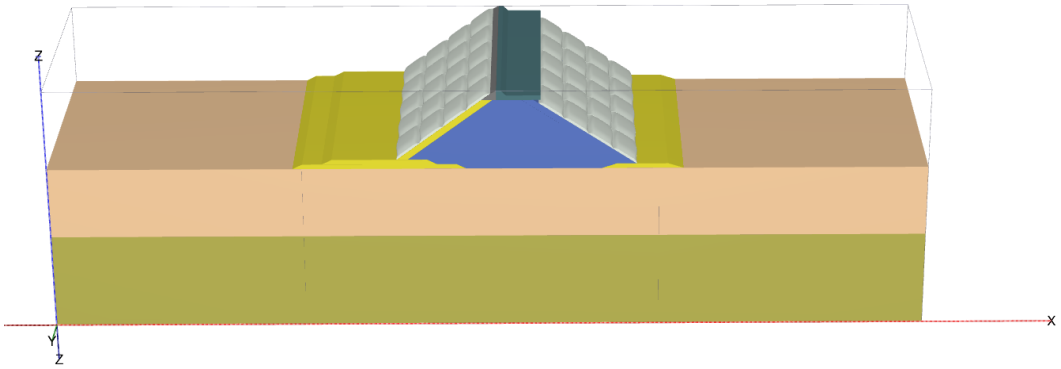

Figure 3.10 Numerical model of a reinforced RM breakwater

3.8 SUMMARY

This chapter provides an overview of newly developed resilient models for breakwaters, as well as physical and analytical studies conducted to evaluate their effectiveness in mitigating the impact of tsunamis. The methodology adopted in this study begins with the development of new countermeasure techniques for RM breakwaters, including the gabion-reinforced model, geobag-reinforced model, geogrid-reinforced model, and wrap-faced geogrid reinforced model. The RM breakwater, located on the northern side of Ennore port, Chennai, India, has been chosen as a prototype breakwater. The significance of the prototype is its location along the Coromandel coast, which was subjected to the 2004 Indian Ocean tsunami. Several physical model tests were conducted by modelling the seabed and the breakwater in the developed tsunami flume apparatus. Several instruments are used for the displacements and pore water pressure. Analytical studies are then conducted, focusing on quantifying the damages on RM breakwaters. Finally, numerical analyses were carried out to assess the efficacy of the resilient models.

CHAPTER 4
GEOBAG-REINFORCED RM BREAKWATER

4.1 INTRODUCTION

During the physical model tests, it was observed that the conventional RM breakwater undergoes large deformations and scouring under tsunami overflow. However, the reinforced RM breakwater was resilient against tsunamis. Geogrid layers, geobags, sheet piles and crown walls (with shear key) are adopted as countermeasure elements against the tsunami. The reinforced RM breakwater was made of geobag. A comparative analysis of the behaviour of both breakwater models under tsunami overflow conditions was evaluated using the results obtained from displacement and pore water pressure gauges. The amount of damage that occurred to the breakwater was quantified through an analytical study. However, a more precise analysis of the breakwater deformation was done by plotting a three-dimensional profile before and after tsunami overflow using a robotic profile mapper. Moreover, the high-quality video footage recorded during the tests was post-processed using digital image correlation (DIC) techniques to understand the strain patterns developed in the RM breakwater during tsunami overflow.

4.2 PHYSICAL MODEL TEST

4.2.1 Settlement

In the tsunami overflow tests conducted, a significant scouring was observed in the conventional RM breakwater. By the end of a tsunami overflow test, 50 mm (5 m in the prototype) of the breakwater crest was scoured. It can be noted from Figure 4.1 that the average settlement measured from either side on the crest initially increases abruptly. The sudden uprise of water in the seaside created enormous lateral thrust on the breakwater. Moreover, a sizeable hydraulic gradient was developed due to the sea level difference on either side of the breakwater.

Consequently, severe seepage occurred through the RM and foundation seabed soils. The combined action of these forces resulted in the rapid settlement of the crest in conventional RM breakwater. Instead, the reinforced RM breakwater remained intact

and stable throughout the entire duration of tsunami overflow tests. The extra stability was offered by the heavier geobags that replaced armour blocks. Also, the placement of geogrid along the slopes improved the stability of the mound by interlocking the rubbles. The reduction of seepage through the seabed by sheet pile walls has also played a crucial role in reducing the vertical settlement of the RM.

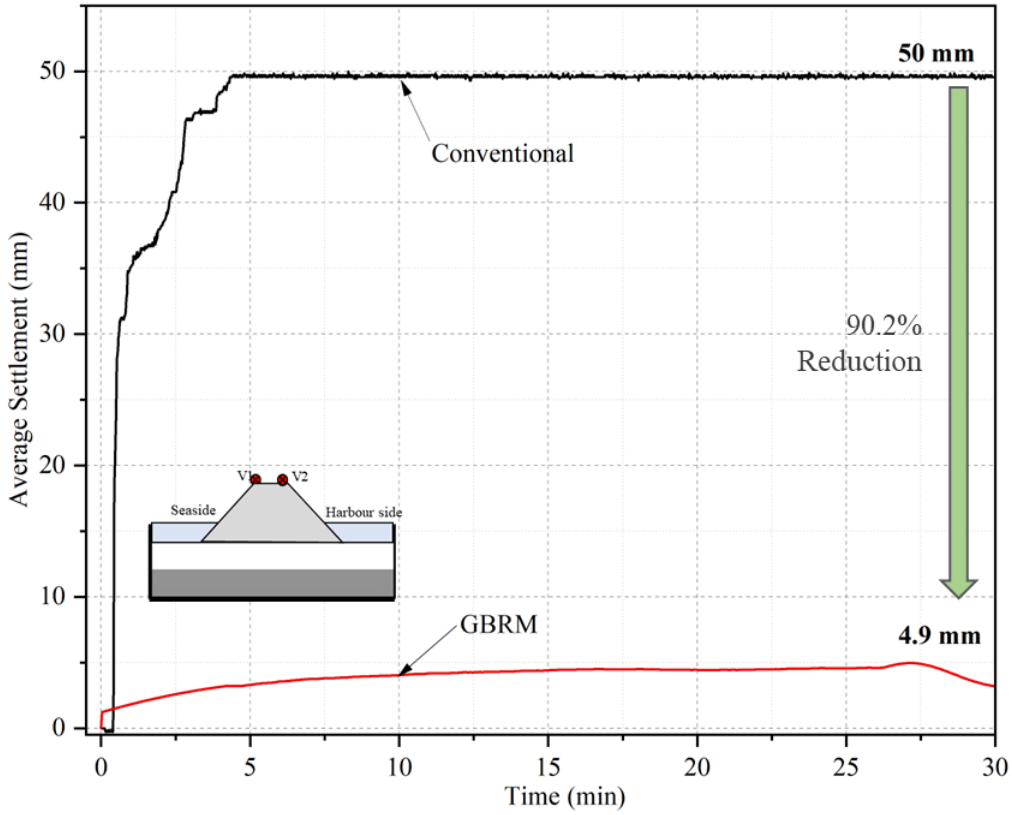

Figure 4.1 Settlement of the crest for conventional and GBRM models

4.2.2 Lateral Displacement

During the tsunami overflow, large hydraulic forces acted on the RM. The lateral thrust of tsunamis displaced the armour units from the seaside to the harbourside. The displaced armour units exposed the core layer of lesser weights. Rubbles in the crest were also displaced towards the harbour side along the direction of the flow of tsunamis. The average displacement measured from the crest is shown in Figure 4.2. It could be observed that the displacement and settlement curves increase abruptly in the beginning and eventually reach a constant stage. Due to scouring, the volume of the RM obstructing the tsunami was reduced. The scouring continued significantly until the

majority of the rubbles above sea level were displaced. The rate of scouring reduced as the height of the breakwater obstructing tsunamis reduced. Even though the scouring of the mound almost reached an equilibrium, relatively small displacements of rubbles were still observed due to the drag forces of tsunami overflow. However, these small displacements were not prominent in the displacement curves since they were insignificant compared to the initial scouring.

On the other hand, in reinforced RM breakwaters, the lateral displacement was reduced entirely. The stability of the RM was improved when armoured with heavier geobags. The lateral displacement of geobags was prevented by tying to the underlying geogrid layer. The interlocking mechanism of geogrid held the core layer together from dislocation. Further, inserting a shear key of the crown wall into the RM also offered better resistance to the crown wall against the lateral forces of tsunamis.

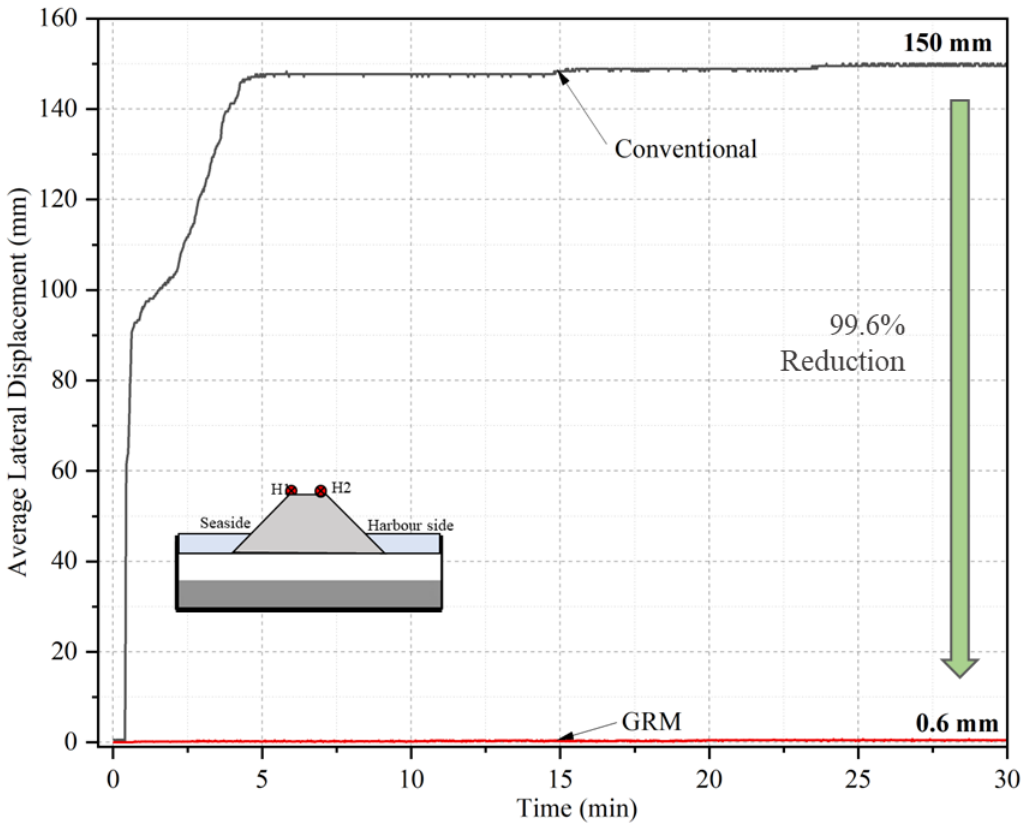

Figure 4.2 Lateral displacement of the crest for conventional and GBRM models

4.2.3 Incremental Pore Water Pressure

Pore water pressure developed in the seabed soils and body of the breakwater during tsunami overflow highlighted that the collapse of conventional RM breakwater was also caused by higher pore water pressure. The pore water pressure measured before the tsunami overflow was deducted from the measured readings during tsunami overflow to get the increment in pore water pressure. It was this IPWP that resulted in the reduction in the shear strength of the RM and seabed soils. From Figure 4.3, it can be inferred that the steep gradient between IPWP from the seaside to the harbour side induced seepage through the seabed. Even though a considerable volume of seepage occurred through the body of the breakwater, some significant seepage has also occurred through the seabed. Here, the seepage occurring in lateral directions could exert seepage pressure on the soil particles that could eventually displace them. A prolonged duration of such a process could result in piping, which reduces its bearing capacity and eventually leads to the settlement of the RM. These impermeable structures discontinued seepage flow paths beneath the breakwater when sheet piles were introduced into the seabed. Consequently, the possibility of piping action was reduced. The numerical analysis also showed the mechanism of sheet pile walls in reducing seepage through the seabed.

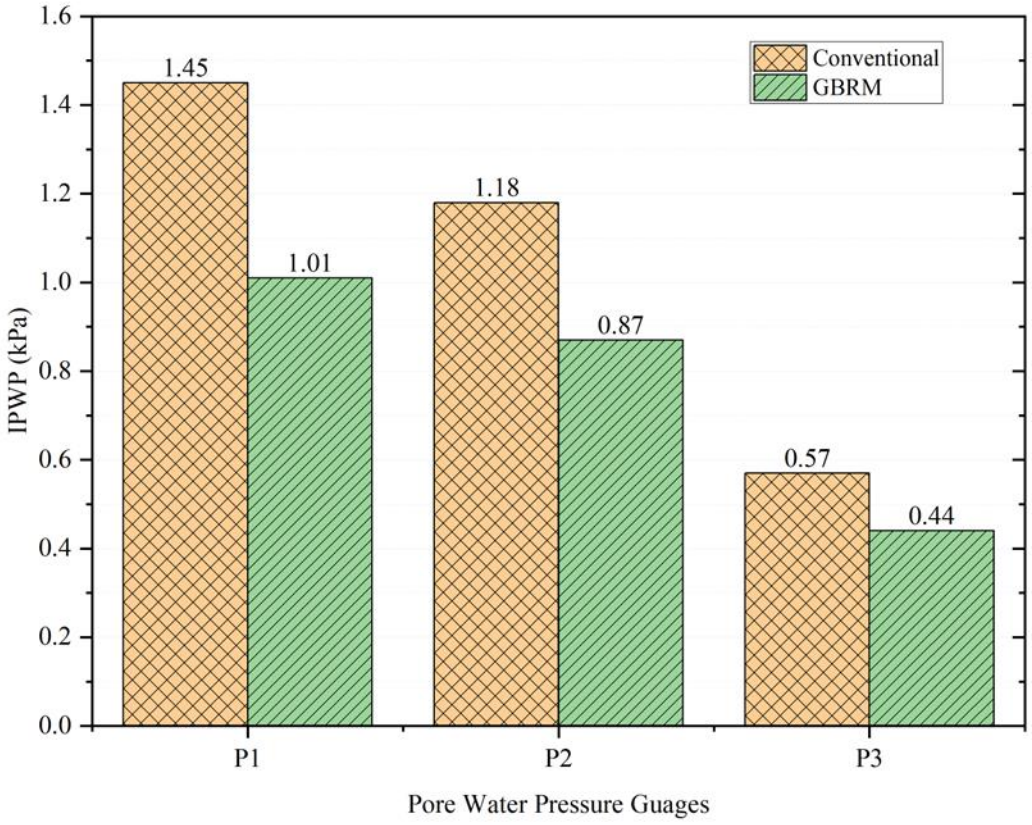

Figure 4.3 IPWP measured during the tsunami overflow for conventional and GBRM models

4.2.4 Deformations of the Breakwater

The conventional breakwater was scoured by 50 mm (5 m in the prototype) during the tsunami overflow. The scoured-off rubbles were deposited over the harbour side seabed by the drag forces of the overflowing tsunamis. However, the reinforced breakwater withstood tsunami overflow without undergoing any deformation, as shown in Figure 4.4.

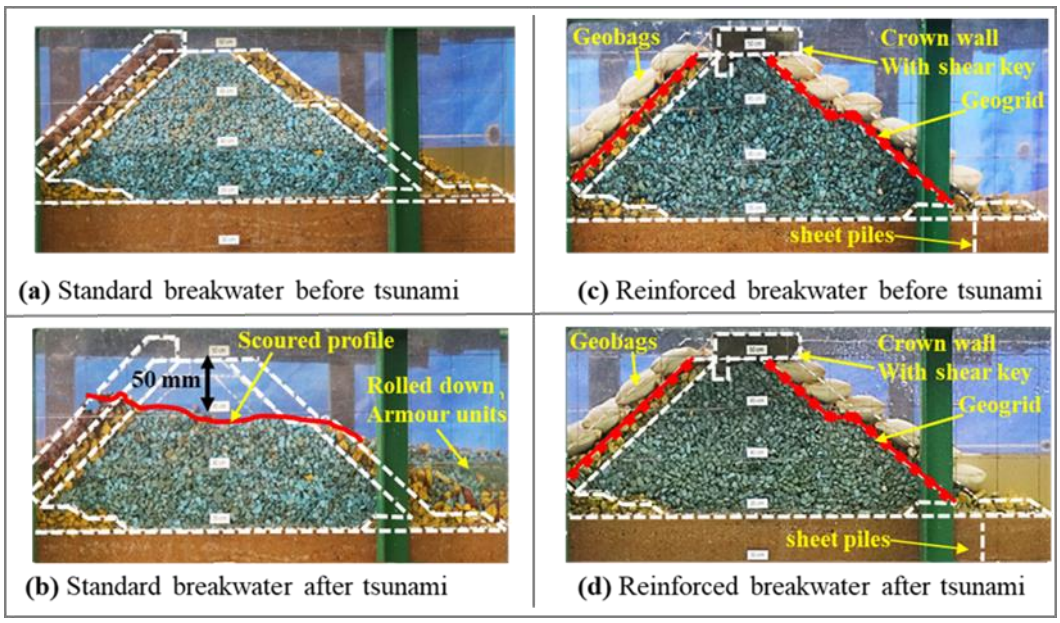

Figure 4.4 Deformation of conventional and GBRM models when subjected to tsunami overflow

A series of time frames highlighting the change in the profile of conventional RM breakwater under tsunami overflow is shown in Figure 4.5. Frame I denote the stable state of the breakwater before tsunami overflow. At t = 10 s, the tsunami reached the height of the breakwater and began to overflow. Before the overflow starts, a considerable volume of water seeps through the body of the breakwater, which is responsible for dislocating secondary armour units, as shown in frame III. Scouring of the crest was initiated owing to the dislocation of rubbles in the harbourside, which eventually moved even heavier primary armour units, as seen in frame IV. The displacement of rubbles was caused by the combined action of lateral forces by tsunami and seepage forces that developed within the breakwater. In frame V, the difference in the hydraulic head on either side of the breakwater still pertains. The seepage forces were disturbing the primary armour units' stability, thereby rolling these rubbles down to the harbourside. The water level at the seaside begins to reduce by the end of 60 s. The scoured profile reached almost the water level at the harbourside. The scouring of the primary armour layer and most of the core layer continued further. A reduction in the breakwater height at the seaside can be seen through frames VII and VIII. The dislodged rubbles were piled up at the harbour side seabed. An increase in the volume of piled rubbles denotes the continuation of scouring in frame IX. Beyond 15 min,

significant scouring was not observed, as shown in the tenth frame. It was observed that the scoured profile reached an equilibrium state once the breakwater height was reduced till the water level on the harbour sea level. As the scouring of breakwater rubbles progresses from the crest during a tsunami, the displaced rubbles are deposited on the harbour-side seabed, effectively increasing the width of the breakwater. In the physical model experiments, it was observed that this scouring and deposition process continues until the buildup of rubbles on the harbour side nearly matches the level of scouring on the breakwater itself. At this stage, equilibrium is achieved because the emerged portion of the breakwater has been fully scoured, while the submerged section, now with increased width, experiences equal water pressure from both the tsunami and the harbour side. This balance in forces effectively opposes further tsunami-induced deformation, leading to a stabilization of the breakwater. Comparing all the frames, it could be inferred that scouring was initiated from the harbourside and propagated towards the seaside. Seepage forces had dislocated the rubbles along the harbourside even before the impact of the overflowing tsunami.

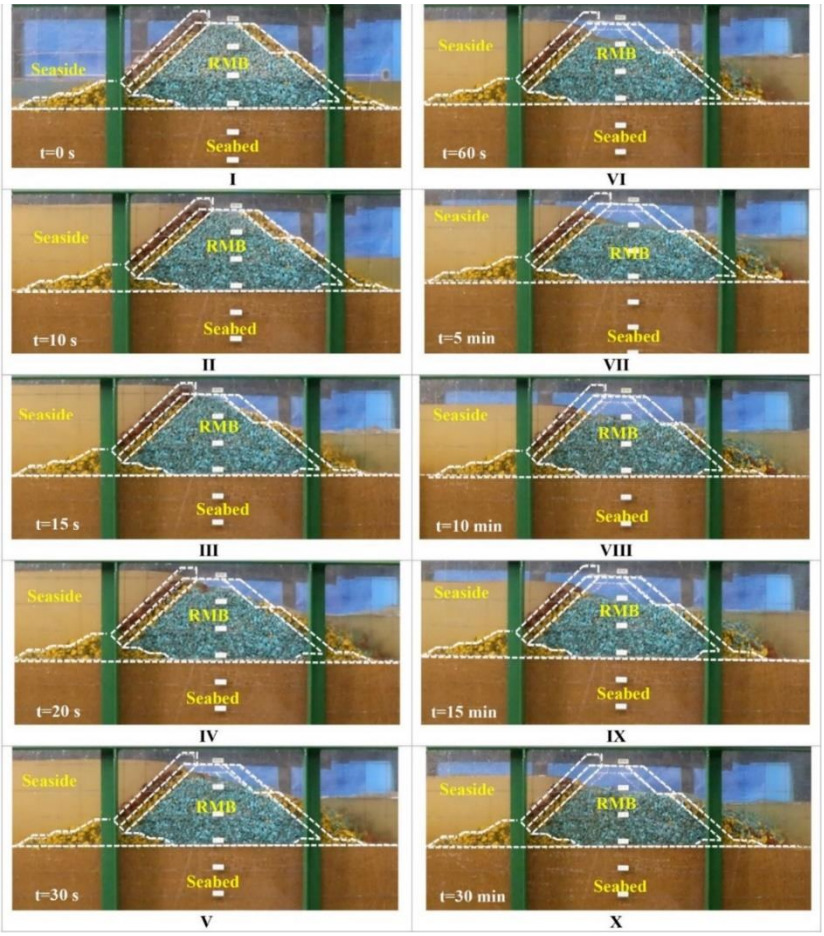

Figure 4.5 Behaviour of the conventional model during the tsunami overflow

Similar time frames of reinforced RM breakwater under tsunami overflow conditions are shown in Figure 4.6. It can be noted in every frame that the reinforced RM breakwater effectively withstands tsunami overflow for a long duration. This appreciable stability of the reinforced RM breakwater is due to the combined effect of each reinforcing element. In the place of primary and secondary armour units of conventional RM breakwater, reinforced RM breakwater has geobags and geogrids. A tsunami imparted significant lateral stresses, which were withstood by increasing the inertial mass of the breakwater. The combined effect of heavier sand-filled geobags evenly placed and tied over the geogrid layer improved the total inertial mass as well as the stability of the breakwater. Geogrid layers stabilised the slopes of the RM on either side through the interlocking mechanism. It also acted as a flexible base that held each row of geobags against the seepage forces. Both geobags and geogrids are

permeable reinforcements and, thereby, have not hindered the dissipation of wave energy through the body of the breakwater.

Moreover, the placement of a crown wall over the crest of the RM with shear key inserted into the mound offered better resistance against lateral forces. The stabilised side slopes, along with the protected crest, made the reinforced RM breakwater an intact offshore structure even under devastating tsunamis. Similarly, it was observed from the pore water pressure readings that a considerable amount of seepage occurs through seabed foundation soils. Sheet piles were provided in the seabed to arrest this seepage. The depth of piles was extended to a dense sand layer to ensure proper blockage of flow lines. The confined space between sheet piles beneath the breakwater has stabilised the seabed by improving the density and reducing seepage forces. The combined action of proposed countermeasures improved the resiliency of the RM breakwater against tsunami.

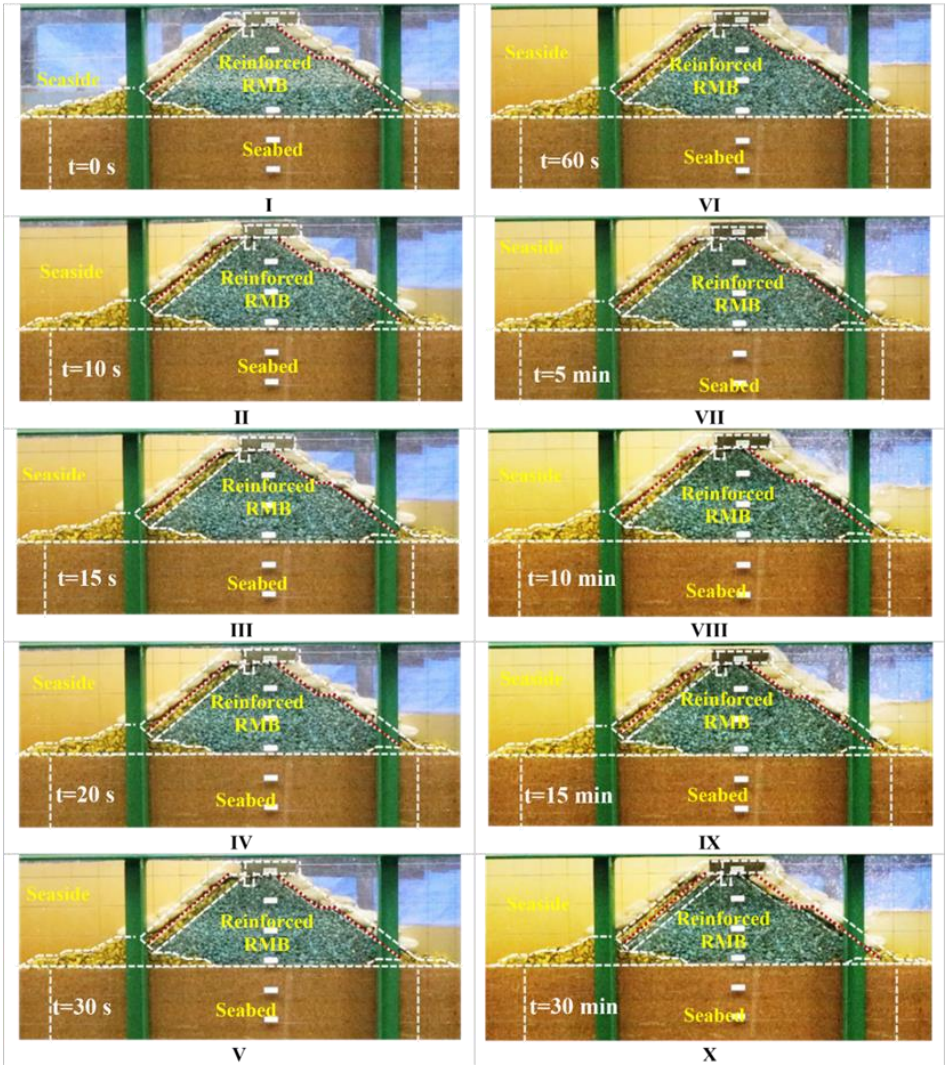

Figure 4.6 Performance of the GBRM model during the tsunami overflow

4.2.5 Mechanism of Deformation

The mechanism behind the enormous deformations observed in the RM was evaluated using the DIC technique. In this method, the high-quality images of an area subjected to deformation are analysed using complex algorithms by tracking the changes in each image pixel. Consequently, strain distribution contours of the area can be precisely plotted. The technique has been successfully adopted in several studies to track the movement of soil grains and rubble from recorded image footage of experiments (Kato et al. 2012; Sassa et al. 2016; Takahashi et al. 2014b; Takano et al. 2015). The shear strain contours developed inside conventional and reinforced RM breakwaters are shown in Figure 4.7 and Figure 4.8, respectively. It can be seen that the initial shear strain values are negligibly smaller before the overflow of the tsunami. The

development of shear strain contours during tsunami over conventional RM breakwater is shown in Figure 4.7. When compared to the corresponding time frame images shown in Figure 4.5, it can be observed that strain contours propagate from the harbour side face to the seaside face along the crest region of the breakwater. An additional frame at t =12 s is given in Figure 4.7. The development of shear strain at the harbour side slope can be clearly seen in this frame even before the overtopping of the tsunami. This indicates that the seepage through the body of the breakwater was the reason behind the initiation of scouring at the harbourside. The present DIC technique is limited to represent only on the strain captured at the localized surface deformations. However the surface strain distribution represented the initial phases of erosion and the corresponding breakwater response during tsunami overflow.

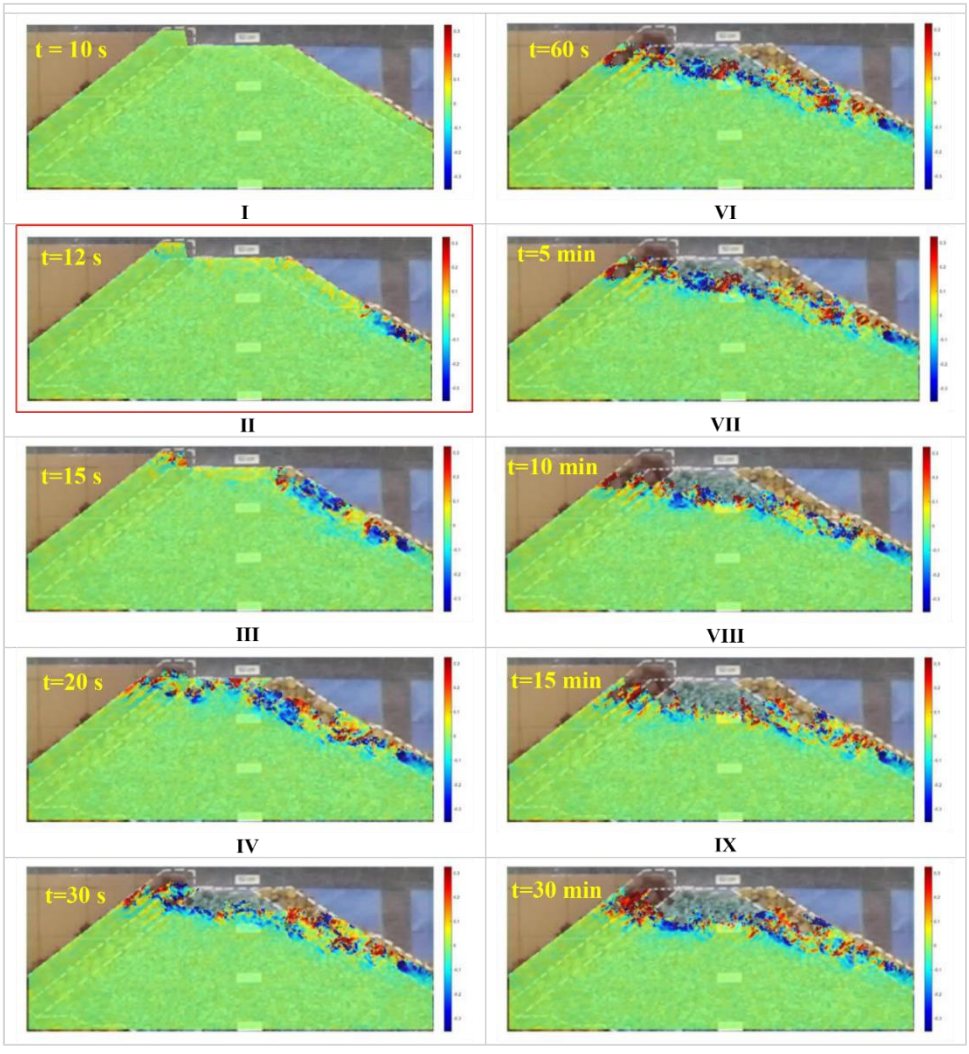

Figure 4.7 Shear strain contours of the conventional model during tsunami overflow

The shear strain contours plotted for reinforced RM breakwater were found to be almost constant throughout the experiment, as seen in Figure 4.8. In other words, the reinforced model was stable enough to prevent any slightest movement in the core rubbles of the breakwater. However, a slight concentration of shear strains beneath the crown wall can be observed towards the end of the experiment. The effects of these shear strains can be neglected since the magnitude of these strains is much less compared to shear strains developed in a conventional RM breakwater model.

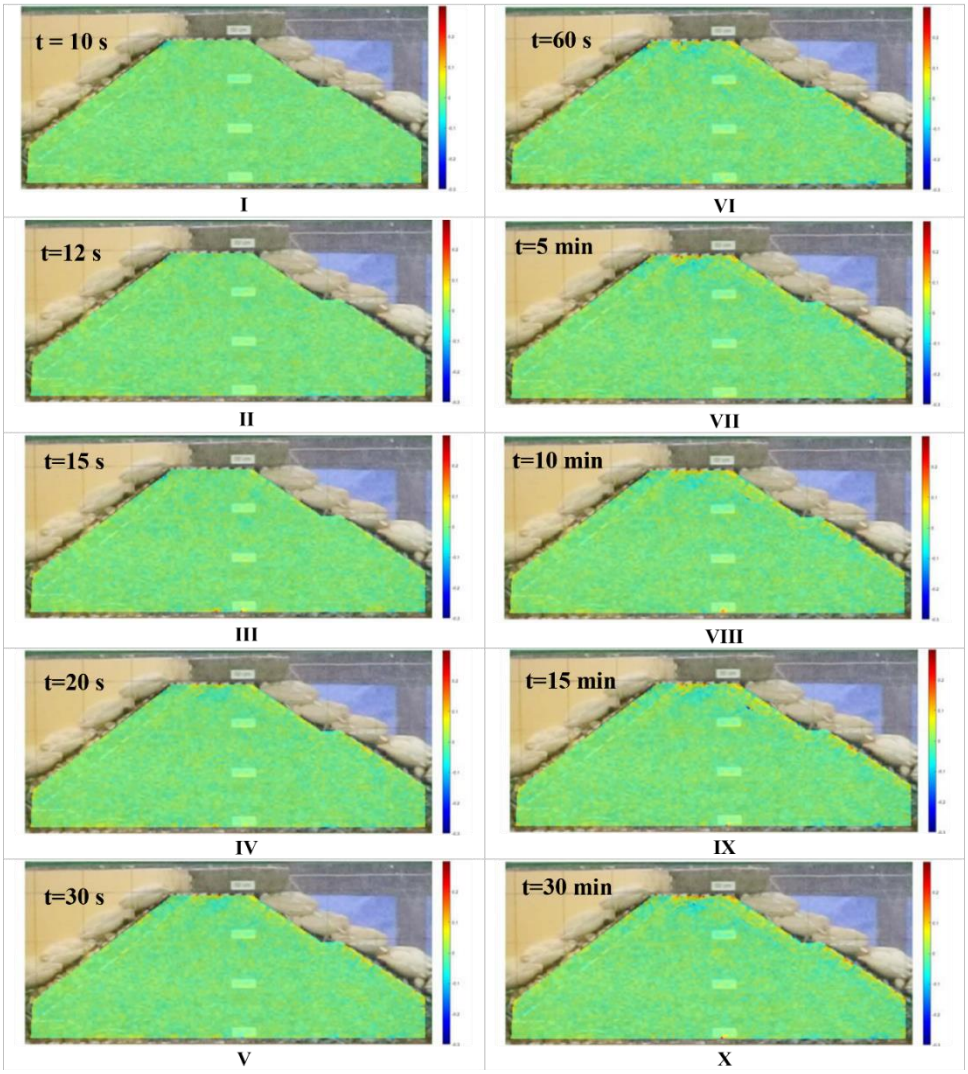

Figure 4.8 Shear strain contours of the GBRM model during tsunami overflow

4.3 ANALYTICAL STUDY

In Figure 4.9, the displaced armour blocks can be identified from the top view of the conventional model after tsunami overflow. Whereas in the reinforced model, the

geobag armour units were not displaced at the end of the experiment. This clearly indicates the efficiency of the proposed reinforcements in resisting tsunamis. Several analytical methods are available in the literature to quantify the damages on RMs. Some of those critical parameters are detailed in this section.

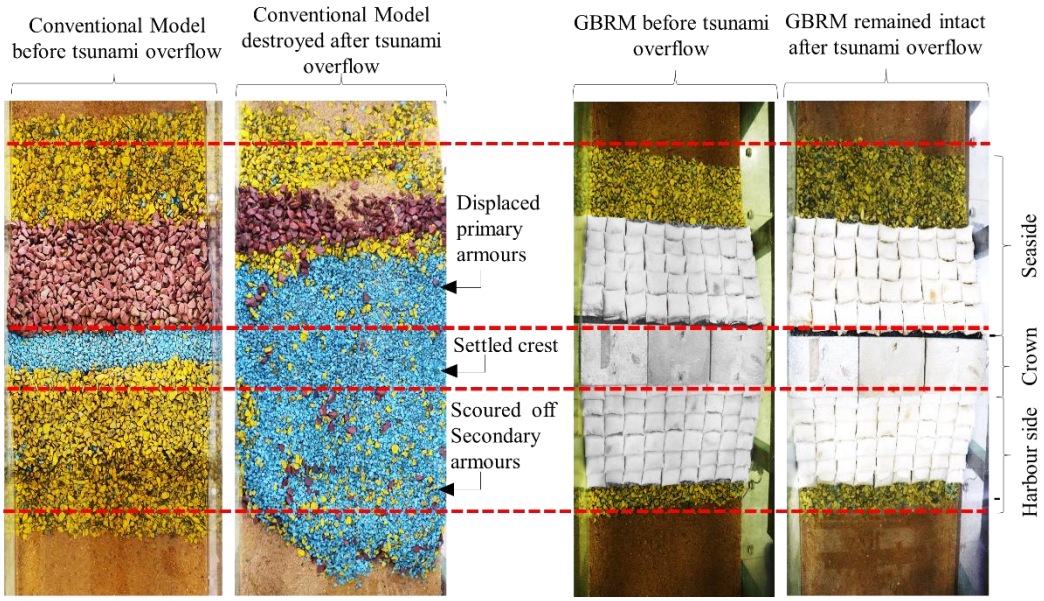

Figure 4.9 Comparison of conventional and GBRM models (top view) before and after tsunami overflow

4.3.1 Relative Displacement

Specific analytical approaches were utilised to quantify the amount of damage that occurred on the RM breakwater under tsunami overflow. Several parameters are available in the literature to account for the damage to RM breakwater both quantitively and qualitatively (Campos et al. 2020a). The majority of these parameters depend on the number and size of rocks used in the armour layer. One such parameter is the relative displacement (R_d), which defines the percentage of armour blocks displaced when compared with the initial number of armour units. Figure 4.10 highlights that 44% of the armour blocks (red coloured) were displaced under the tsunami overflow.

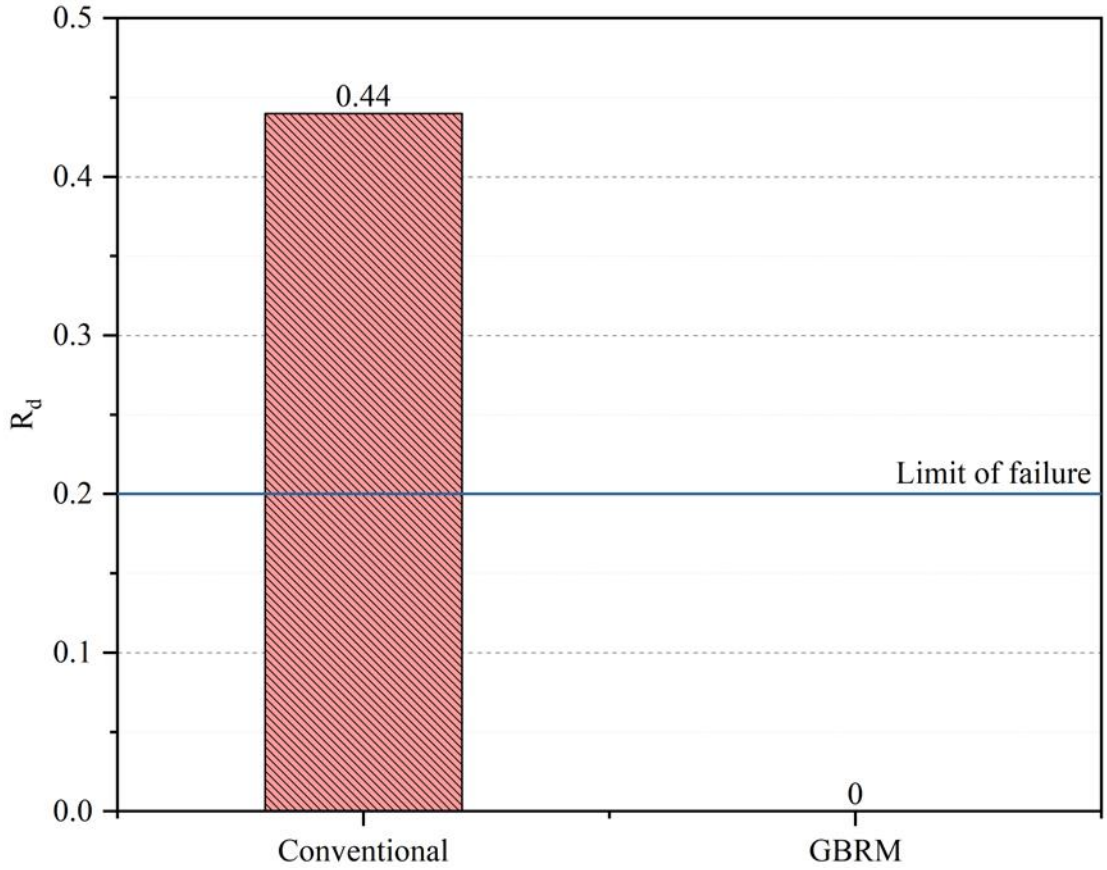

Figure 4.10 Relative displacement of armour units in conventional and GBRM models after the tsunami overflow

4.3.2 Relative Eroded Area

The average eroded area is expressed in terms of the nominal diameter of armour units by the parameter relative eroded area (S) (Broderick 1984). The average eroded area was estimated to be 172 cm^2 based on the number of armour units displaced (Vidal et al. 2004). The relative eroded area was found to be 43 in conventional RM breakwater, which is represented in Figure 4.11. However, in the reinforced model, the geobag armour units laid over the geogrid layer were highly stable against destabilising tsunami forces. None of the geobags was observed to be displaced during the tsunami overflow.

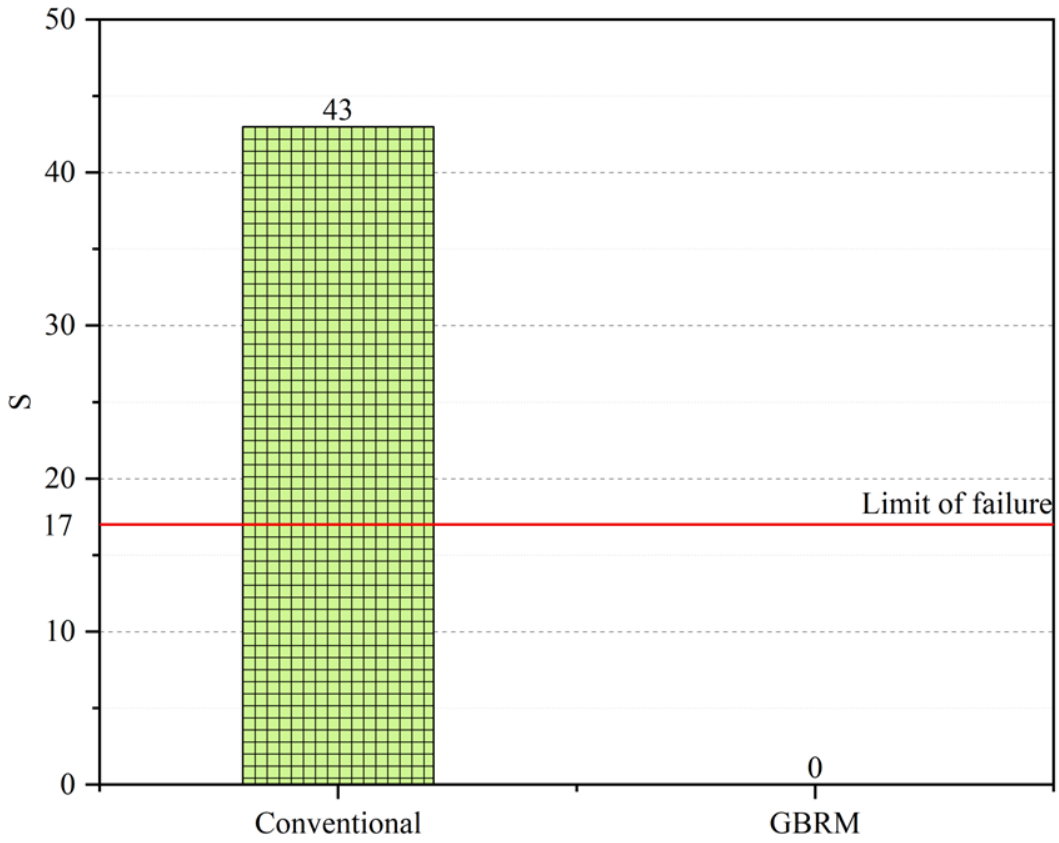

Figure 4.11 Relative eroded area in conventional and GBRM models after the tsunami overflow

A qualitative relation between relative displacement (R_d) and the degree of damage has been summarised in the Coastal Engineering Manual (United States Army Corps of Engineers 2002). A similar relation was established for the relative eroded area (S) in other literature (Campos et al. 2020b). Table 3.6 summarises the limits of these parameters corresponding to the amount of damage to the RM breakwater. The relative displacement was 54.5 % more than its limiting value of failure. Similarly, the relative eroded area was 60.47 % more than its threshold of failure. The relative displacement and eroded area of a conventional RM breakwater cross the threshold of failure. However, in the reinforced models, zero displacements were observed. The relative eroded area for a solitary wave of the same height as the tsunami was found to be 0.55. This clearly indicates that a tsunami can induce larger destabilising forces on an RM than a storm wave of similar height. The proposed reinforced RM breakwater was observed to withstand the rigorous tsunami load without any deformation. In reference to the criteria for damages in geobag reinforced structures defined by Dassanayake and

Oumeraci, (2012), the geobag reinforced RM breakwater model in the present study can be categorised as ‘stable’.

4.4 PROFILE MAPPING

The initial and final profiles of reinforced RM breakwater during tsunami overflow remained intact without any significant deformation. Figure 4.12 shows the profile of the reinforced RM breakwater generated from CloudCompare after post-processing the scanned data from the robotic mapper. The elevation difference between every point in the breakwater was plotted as a surface of the scoured profile. The surface was almost planar, which clearly indicated that the volume of the reinforced RM breakwater had not undergone any change during the tsunami overflow.

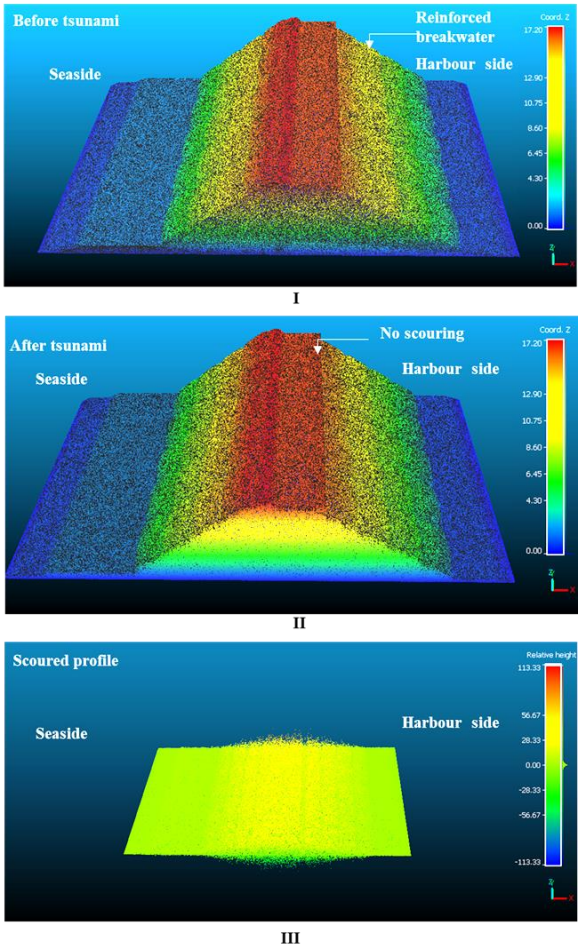

Figure 4.12 Comparison of the reinforced model profile before and after tsunami overflow (all dimensions are in cm)

4.5 NUMERICAL SIMULATION

From the shear strain contours developed by the DIC technique, it was observed that the excess seepage initiated the scouring of conventional RM breakwater through the body of the breakwater. Moreover, the output from pore water pressure gauges in the seabed highlighted that considerable seepage occurs through the seabed soils during tsunami overflow. Even though the effect of seepage was a crucial factor that led to the collapse of conventional RM breakwater, a detailed understanding of the failure mechanism is limited by experimental observations. Numerical simulations of the physical model test could visualise the seepage paths and corresponding strength reduction more precisely. A complex 3D finite element analysis was conducted by utilising the fully coupled flow-deformation analysis module of PLAXIS 3D. The breakwater models (conventional and reinforced) along with seabed soils (loose top layer and dense bottom layer) were numerically modelled, as shown in Figure 4.13. The rubble layers of the breakwater were modelled using constitutive soil models. A similar method was adopted in the studies by Cihan et al. 2012, Cihan and Yuksel (2011, 2013). In reinforced RM breakwater, sheet piles were modelled using plate elements, and the geogrid layer was modelled using a geogrid element. Interfaces were provided along either side of the plate and geogrid elements. The geobags were modelled with an outer geotextile membrane wrapped over the soil core. The Mohr-Coulomb model was chosen to define the soil parameters. The material parameters of the seabed soils and breakwater rubbles defined in Table 3.2 and 3.4 were given as the input for the numerical modelling.

However, the crown wall units were defined by a linear elastic non-porous soil model. The seabed and breakwater volumes were meshed using tetrahedral elements with three nodes on every edge. Sheet piles and geogrid elements were meshed with six nodes to match the three edge nodes of the tetrahedron. A medium-dense meshing with local mesh refinement was used to discretise the geometries. The conventional model has meshed into 18325 elements with 29924 nodes, and the reinforced model has meshed into 41995 elements with 67221 nodes. The MSL before tsunami arrival and during tsunami overflow was defined as separate water levels in the flow conditions mode. The exposed surfaces of the seaside seabed and breakwater slopes, in both conventional

and reinforced models, were assigned as hydraulic boundaries that allow seepage of water through them. However, in the reinforced model, interfaces of sheet piles were defined with zero cross-flow. This ensured the simulation of sheet piles as cut-off walls that block seepage paths through the seabed. However, it is important to note that the software did not simulate the erosion of the rubble mound breakwater, which is a limitation of the current analysis.

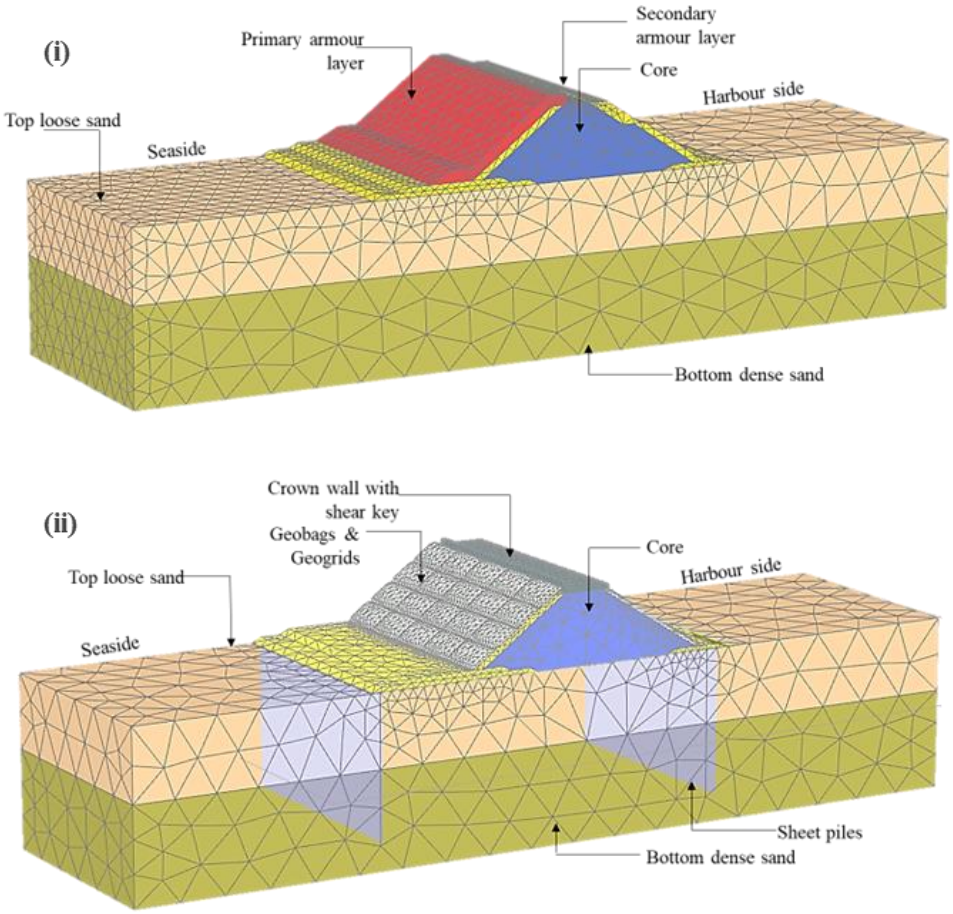

Figure 4.13 Numerical modelling of (i) conventional and (ii) reinforced model

4.5.1 Validation

The numerical model was validated with the pore water pressure readings taken from experimental data. The location of sensors P1 to P4 was marked in the numerical model as points of interest. Further, active pore water pressure for each case was determined from two calculation stages before and during the tsunami overflow. Figure 4.14 depicts the IPWP plotted across the length of the breakwater along the locations of the pore

pressure transducers. It can be inferred from the figure that the developed numerical model can seemingly predict the behaviour of both conventional and reinforced RM breakwaters. Hence, the numerical models are validated with the experimental results.

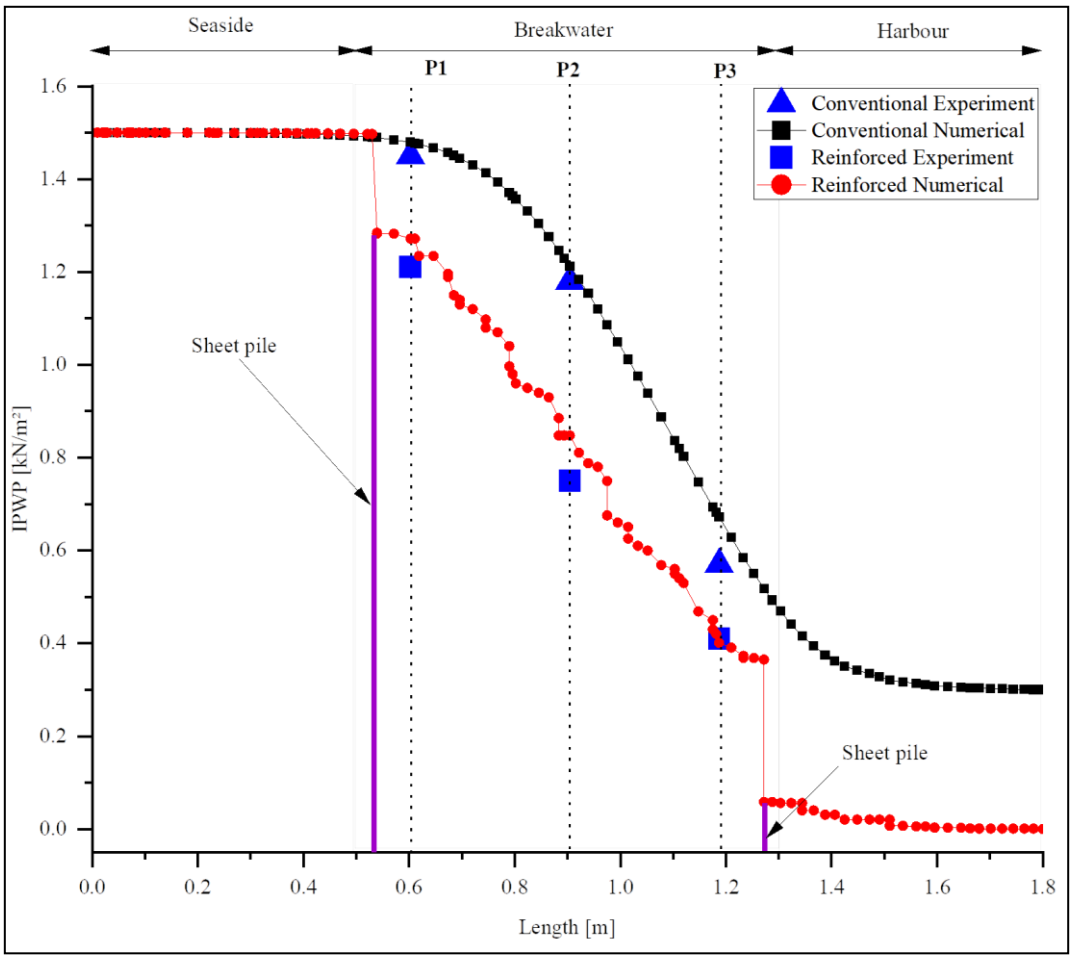

Figure 4.14 Validation of numerical model with the experimental results

4.5.2 Seepage Analysis

The flow vectors of seepage through the seabed can be identified prominently in the conventional RM breakwater under tsunami overflow, as seen in Figure 4.15. With the insertion of a sheet pile, the seepage through the seabed has been considerably reduced. The reduced seepage can be identified from the reduction in seepage flow vectors through the seabed. Even though the presence of sheet pile walls has prevented seepage through the seabed, some flow vectors still prevail due to the infiltration of water from the RM. The presence of sheet piles has diverted the path of seepage around it. Therefore, the length of the sheet pile has to be embedded in the dense soil layer to

prevent flow paths around the tip of the pile. Seepage through the body of the breakwater is another predominant phenomenon that results in the collapse of conventional RM breakwater during tsunami overflow. However, one of the primary functions of an RM breakwater is the dissipation of incident wave energy by transmitting the waves through its permeable body. The permeability of RM breakwater is a critical factor that determines its performance. During tsunami overflow, a large volume of water permeates through the body of the breakwater. This excess seepage imparts destabilising forces that initiate the scouring of armour units from the harbourside. This phenomenon was observed in the shear strain contours of the breakwater during tsunami overflow. In Figure 4.15, it can be seen that the geobag armour units have reduced the seepage through the body of the reinforced RM breakwater. Whereas seepage still prevails through the RM, ensuring that the wave energy dissipation functionality of the breakwater is not compromised.

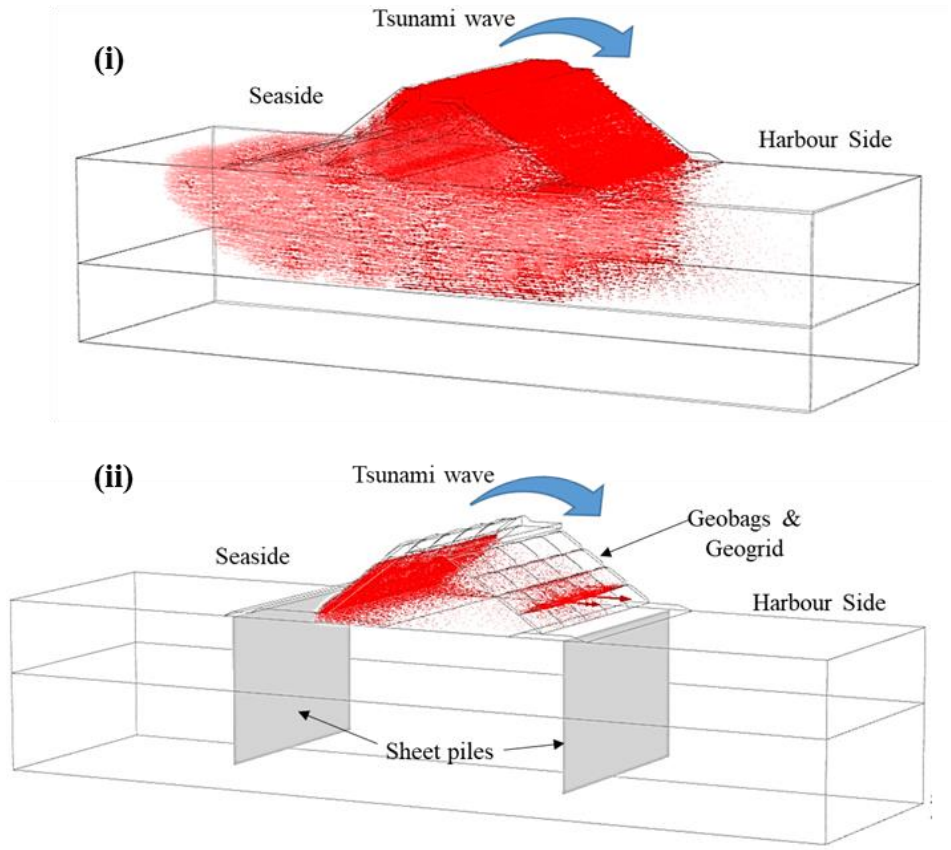

Figure 4.15 Seepage flow vectors under the tsunami overflow (i) conventional and (ii) reinforced model

4.5.3 Stability of Breakwater

The stability analysis of the numerical models was conducted using the safety analysis method, in which input shear strength parameters of soil are varied against the reduced shear strength values to determine the maximum safety factor possible under defined loading conditions. While the method does not address erosion observed in model tests, the factor of safety was assessed to gauge the stability of the intact breakwater during the specific condition of tsunami overflow. The study aimed to understand how reinforcement improves stability by comparing the factor of safety in both conventional and reinforced designs, offering a crucial measure for early-stage design considerations.

The global factor of safety for both conventional and reinforced RM breakwaters was determined under tsunami overflow conditions using the strength reduction method. The angle of internal friction (ϕ) parameter was gradually reduced by a small percentage until failure occurred. Failure was identified when the factor of safety ceased to show significant variations with further reductions in the shear strength parameters—the parameter Msf was used as a multiplier to reduce both c and φ values in stages. The cumulative sum of the safety factors at each load increment stage is denoted as ΣM_{sf}. At any particular stage, the corresponding factor of safety was determined using the following equation (**4.1**)

$$\sum M_{sf} = \frac{(\text{Shear strength})_{\text{Input}}}{(\text{Shear strength})_{\text{reduced}}} \qquad \textbf{(4.1)}$$

The value of ΣM_{sf} was plotted against the displacement of a node selected at the crown. The displacement denoted in the abscissa of curves plotted in Figure 4.16 has no physical significance. The reinforced model is 61% more stable than conventional RM breakwater when subjected to a tsunami height of 150 mm.

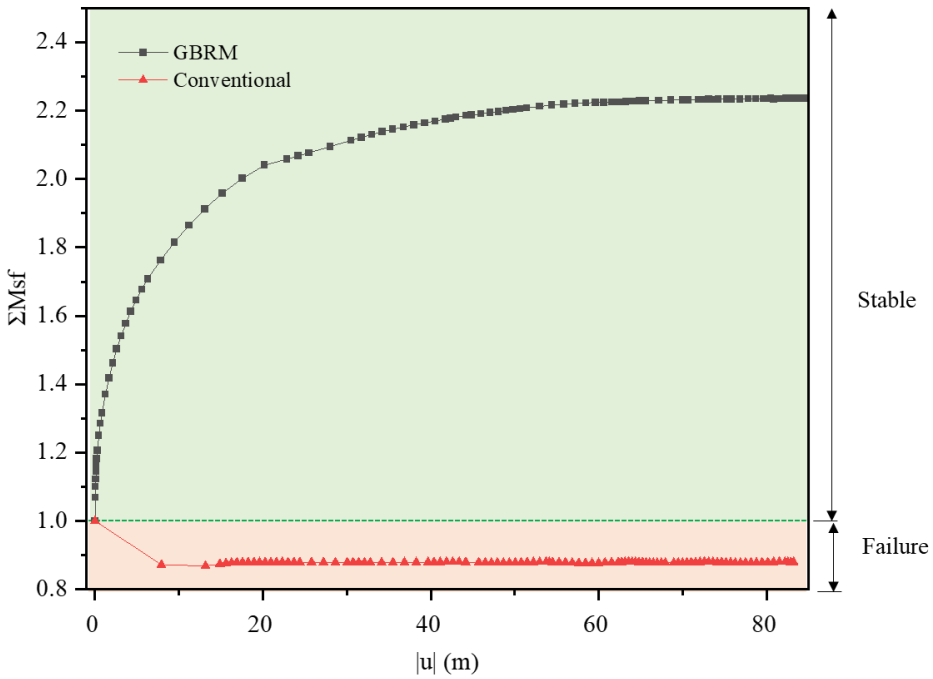

Figure 4.16 Stability of the conventional and reinforced model under the tsunami overflow

However, it could be seen that in reinforced RM breakwater, the safety factor was higher than unity, which clearly indicates a stable structure even after the tsunami overflow. This is clearly seen in the lack of failure surface in reinforced models, as shown in Figure 4.17. Some contours were seen at the overlapping regions between each layer of geobags. However, any possibility of displacement of geobags along these overlapping areas is prevented by the connection to the underlying geogrid layer. At the same time, the critical failure surface of conventional RM breakwater can be distinguished distinctly. From the physical model tests, a similar type of scouring was observed along the crest and harbour side slope of the RM. However, the harbour side slope was not scoured till the base. The piling up of rolled-down rubbles on the harbour side seabed has indirectly increased the width of the breakwater to a certain height above the seabed. The more comprehensive section has thus arrested the propagation of the failure surface to the heel of the RM. This extra stability due to the heaving up of the rolled-down rubbles was not considered in numerical simulations.

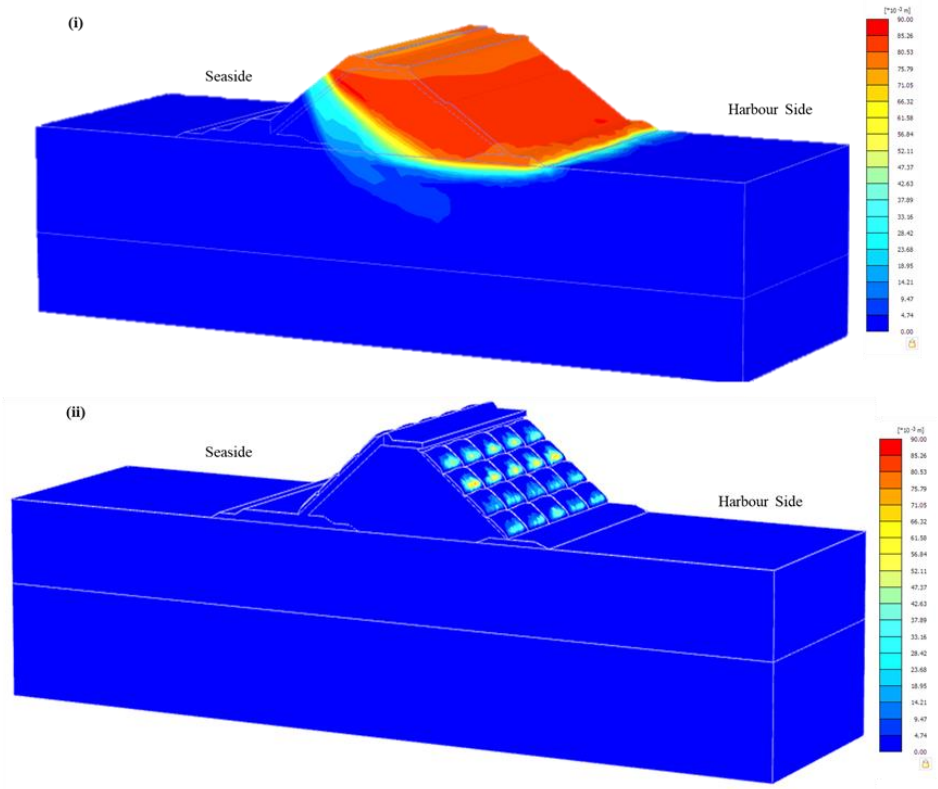

Figure 4.17 Failure surface of (i) conventional and (ii) reinforced model under the tsunami overflow

4.5.4 Effect of Tsunami Height

Another critical parameter that had a significant influence on the stability of the breakwater was the height of the tsunami (h_t). In physical model tests, the conventional RM breakwater collapsed under a tsunami height of 150 mm (15 m in prototype). The stability of the breakwater at every 200 mm (2 m in prototype) rise of the tsunami was monitored in the numerical analysis. The depth of MSL (h_w) was 50 mm in the physical model tests. Figure 4.18 describes the effect of the dimensionless parameter (h_t/ h_w) on breakwater stability. As the height of the tsunami increases, a noticeable reduction in breakwater stability is observed. The increased lateral thrust on the RM and higher seepage rate through the body of the breakwater are the key factors that reduce breakwater stability. At the beginning of the physical model test, the initiation of RM scouring occurred when the height of the tsunami reached nearly 100 mm. A similar trend was observed from the numerical simulations, where the stability of the breakwater was compromised when tsunami height reached 110 mm, as shown in

Figure 4.18. The stability factor $\Sigma M_{sf\ was}$ reduced by 38% as the ratio h_t/ h_w increased up to 3. The rise of tsunami level beyond h_t/ h_w = 1.4 has generated an abrupt 23% increase in destabilising forces on the breakwater. The sudden reduction in the stability was a result of the seepage forces from the sea-level difference between the seaside and harbourside. Moreover, the width of the breakwater cross section reduces towards the top. Therefore, the stability of the mound reduces with an increase in tsunami height.

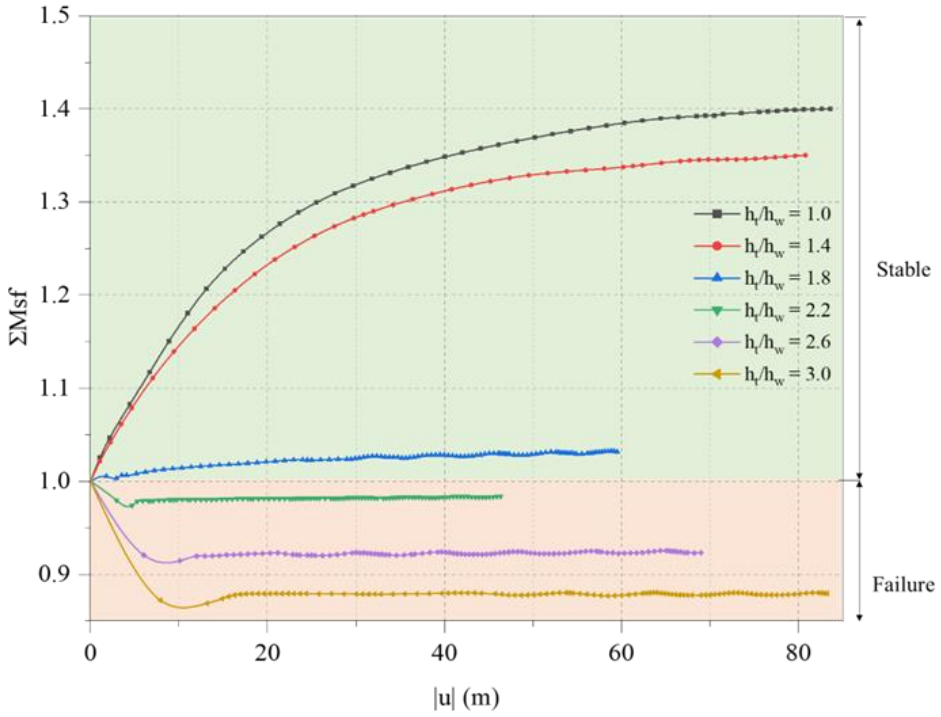

Figure 4.18 Stability of conventional model under various tsunami impact heights

The critical slip surface corresponding to each increment in tsunami height is shown in Figure 4.19. The figures solely represent the possible mode of failure that was obtained during the safety analysis of the conventional RM breakwater. It could be seen that the increase in relative tsunami height beyond 1.8 has destabilised the seaside slope more than in the previous stages. With a further increase in tsunami height, the beginning of the failure surface moves towards the seaside slope. This was evidently seen in the physical model tests, where the seaside armour units were also scoured away by the tsunami of 150 mm in height. However, in the physical model test, the scouring was not extended till the heel of the breakwater at the harbour end. This was possibly due to the piling up of scoured rubbles on the harbourside. This heaving of rubbles

effectively increased the width of the breakwater, which arrested the continuation of the failure surface beyond a certain level.

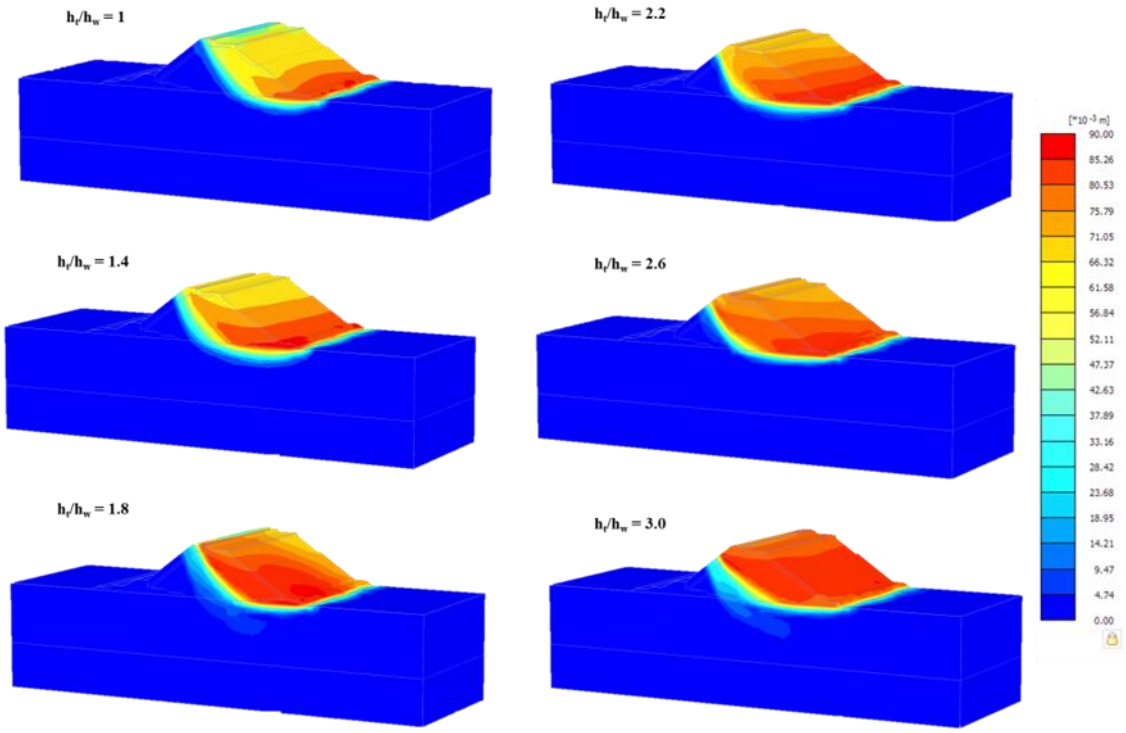

Figure 4.19 Failure surface of the conventional model under different tsunami impact heights

4.6 SUMMARY

Detailed experimental and numerical studies revealed that the conventional RM breakwater was destroyed during the tsunami overflow. The displacement of armour rubbles under the enormous lateral thrust of the tsunami, dislocation of core and armour rubbles due to excess seepage pressure and scouring of armour rubbles due to the breaking of the tsunami along the harbour side slope were the predominant failure mechanisms. In comparison, reinforced RM breakwater offered higher resiliency by withstanding the tsunami overflow without any noticeable deformation. The following inferences can be summarised from the present study,

- Severe damage was observed on the conventional RM breakwater during the tsunami overflow tests. The breakwater crest settled by 50 mm (5 m in prototype) under the overflow of a 150 mm height tsunami. Armour units in the crest region were displaced by 150 mm (15 m in prototype) to the harbour side under the tsunami forces.
- During the tsunami overflow tests, a significant difference in hydraulic head between the seaside and harbour side of the breakwater occurs. Consequently, excess seepage pressure is developed in the RM. It was evident from the distribution of shear strain contours inside the breakwater that the seepage forces initiated scouring by displacing armour units from the harbour side even before the impact of the overtopping tsunami on harbour side slopes.
- Geosynthetic reinforcements of the breakwater impart resiliency to the breakwater during the tsunami overflow. The reinforced RM breakwater was decidedly stable to withstand the numerous failure mechanisms induced by an overflowing tsunami.
- The settlement of the breakwater crest was reduced by 90.2% and lateral displacement by 99.6% in the GBRM model. The higher mass of geobags compared to rubbles improved the total inertial resistance of the breakwater against the lateral forces of the tsunami. Additionally, the binding to the geogrid layer ensures extra stability against the seepage forces through the body of the breakwater.
- The provision of crown walls with shear key protected the crest of the RM breakwater from scouring during the tsunami overflow. Moreover, the shear key of crown walls improved their stability against the destabilising lateral forces of the

tsunami. The insertion of sheet piles into the seabed acted as cut-off walls that reduced excess seepage through the seabed, which could result in the strength reduction of the foundation soils. The IPWP at the seabed soils beneath the breakwater was reduced by 26.3% in the GBRM model. Thus, the proposed reinforced RM breakwater was observed to be highly resilient against tsunami overflow.

The novel technique of replacing armour blocks with a combined geobag-geogrid system can be adopted to mitigate tsunami-induced damages on breakwaters. The replacement of concrete armour units with a geobag-geogrid system is an environmentally friendly approach which depletes the carbon footprint of cement used to make precast armour blocks. This can be adopted in practical applications on the ground.

CHAPTER 5
GABION-REINFORCED RM BREAKWATER

5.1 INTRODUCTION

The effectiveness of the proposed reinforced model of the RM breakwater is evaluated by conducting physical model tests and analytical theories. Gabions, sheet piles and crown walls (with keys) are proposed as countermeasure elements. To the end, responses of the reinforced breakwater are compared with those of conventional breakwater in order to examine the performance of the proposed countermeasures. The height of the tsunami was 150 mm (15 m in prototype) in the physical model tests. In the tests, displacement gauges, pore pressure gauges, and profile mappers are used to measure settlements and lateral displacements, and complete 3D profiles are plotted. Analytical studies are also done to determine the effects of these countermeasures on the stability of the breakwater during the tsunami. Finally, numerical simulation is also carried out to clarify the mechanism for both conventional and reinforced breakwaters.

5.2 PHYSICAL MODEL TEST

5.2.1 Settlement

In the physical model tests on the conventional breakwater, it was observed that nearly 50 mm (5 m in prototype) of the breakwater was scoured entirely away by the tsunami. The addition of gabions on both sides of the mound improved its intactness, which eventually helped reduce the settlement of the breakwater crest, as observed in the evolution of the mound profile during the overflow of the tsunami. It was also evident from tests and the comparative analysis of the mound profile before and after the tsunami impact that the volume of rubble scoured was negligible or even zero. The gabions, shear keyed crown wall, and sheet piles were found to be very effective countermeasures in reducing the settlement of the mound during the tsunami overflow test, as shown in Figure 5.1. The heavier gabion unit (compared to an armour unit) has improved the mass inertia of the armour layers. Further, the gabion has more extensive base/ contact areas compared to rubble, which provides higher frictional force and, thereby, better resistance against dislocation. Comparatively heavier gabions were not scoured. While gabions stabilized the slopes of the mound, the crest was protected by

a shear-keyed crown wall unit. The embedment of the shear key into the mound along the seaside face has provided better resistance against sliding and overturning of crown wall units (there was high scouring at the top of the breakwater in the case of the conventional breakwater). Thus, the crown wall and gabions acted as a protective outer layer to the core and side slopes of the breakwater. In addition, the mound foundation seabed was reinforced with two rows of sheet piles, one beneath the seaside slope end and another beneath the harbour side slope end. These sheet piles act as cut-off walls and arrest the seepage of water through the seabed soils, which would otherwise have reduced the shear strength reduction of the foundation. Such failures were observed beneath caisson-type breakwaters in previous studies (Chaudhary et al. 2018c; b, 2019; Chaudhary and Hazarika 2018). Thus, the combined effects of all three reinforcing measures nullified the settlement of the RM breakwater under severe conditions like a prolonged tsunami overflow. It can be seen in Figure 5.1 that the conventional breakwater settled around 50 mm during the tsunami; however, it is almost zero for the reinforced breakwater.

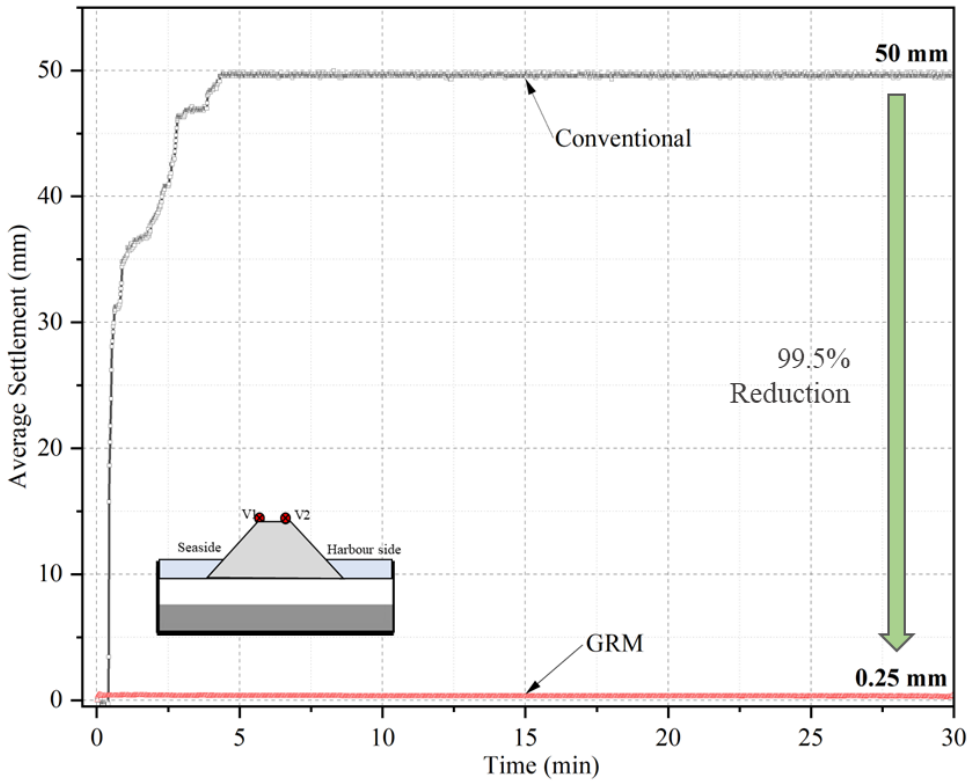

Figure 5.1 Settlement of the crest for conventional and GRM models

5.2.2 Lateral Displacement

During the tsunami inundation, powerful hydraulic forces exerted themselves upon the rubble mound (RM). The sideways thrust of the tsunami caused the armour units to shift from the seaward side to the harbourside. This displacement of armour units exposed the lighter core layer beneath. Figure 5.2 illustrates the average displacement measured from the crest, indicating an initial rapid increase in displacement and settlement, followed by a stabilization phase. The volume of the RM obstructing the tsunami diminished due to scouring, which persisted until most of the rubble above sea level was displaced. As the height of the breakwater-blocking tsunami decreased, the rate of scouring also diminished. Although the scouring nearly reached equilibrium, minor displacements of rubble persisted due to the drag forces of tsunami overflow. However, these small displacements did not significantly affect the displacement curves, as the initial scouring overshadowed them.

Conversely, in reinforced RM breakwaters, lateral displacement was mitigated entirely. The stability of the RM was notably enhanced when armoured with heavier gabions. Additionally, inserting the shear key of the crown wall into the RM provided enhanced resistance against the lateral forces of the tsunami.

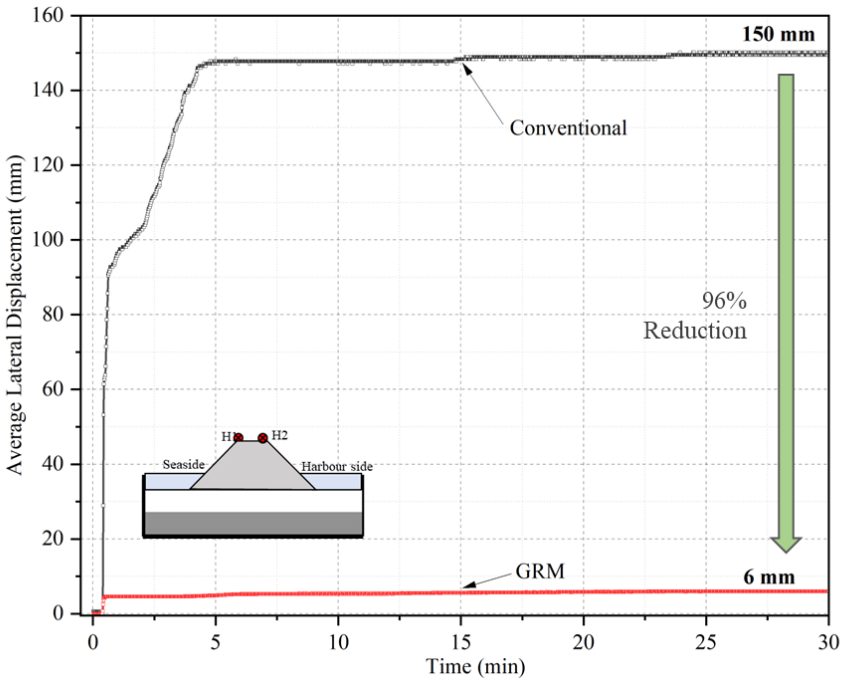

Figure 5.2 Lateral displacement of the crest for conventional and GRM models

5.2.3 Incremental Pore Water Pressure

The effects of the placement of the sheet piles inside the seabed were clearly highlighted in Figure 5.3, where a reduction in the increase in pore water pressure during the tsunami was observed in the pore water pressure gauges' readings. The pore pressure transducers were placed at three different locations in the seabed soil- P1 placed beneath the seaside end of the mound, P2 directly beneath the mound and P3 beneath the harbour side end of the mound. The transducers at the seaside registered the highest increment in pore water pressure during the tsunami as the height of the tsunami water raised abruptly high at the seaside. On the other hand, the water level at the harbour side was always maintained at MSL by continuously pumping out excess water. This head difference in the water level between the seaside and harbour side has resulted in the high seepage of water through the seabed and breakwater body and also caused an increase in the pore water pressures measured at P2 and P3 locations. The increase in pore water pressure is termed IPWP. However, the IPWP beneath the centre of the mound and harbour side was less than that at the seaside. This reduction in the IPWP was evident as the seepage length increased from one sensor to another. The insertion of sheet piles into the seabed has reduced the seepage considerably, which was evident from the reduction in the IPWP by an average of 27% at each location. The sheet piles acted as cut-off walls and restricted the direct flow of water through the loose sand layer (upper seabed layer). Since the sheet piles were provided till the depth of the dense sand layer of lower permeability, the possibility of generation of seepage path around the sheet pile was arrested.

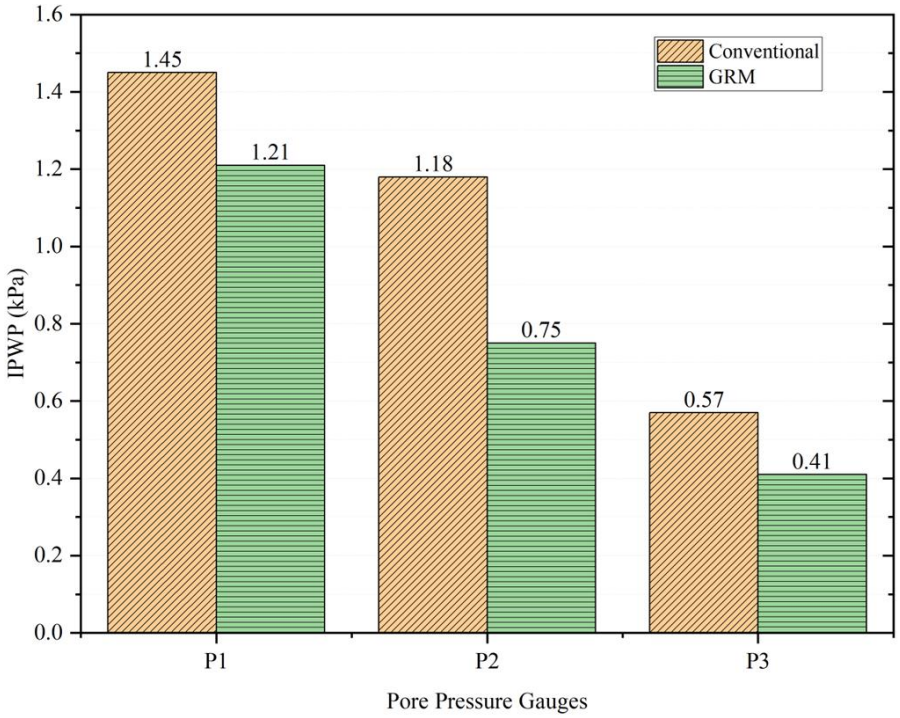

Figure 5.3 IPWP measured during the tsunami overflow for conventional and GRM models

5.2.4 Deformations of the Breakwater

Photographs of the RM breakwater taken before and after the tsunami overflow tests are shown in Figure 5.4. The crown unit played an essential role in reducing the scouring and increasing the stability of the reinforced breakwater. The provision of shear key in the crown wall unit was found to be very efficient in holding the crown wall against sliding and over-turning under the impact of the tsunami. In the case of the conventional breakwater, the initial scouring of armour units from the harbourside exposed the core layer, which was later scoured off along with the primary armour units. The scouring of nearly 5 m in the prototype breakwater destroyed 96% of the freeboard height (Figure 5.4 (b)). It ultimately caused the breakwater to fail to block the tsunami. This would give unfettered access to the tsunami in the coastal areas, which would create massive damage to life and property. However, the proposed reinforcements are found very effective for the breakwater to make it stable against the tsunami overflow for a longer duration without any damage. Moreover, this made the breakwater resilient against tsunami-induced damage.

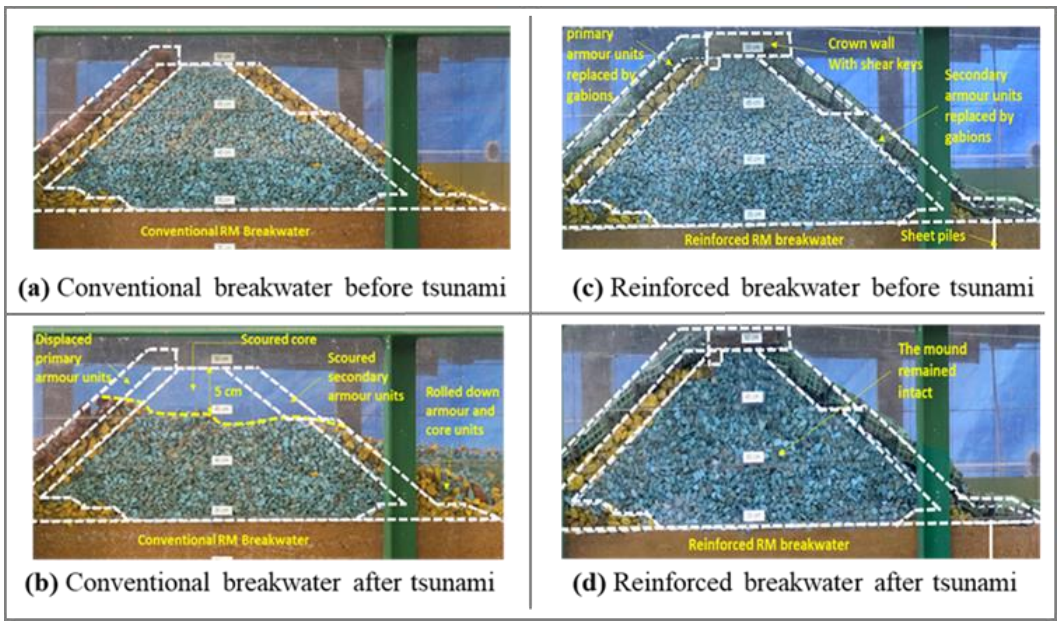

Figure 5.4 Deformations in conventional and GRM models when subjected to tsunami overflow

The conventional RM breakwater was observed to be scoured considerably under tsunami overflow conditions. Figure 5.5 shows the evolution of scouring on the breakwater during the tsunami overflow tests. It is evident that the rubbles of the mound were scoured from the crest nearly by 50 mm (5 m in the prototype) due to the continuous overflow of the tsunami. The breakwater before the tsunami impact is depicted in Figure 5.5 (a), a photograph taken at t = 0 s.

The beginning of tsunami overflow is shown in Figure 5.5 (b) at time t = 10 s, where the water level in the seaside raised to the height of the breakwater. After 5 seconds of overflow, the armour units at the harbour side were rolled down Figure 5.5 (c). Within the next 5 s (i.e., t = 20 s) of the overflow, the top of the RM started to scour off, as shown in Figure 5.5 (d). It can also be seen that the tsunami has carried away one primary armour unit. The scoured profile in Figure 5.5 (e) shows that the mound was scoured more towards the harbourside. This immediate scouring was due to the excess seepage of water through the body of the breakwater under pertaining water level differences between the seaside and harbourside. Tsunami impact force also played a role in this. The secondary armour on the harbour side, along with some core materials, displaced more under the impact of the overtopping tsunami. The displaced rubbles

were found to be deposited over the seabed on the harbourside. At the end of t = 1 min, a few primary armour units on the seaside were scoured by the continuously overflowing tsunami and deposited on the harbourside, as shown in Figure 5.5 (f). By t= 5 min, more rubbles from the seaside were scoured away, as seen in Figure 5.5 (g).

In Figure 5.5 (h), it can be seen that the scoured rubbles were observed to be piled up on the seabed at the harbourside. Since there was no crown unit over the breakwater, the high impact forces of the overflowing tsunami near the rubbles were forcing the rubbles to roll down to the harbourside. Due to the tsunami's blockage by the breakwater, some eddy-like waves formed near the breakwater. The combined effects of these forces have pulled even the heavier primary armour layer (red coloured) from the seaside and deposited over the seabed on the harbourside. The amount of scouring has reached almost an equilibrium state for the tsunami at the end of t = 15 min, as seen in Figure 5.5 (i).

It was observed that the water level in the harbour side has a more significant role in adding stability to the RM during a tsunami impact. Almost the whole portion of the RM that was standing above the sea level was scoured off entirely during the tsunami overflow, as seen in the photograph Figure 5.5 (j).

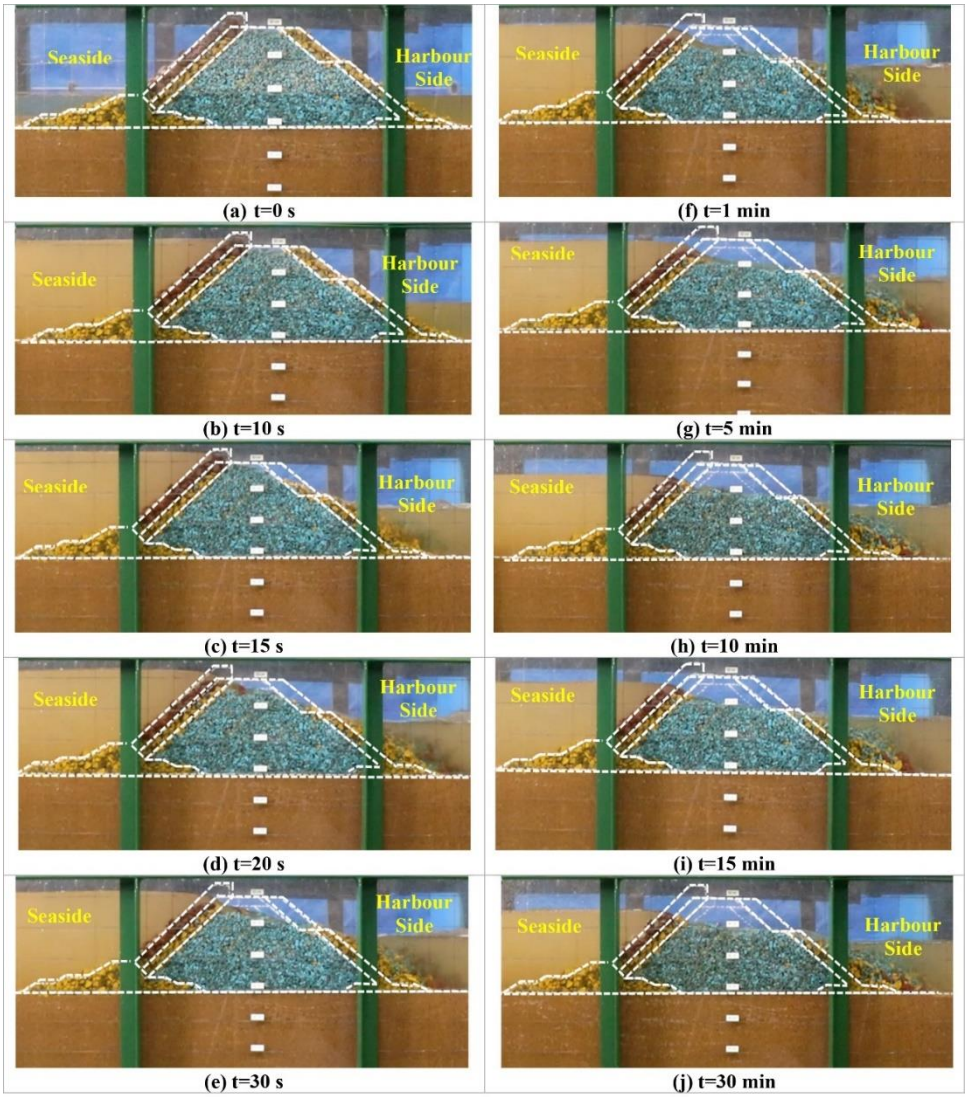

Figure 5.5 Behaviour of the conventional model during the tsunami overflow

The addition of reinforcements such as gabions, sheet piles and crown walls with shear key to the conventional RM breakwater showed improved resistance to the tsunami overflow. The mound remained intact throughout the tsunami overflow test. This was evidently seen in every photograph captured during the experiment, as shown in Figure 5.6. The gabions were provided as a replacement to the armour layers in the reinforced breakwater. Each gabion was heavier than a single armour unit. This heavier gabion could not be scoured easily. In addition, their extra weight and large contact areas, compared to the rubbles, provide extra stability for the mound. Even though the irregular angular armour rubbles have good interparticle locking, the gabions have more contact areas (base contact area) over which it was standing. So, the greater the contact

area and heavier weight of the gabion, the higher the frictional forces are, and thus, the more significant the stability of the gabion-reinforced slopes of the mound.

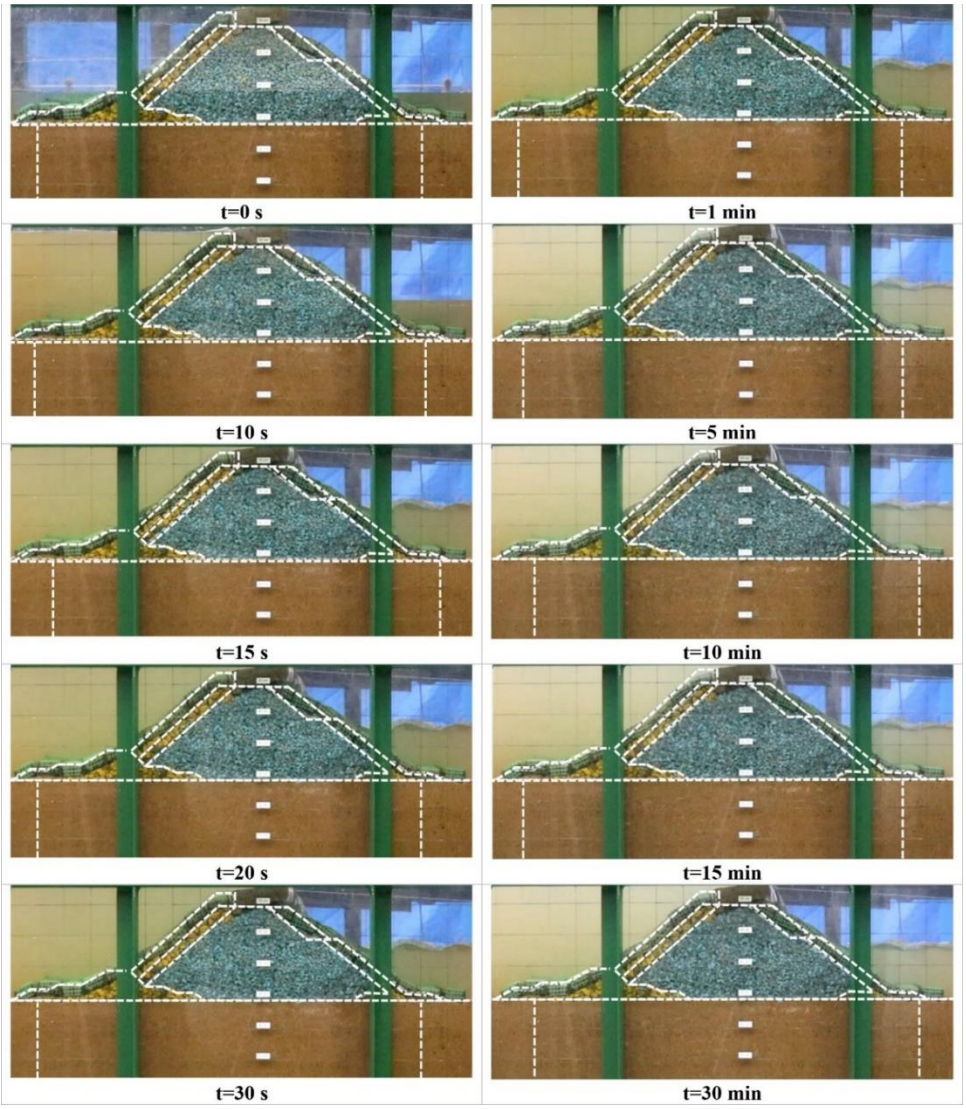

Figure 5.6 Performance of the GRM model during the tsunami overflow

5.3 ANALYTICAL STUDY

The damage to the RM during tsunami overflow was quantified using different damage parameters. The damage parameters were expressed regarding the number of displaced armour units after a tsunami overflow. For differentiating between each layer, the rubbles were coloured. Figure 5.7 highlights the displaced armour units after a tsunami overflow in the conventional type and the intact mound with no displacement of armour units in the reinforced type. The stability number Ns for armour units could represent

the destabilising forces that acted upon the breakwater under the tsunami overflow. It was estimated that, for a tsunami height of 120 mm, the stability number was 3.78.

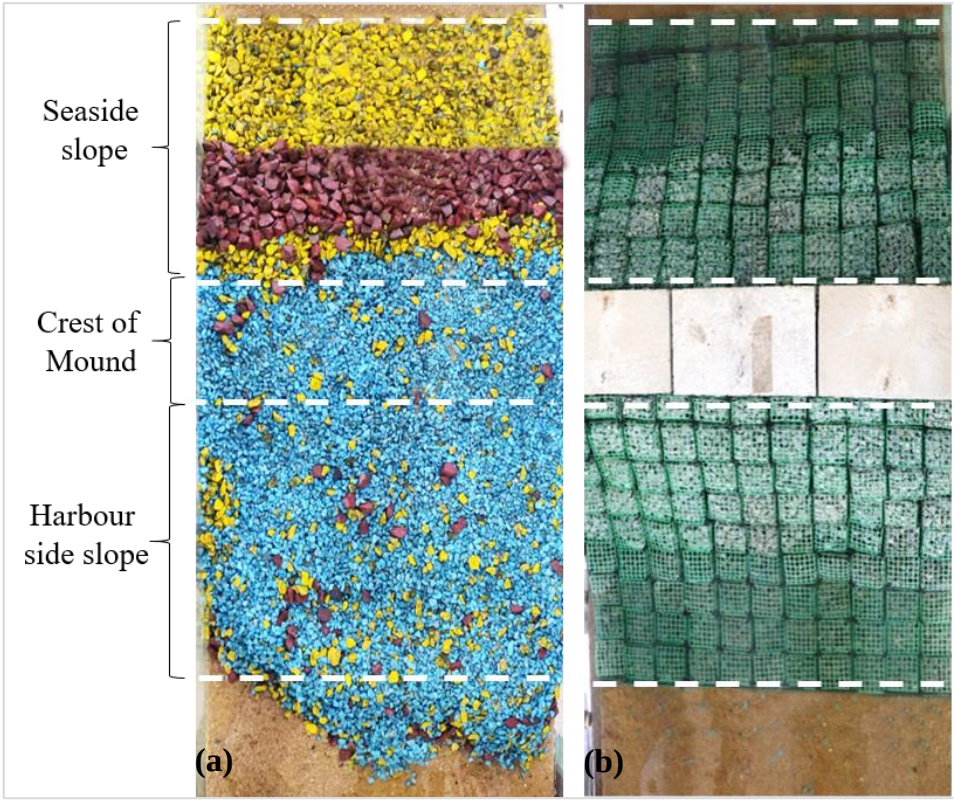

Figure 5.7 Comparison of top view of the (a) conventional (b) GRM models after tsunami overflow

5.3.1 Relative Displacement

The relative displacement (R_d) was determined by counting the total number of the primary armour units displaced after the tsunami overflow. A total of 971 armour units were used to prepare the primary armour layer in the physical model, out of which 430 units were entirely displaced from their initial positions. The relative displacement for the conventional breakwater was 0.44. However, after the inclusion of reinforcements, the RM remained intact during the tsunami overflow experiments, as shown in Figure 5.8.

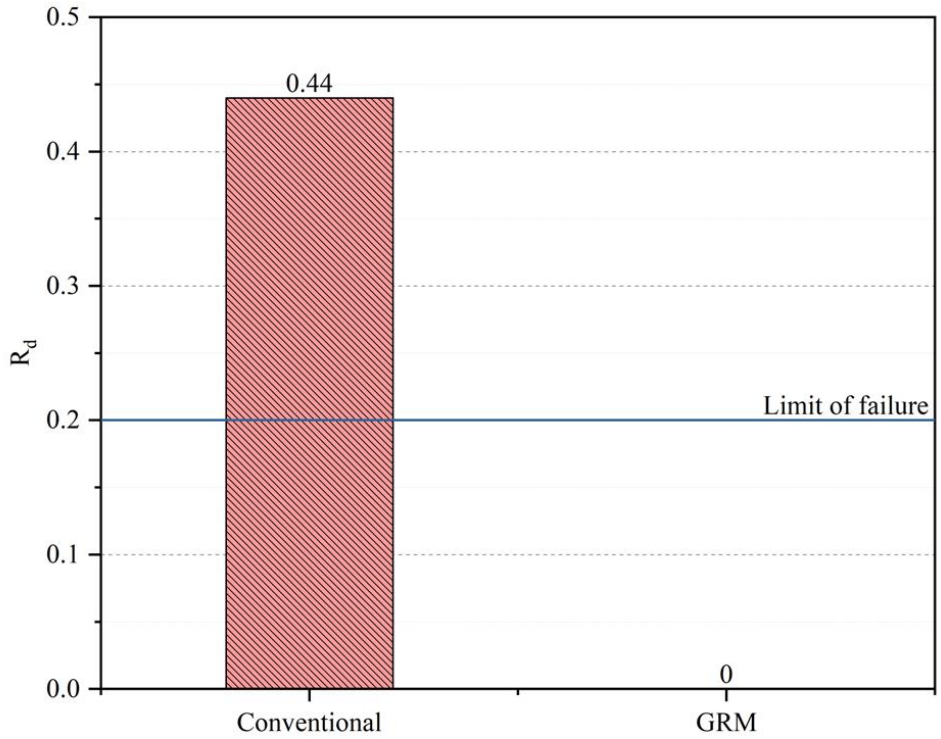

Figure 5.8 Relative displacement of armour units in conventional and GRM models after the tsunami overflow

5.3.2 Relative Eroded Area

The width of the model cross-section, B, which is 0.4 m in this study, is also significant in the average eroded area. Based on the range of values obtained for S, for breakwater slope (cot α) varying from 1.5 to 4, the damages that occurred on the RM can be categorised as per Table 3.6 (Campos et al. 2020b). The relative eroded area (S) was determined for the conventional breakwater; it was found to be 43. This type of scoured profile is higher than the destruction threshold, as mentioned in the qualitative damage assessment on RM breakwaters tabulated in Table 3.6. As suggested by Xu et al. (2020), the S parameter can be determined for armour units under the impact of a solitary wave of 150 mm in height according to the equation proposed by Aniel-Quiroga et al. (2018). It was found that the value of S was 0.18, which was a significantly smaller value than that of a similar tsunami impact. This possibly explains the severe damage that was observed during the tsunami overflow, where the layer below armour units was exposed to further wave impacts, which eventually led to the failure of the mound. However, replacing armour units with gabions and placing crown walls (with shear key) imparted

resiliency to the breakwater such that no armour units were displaced at the end of the tsunami overflow test, as highlighted in Figure 5.9.

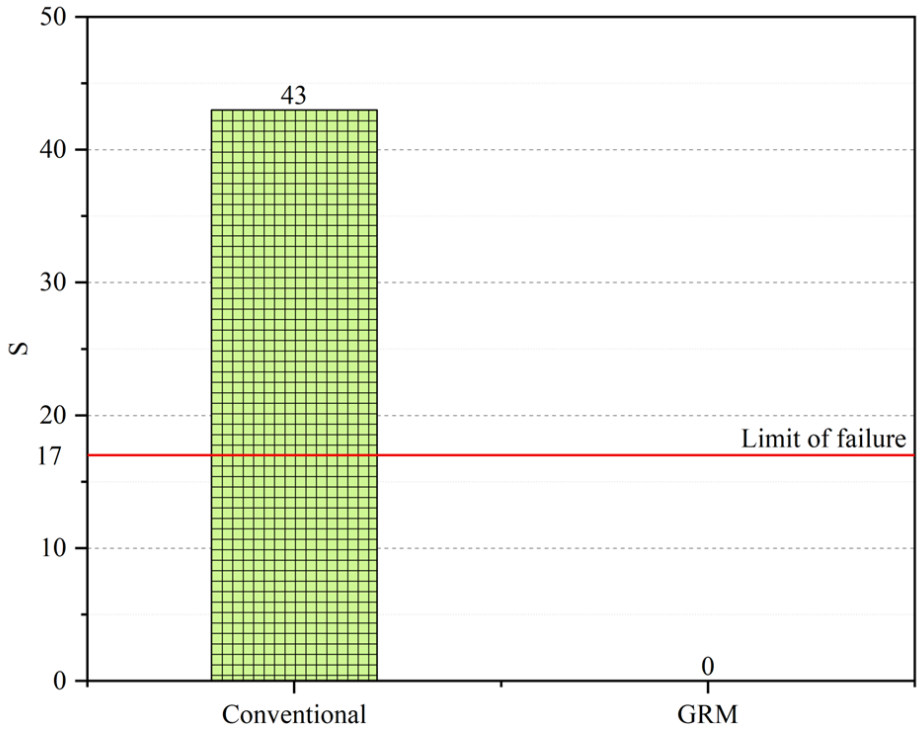

Figure 5.9 Relative eroded area of armour units in conventional and GRM models after the tsunami overflow

5.4 PROFILE MAPPING

The scanned profile of the conventional breakwater mound before and after the tsunami overflow is shown in Figure 5.10. The crest of the mound scoured almost the same depth across the width of the breakwater. A total volume of 4016.71 cc was scoured off from the top region of the mound. The scoured materials rolled down towards the harbour side, resulting in 2800.78 cc of piled-up rubbles on the harbour side seabed. The coloured bands of the scoured depth profile in Figure 5.10 (c) represent the difference between a point on the mound before and after scouring. The whole breakwater model was scanned by the profile mapper before and after the tsunami overflow tests. The scour depth is calculated as the relative difference between elevations of every point on the breakwater profile before and after the tsunami overflow. Maximum scouring was observed beneath the crest of the mound, and upheaval was observed due to the deposition of rolled-down rubbles towards the

harbourside. It can be noticed that the seaside portion beneath the sea level was not affected much by the tsunami overflow. The hydrostatic forces exerted by an equal depth of water in the harbour side must have provided extra stability to the region beneath the MSL. However, no deformation was observed in the reinforced breakwater. Hence, the scanned profile of the breakwater before and after tsunami overflow was the same as that of a flat scour depth profile, as shown in Figure 5.11.

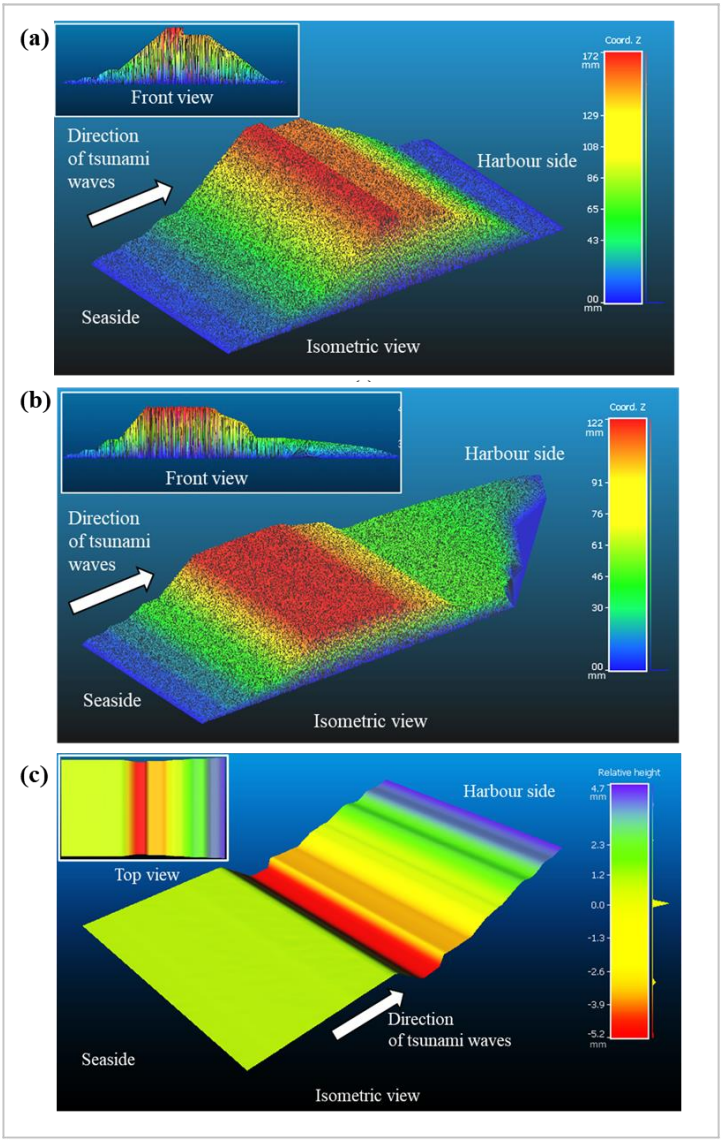

Figure 5.10 Scanned profile of the conventional model (a) before tsunami overflow (b) after tsunami overflow (c) depth profile of scoured volume

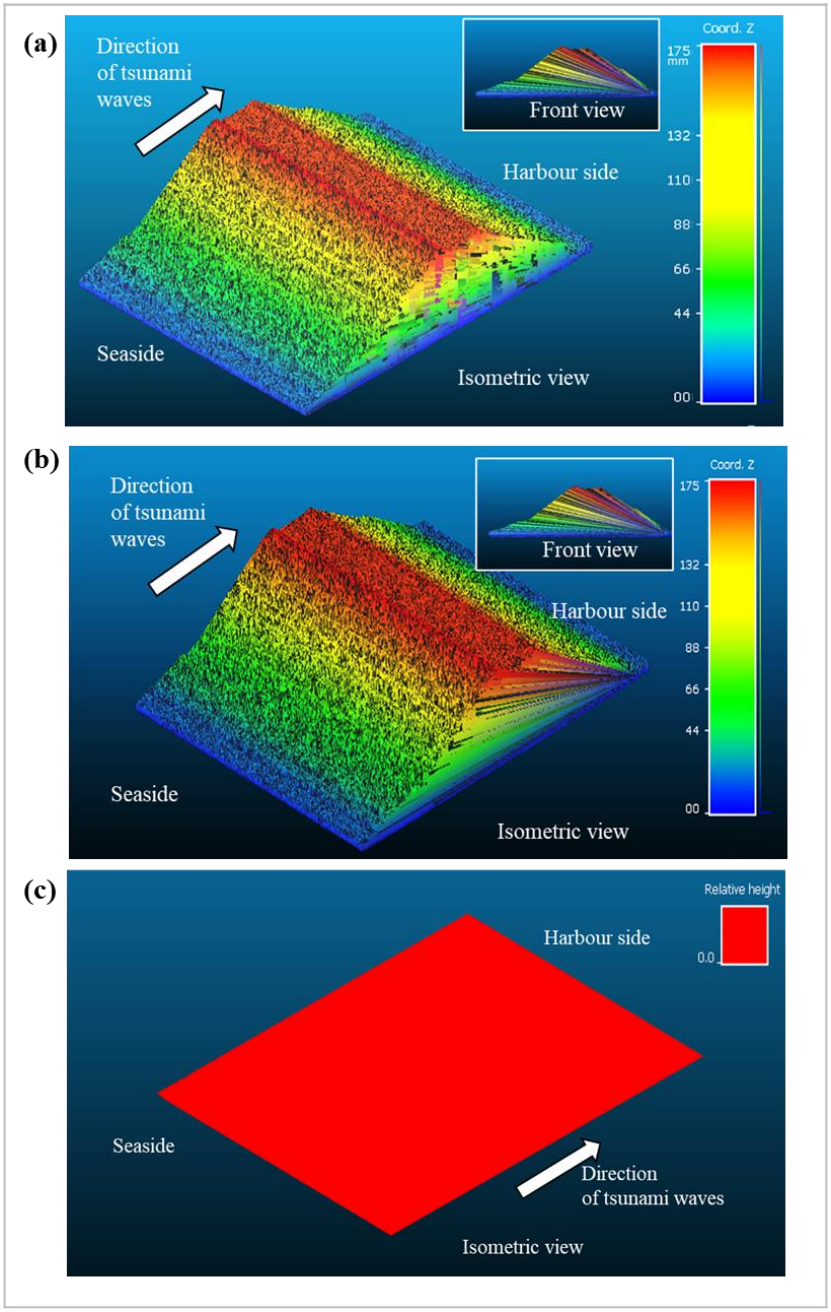

Figure 5.11 Scanned profile of the reinforced model (a) before the tsunami overflow (b) after the tsunami overflow (c) depth profile of scoured volume

5.5 NUMERICAL SIMULATION

The seepage that occurs due to the sea water level difference between the seaside and harbour side during the tsunami overflow is studied in detail by using the flow calculation module in PLAXIS 3D. The numerical model has been defined with a soil domain of 1800 mm length, 350 mm depth and 500 mm width, as shown in Figure 5.12. The soil was modelled as two separate sand layers, as done in the physical experiments, with a lower dense layer and a loose upper layer. The Mohr-Coulomb soil model has been selected to model the top and bottom soil layers. The properties of materials used for defining the numerical model is tabulated in Table 3.2 and 3.4. A Mohr-Coulomb soil model was used to model the armour and core layers of the breakwater. It was observed in previous research that constitutive soil models could effectively simulate the behaviour of RM breakwaters (Cihan et al. 2012; Cihan and Yuksel 2011, 2013). The crown wall was modelled as a non-porous linear elastic layer. The numerical modelling was particularly focusing on the seepage effects of the tsunami and hence, the erosion of breakwater was not considered in the numerical study.

Groundwater flow boundary conditions were defined such that the boundaries on either end and top were assigned as ‘open’ boundaries. In contrast, the bottom boundary was defined as ‘closed’. The ‘open’ boundaries permit the flow of water across the boundary, and the ‘closed’ boundaries prohibit the flow of water across boundaries. The ‘open’ and ‘closed’ groundwater boundary conditions were defined to simulate the semi-infinite soil medium. However, the ‘seepage’ type boundary condition was defined for the top boundary of soil as well as the outer boundaries of the RM breakwater. A refined element distribution with enhanced mesh refinement has been chosen for meshing the modelled geometries. The geometries meshed into 18,325 elements and 29,924 nodes in the conventional model and 20,242 elements and 34,530 nodes in the reinforced model. Tetrahedral elements with ten nodes were used to mesh the soil body. The sheet piles were modelled as plate elements with six nodes and interfaces of the sheet piles with interface elements of 12 nodes.

The analysis was then performed based on the transient groundwater flow analysis, where the time-dependent changes due to defined water levels are calculated. The duration of tsunami overflow was set to 30 min. The permeability of the soil and RM

must also be given as mandatory input parameters for conducting a flow-deformation analysis. A Chart Datum (CD) of 50 mm was defined as the initial global water level. A new water level was created with a profile of surface water resembling the overflow of a tsunami over the RM. The analysis was carried out in two stages resembling the conditions before and during the tsunami overflow.

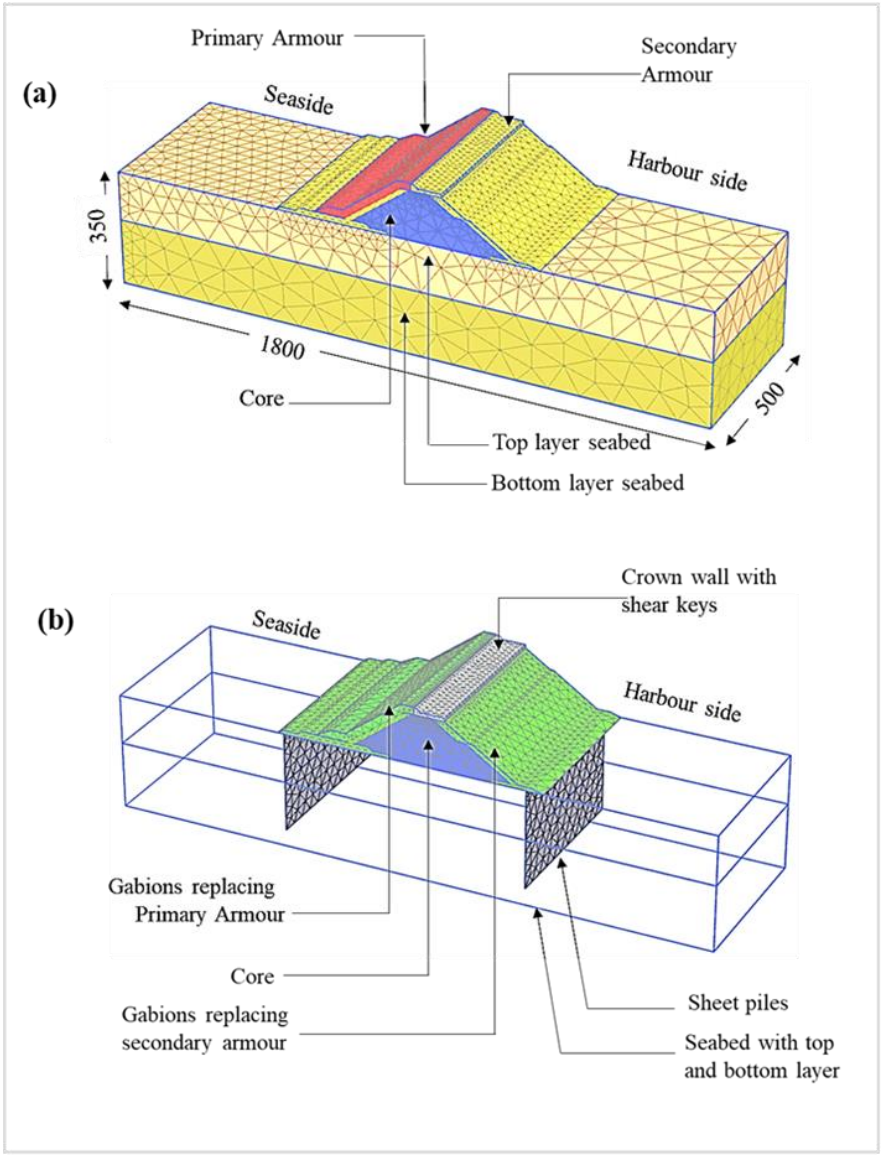

Figure 5.12 Numerical models developed (a) conventional and (b) GRM model (all dimensions are in mm)

5.5.1 Seepage Through the Seabed

In conventional RM breakwater, the potential head difference between the water level in the seaside and harbour side generates a continuous seepage of water through the

seabed beneath the mound. However, the seepage is lesser through the seabed layer compared to the permeation of water through the body of the breakwater due to its higher permeability. This is evident in the increased density of groundwater flow arrows inside the breakwater, as shown in Figure 5.13. The seepage that occurs through the seabed would considerably reduce the shear strength of the seabed soil, which would eventually lead to massive settlement of the RM. In the studies conducted by Takahashi et al. (2014b), it was clearly seen that the seepage forces could reduce the bearing capacity of the foundation beneath breakwaters. The lesser density of groundwater flow vectors through the topsoil layer after the inclusion of sheet piles highlights the reduction in seepage. A similar effect was observed in the abrupt changes to the IPWP curve in Figure 4.14 at the locations of sheet pile walls. Here, the sheet piles acted as cut-off walls, which restricted the seepage of seawater through the seabed.

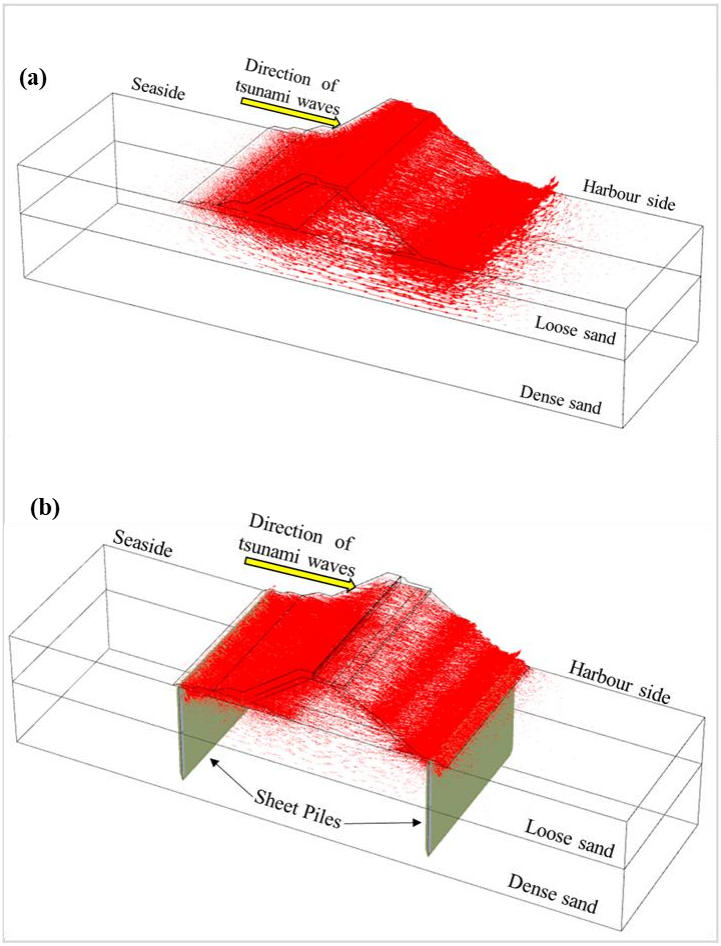

Figure 5.13 Seepage during the tsunami overflow tests (a) conventional model (b) GRM model

5.6 SUMMARY

Several RM breakwaters failed during past tsunamis. Therefore, an attempt in this study has been made to investigate the behaviour of the breakwater during a tsunami. To this end, a series of physical model tests were conducted for a scaled model of the RM breakwater, which was subjected to tsunami in a tsunami flume. Since sometimes, the tsunami height can be higher than the designed tsunami level. Hence, the overflow of the tsunami was allowed during the tests. In the test, several parameters were measured and analysed to get a clear understanding of the response of the breakwater under tsunami overflow. The failure mechanisms were analysed with the aid of analytical studies and numerical simulations. Later, countermeasures were developed to make the breakwater resilient against tsunami-induced damage.

Moreover, the effectiveness of the reinforced breakwater (with countermeasures) was evaluated by conducting the tsunami overflow tests. The same was re-examined by performing analytical studies. Further, numerical simulations were carried out to make the mechanism clearer. Based on the present study, the following conclusions are drawn,

1) The majority of the RM that stood above the sea level was scoured away due to the intense drag forces of the overflowing tsunami. However, the presence of the crown walls and gabions has wholly prevented the scouring of the reinforced breakwater. The settlement of the breakwater crest was reduced by 99.5% in the GRM model. Moreover, the lateral displacement of the crest was reduced by 96%.
2) It was observed in the physical model test on the conventional RM breakwater that the breakwater crossed the damage threshold limit of destruction during the tsunami overflow test. The sudden upraise in the water on the seaside had not only induced high seepage through the body of the breakwater but also upward buoyancy forces on the rubbles, which resulted in deep scouring and rolling down of the rubbles. The combined effects of all these forces destroyed the breakwater.
3) The replacement of armour layers with gabions, insertion of sheet piles in the seabed soils and placement of crown wall (with shear key) imparted high

resiliency to the breakwater against tsunami. The reinforced RM was observed to withstand the severe tsunami overflow without any damage. This higher resiliency was aided by the comparatively heavier gabions, which had better resistance against scouring. Also, the shear key of the crown wall unit was effective in resisting the sliding and overtopping of the crown, which protected the scouring of the crest and mound materials. Moreover, the sheet piles acted as cut-off walls that arrested the seepage through the foundation seabed soils, which prevented the decrease in shear strength (caused by seepage) of the foundation seabed soils.

4) The inclusions of sheet piles reduced seepage through the seabed by 36.4% beneath the breakwater. The mechanism involved behind the reinforcement with sheet piles was comprehended in the numerical investigation. The effects of sheet pile walls resulted in the reduction of IPWP throughout the length of the breakwater model. The provision of sheet pile walls in the foundation soil of the RM breakwater has considerably reduced the seepage flow through the upper loose sand layers of the seabed during the tsunami overflow. Hence, it can be said that the proposed reinforcing elements can be effective countermeasures to make the breakwater resilient against tsunami-induced damage.

Generally, the primary armour layer of an RM breakwater is made of concrete blocks. The proposed countermeasures, such as gabions as a replacement for armour units, could effectively reduce the carbon footprint of concrete manufacturing.

CHAPTER 6
GEOGRID-REINFORCED RM BREAKWATER

6.1 INTRODUCTION

This study could be a pioneering application of geogrids as reinforcing elements in RM breakwaters to mitigate damages from tsunamis. Geogrid layers are provided on both the seaside and harbourside to mitigate tsunami-induced damage to the breakwater. In addition, a crown wall (with shear key) is also introduced to prevent the scouring of the crest and sheet piles from preventing excess seepage through the seabed. Geogrid placement plays a crucial role in the stability of a reinforced RM breakwater. Therefore, geogrids were placed over the armour layer, and double geogrid layers were placed above and below the armour layer, as attempted in the present study.

Additionally, the effect of extending geogrid beneath the heel of the RM was also considered. Figure 6.1 depicts the details of each model with one conventional (unreinforced) model and three types of reinforced models.

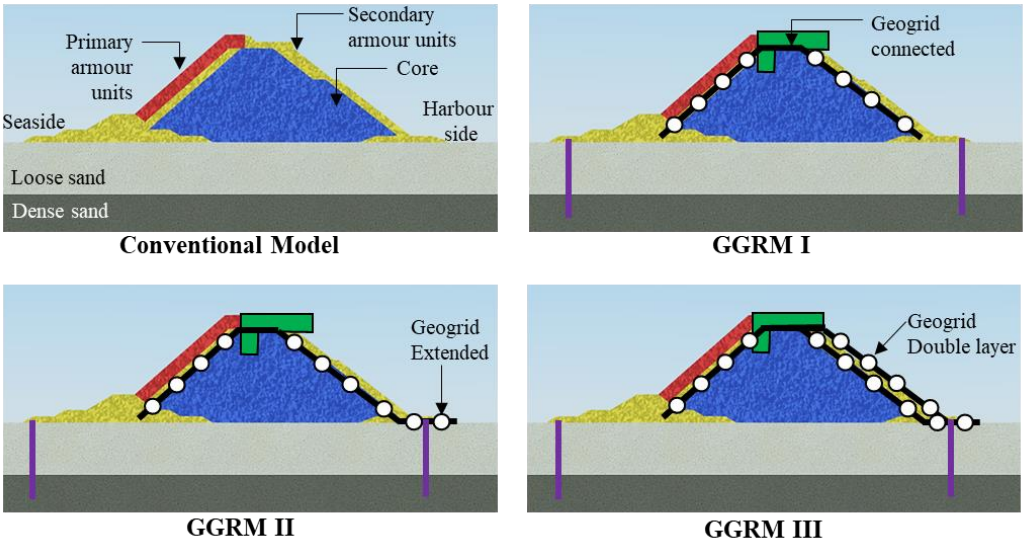

Figure 6.1 GGRM breakwater models developed for physical model tests

The study compared the performance of reinforced and conventional RM breakwaters during a tsunami. Several parameters were analysed during tsunami overflow to evaluate the effectiveness of the reinforced RM breakwater, such as reduction in settling of the crest, the resistance of the crown wall against lateral displacements and the IPWP

developed in the seabed soils. The average of the measurements taken by displacement gauges at two different locations, V1 and V2, was measured to determine the average settlement of the crest. Further, the average lateral displacement of the crest was determined by averaging the measurements taken by displacement gauges at H1 and H2.

6.2 PHYSICAL MODEL TEST

6.2.1 Settlement

The emerged breakwaters are designed with a portion that rises above the freeboard depth, which is the minimum depth required to prevent waves from overflowing. This portion of the breakwater effectively blocks tsunamis. However, if the breakwater height decreases, the tsunami will have unrestricted access to the coastal areas, putting them at risk of severe damage. The reduction in height is expressed in terms of the average settlement of the breakwater crest during tsunami overflow tests. A comparative analysis of the average crest settlement between conventional and reinforced models is presented in Figure 6.2 to evaluate their effectiveness in blocking tsunamis. The analysis results show that the reinforced models significantly reduced the average settlement of the RM breakwater compared to the conventional models. This trend demonstrates the superiority of the reinforced models in blocking tsunamis. During the tsunami overflow tests, the conventional RM breakwater underwent severe deformation, with the rubbles shifting away from the structure and settling the crest vertically. The excess seepage mainly caused this severe deformation through the breakwater and the intense lateral force exerted by the tsunami. However, the reinforced models, which incorporated geogrid, effectively resisted the displacement of the rubbles, resulting in a significant reduction in the crest settlement. This considerable reduction in settlement highlights the importance of incorporating reinforcing elements in breakwaters to enhance their performance against tsunamis.

By providing geogrid along the seaside and harbour side slopes (GGRM I), a 45% reduction in the settlement was observed, as shown in Figure 6.2. The provision of the geogrid layers has provided extra stability to the RM in resisting tsunamis. However, the excess seepage through the mound has displaced the harbourside geogrid layer from

its bottom. The seepage, in turn, resulted in rubble rolling down through the bottom region of the harbourside slope. This erosion of rubbles was overcome by extending the geogrid reinforcements beneath the heel at the harbourside. This extended part of the geogrid layer prevented it from displacing from the bottom under large seepage forces.

Consequently, in the GGRM II, an 81% reduction was observed in the vertical settlement of the crest when compared to the conventional model. However, the rubbles in the core layer were dislodged and mixed with armour layer rubbles. This rubble displacement was prevented by adding one more geogrid layer beneath the secondary armour layer along the harbourside slope. The new geogrid layer prevented the movement of core rubbles under excess seepage forces. Thus, the GGRM III demonstrated a 97% reduction in settlement of the breakwater crest. Therefore, it can be concluded that the reinforced models, particularly model III, demonstrated excellent performance in lowering the average settlement of RM breakwater when subjected to tsunami overflow.

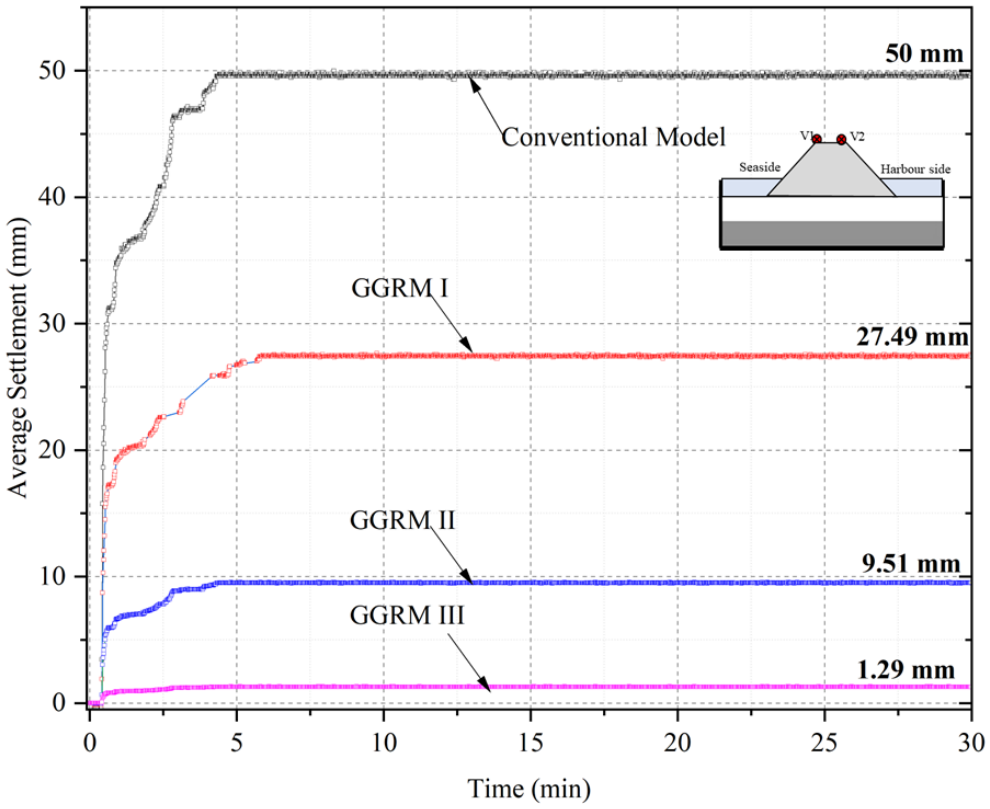

Figure 6.2 Settlement of the crest for conventional and GGRM models

6.2.2 Lateral Displacement

The lateral displacement of the crest of an RM breakwater could expose the core layer to an overflowing tsunami. As core layers are made of lighter rubbles, the rubbles in the core layer would be dislodged under the drag forces of the tsunami. Further, the excess seepage forces exerted by the seawater seeping through the body of the breakwater also result in the lateral displacement of rubbles towards the harbour side during a tsunami overflow. The tsunami exerts immense lateral forces on the mound, causing the crown wall to shift towards the harbourside. It is crucial to minimize or eliminate such lateral displacement during tsunami overflow to enhance the resilience of the breakwater. A comparison of the average lateral displacement of the crest between reinforced and conventional RM breakwater was conducted during tsunami overflow, as shown in Figure 6.3. The results indicate that the reinforced models effectively reduced the average lateral displacement of the crown wall. The geogrid layers were added on both sides of the RM to reinforce the structure. Providing a shear key beneath the crown wall and the geogrid layer on either side of RM reduced the lateral displacement of crown wall units by 69 % in the GGRM I compared to the conventional model. GGRM II demonstrated a 95 % reduction in the lateral displacement of crown wall units compared to the conventional model.

Further, the double-layered geogrid on the harbourside has reduced the dislocation of core rubbles, which was also responsible for the lateral displacement of the crown wall. Thus, the GGRM III has ultimately almost arrested lateral displacements of the crown wall. Consequently, it can be stated that the implementation of GGRM III significantly decreased both the average settlement and lateral displacement of the RM breakwater, thereby enhancing its performance under tsunamis.

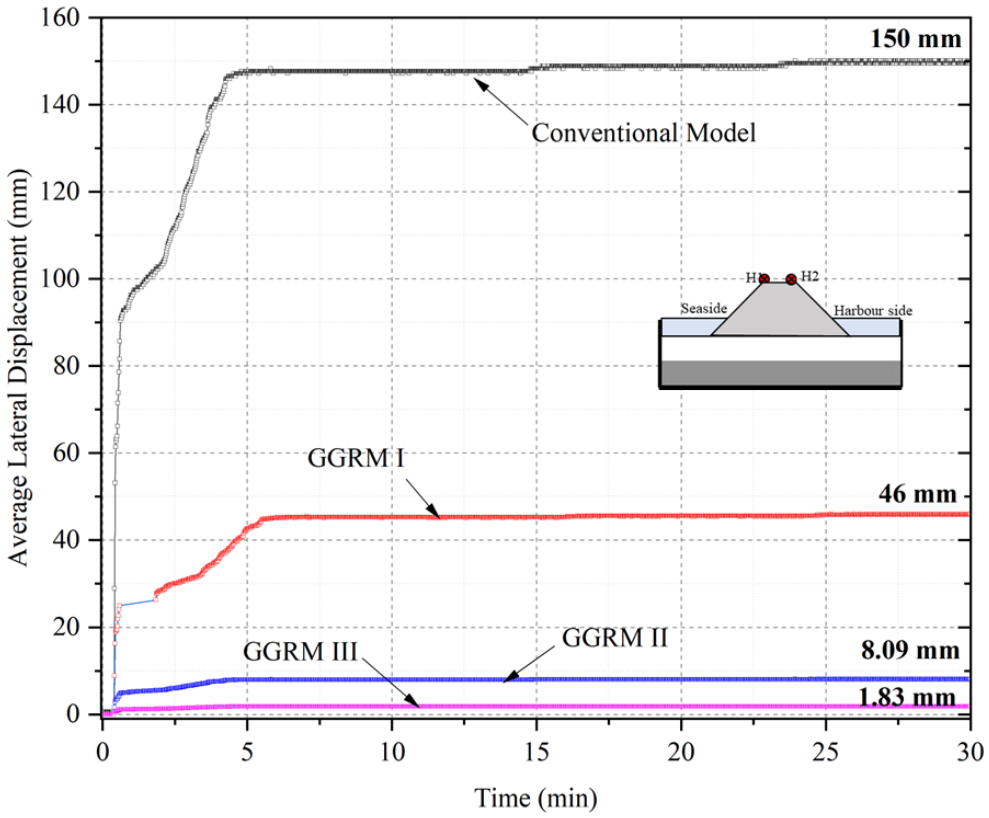

Figure 6.3 Lateral displacement of the crest for conventional and GGRM models

6.2.3 Incremental pore water pressure

Tsunamis significantly impact the stability of RM breakwater due to the additional pore water pressure they generate in the seabed soils and RM, known as IPWP. A comparison is made between conventional and reinforced RM breakwaters during a tsunami overflow to understand how reinforcement affects this pressure. The results showed that IPWP was higher on the seaside of the breakwater during the tsunami than on the harbourside. During the event of a tsunami, the seaside water level abruptly increases—the rise in water level at the seaside results in higher IPWP in the seaside seabed soils. At the same time, the water level at the harbourside will be lower due to the presence of the breakwater.

Consequently, the IPWP in the harbourside seabed soils is comparatively lesser. This significant difference in IPWP on either side of the breakwater causes instability and even failure of the breakwater if not adequately reinforced or designed. It is important to note that the IPWP affects not only the seabed soils but also the body of the RM breakwater, as the pressure difference can lead to a large volume of seepage that can

dislocate rubbles. The seepage through seabed soils reduces its bearing capacity, which can lead to the settlement of the breakwater. Therefore, it is crucial to consider the effect of IPWP in the design of breakwaters to ensure their stability during tsunami events. A 61 % difference was observed in the IPWP measured from harbourside seabed soils compared with that measured from the seaside seabed soils. The considerable difference in IPWP triggered seepage through seabed soils during tsunami overflow. Such seepage forces reduce the bearing capacity of seabed soils and eventually lead to the settlement of the breakwater. However, adding sheet pile reinforcements has reduced the IPWP, as shown in Figure 6.4 in the case of GGRM III. A similar trend was observed in other reinforced models as well. The reinforced models have shown an average 49 % reduction in the IPWP during tsunami overflow. The insertion of sheet piles into seabed soils on either end of the breakwater acted as cut-off walls that prevented seepage from the seaside to the harbourside through seabed soils, significantly reducing the IPWP.

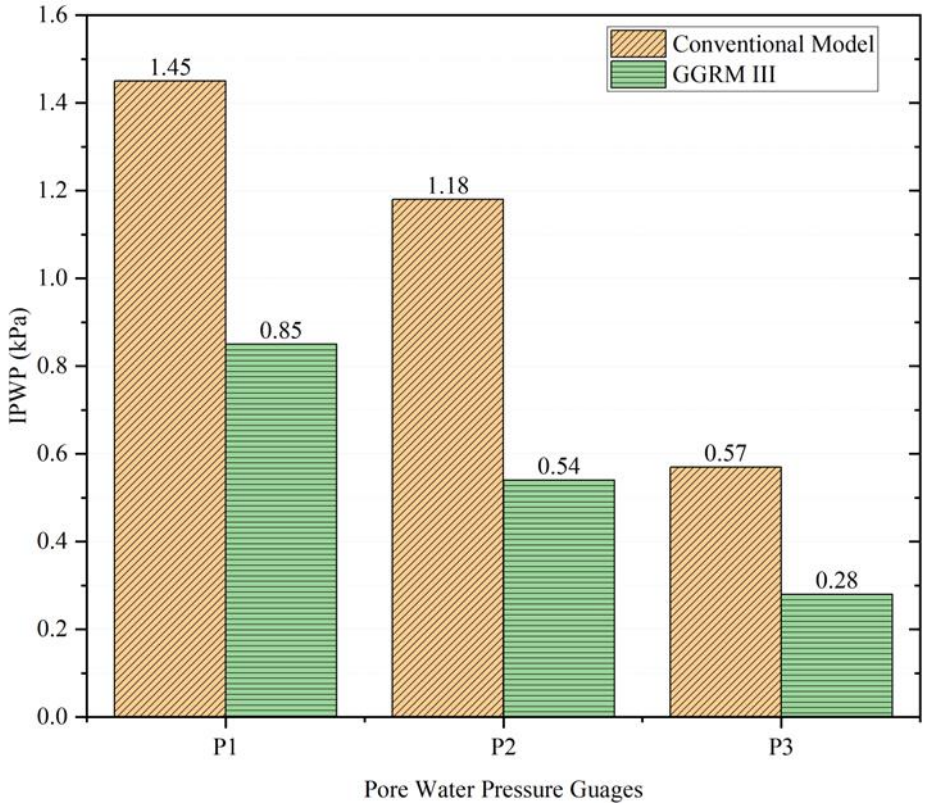

Figure 6.4 IPWP measured during the tsunami overflow for conventional and GGRM III models

6.2.4 Deformations of the Breakwater

The conventional model underwent significant deformation during tsunami overflow, as depicted in Figure 6.5. The excess seepage and intense lateral forces exerted by the tsunami caused the rubbles to dislodge even from the primary armour layer. An overflowing tsunami initiated the scouring of the crest. The armour layer on the harbour side slope of the mound was eroded under the impact of the tsunami, causing the armour and core layer rubbles to roll down towards the harbourside. A scouring of approximately 50 mm (5m in the prototype) was observed in the conventional breakwater, meaning that 96% of the breakwater's height above the freeboard depth was scoured off during the tsunami overflow. This enormous scouring reduced the functionality of breakwater in blocking overflowing waves, leading to potential flooding of coastal areas. As seen in Figure 6.2 and Figure 6.3, scouring of the RM occurred rapidly, indicating that the breakwater could not function immediately after the impact of the tsunami.

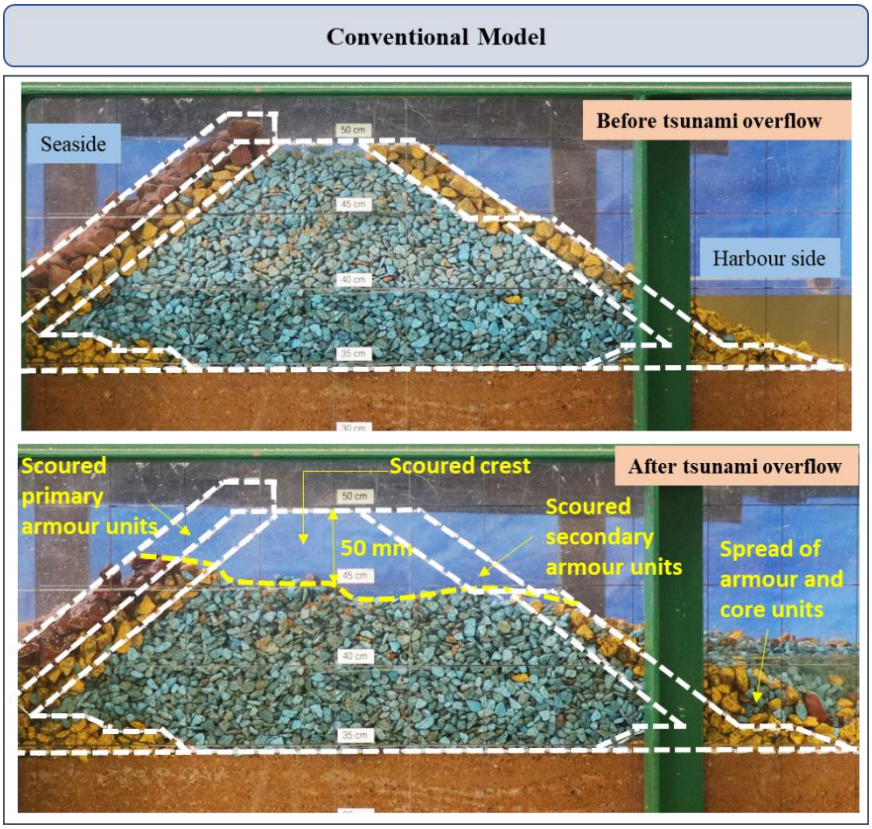

Figure 6.5 Deformations in the conventional model when subjected to tsunami overflow

Adding reinforcing elements to the conventional breakwater enhanced its ability to withstand tsunamis. The placement of geogrid layers created an interlocking mechanism with the rubbles. The aperture size of the geogrids was selected so that the core layer rubbles would not pass through it. With the geogrids placed along the slopes of the mound, the plane of the geogrid layer was oblique to the direction of the tsunami, allowing a significant portion of the excess lateral force exerted by the waves to be transferred to the tensile strands of the geogrid layer. During tsunami overflow, the rubbles were pushed against the tensile strands of the geogrid, creating further interlocking and transferring the stresses to the geogrid layer. Additionally, the dislocation of the rubbles on the harbourside armour layer due to the impact of the overtopped tsunami bore was minimized in the geogrid-reinforced models.

In the GGRM I, the harbourside and seaside geogrid layers prevented the displacement of rubbles due to their interlocking mechanism. This reinforcement method improved breakwater performance during a tsunami overflow than the previous model. However, the bottom area of the harbour side geogrid layer was still displaced, causing the rubbles from the core and armour layers to roll down through the heel of the breakwater. The forces exerted by the overflowing tsunami and excess seepage through the body of the breakwater resulted in the erosion of rubbles through the breakwater heel region. Despite this, placement of the crown wall (with a shear key) prevented scouring of the crest during the tsunami overflow, as shown in Figure 6.6.

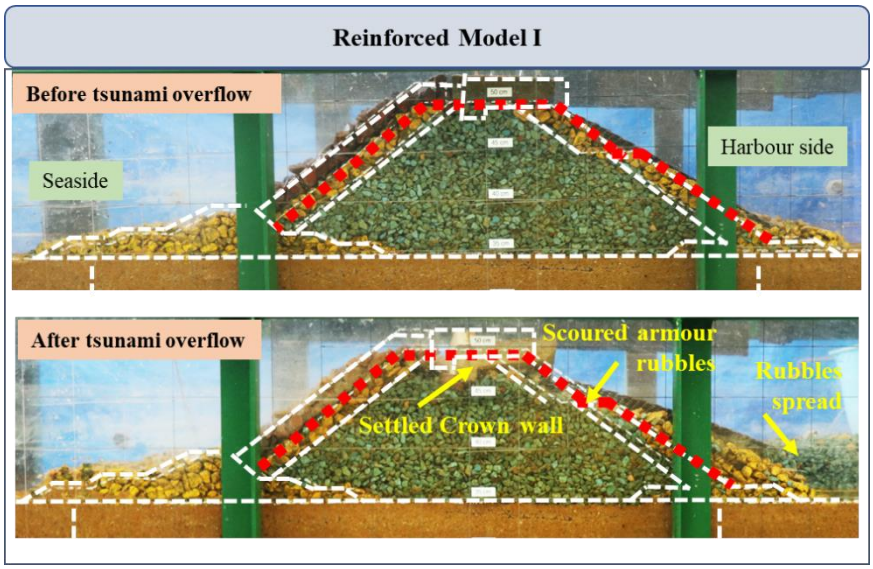

Figure 6.6 Deformations in GGRM I model when subjected to tsunami overflow

The uplift of the geogrid layer from the heel of the breakwater can be effectively prevented by extending the geogrid beneath the heel of the mound, as attempted in GGRM II. As shown in Figure 6.7, the new model was more resilient against tsunamis, and the heel of the breakwater remained intact after the tsunami overflow. However, the crown wall was tilted, and the tsunami overflow dislocated core rubbles at the crest. The excess seepage under tsunami overflow dislodged rubbles from the core layer and moved towards the harbourside. The overflowing tsunami also displaced the armour layer along the harbourside slope, causing scouring where the wave impacted. Furthermore, the shear key in crown wall units prevented the sliding of the crown wall, thereby protecting the RM crest from scouring during tsunami overflow.

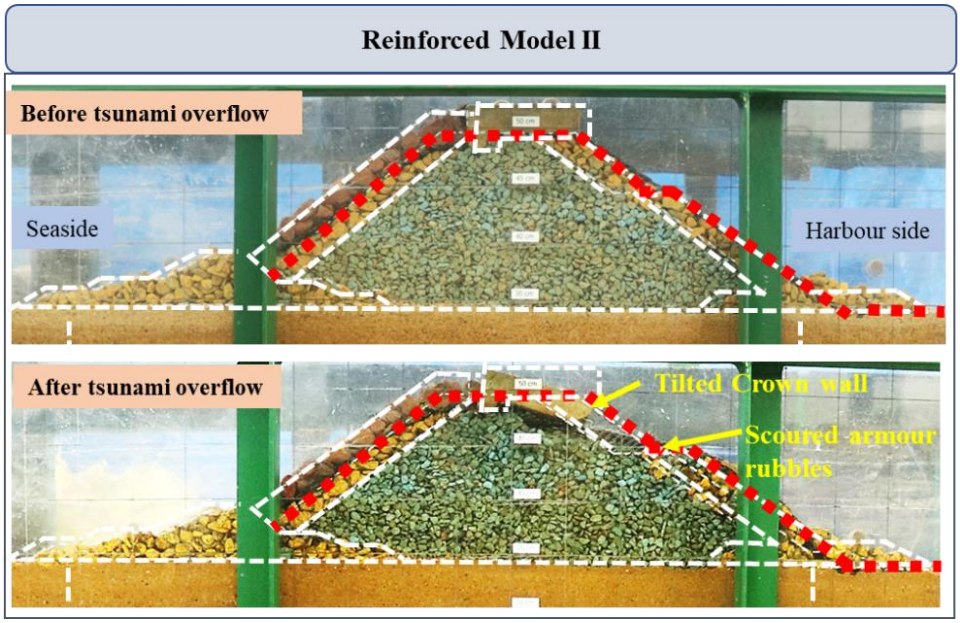

Figure 6.7 Deformations in the GGRM II model when subjected to tsunami overflow

The dislodging of rubbles from the core layer can be prevented by providing an additional layer of geogrid separating the core and the armour layer on the harbourside, as attempted in GGRM III. The goal of the GGRM III was to arrest the dislocation of rubbles from the core layer. The core layer was protected by adding an extra layer of geogrid between the core and secondary armour layer on the harbourside of the breakwater. The results showed that this reinforcement model helped the breakwater remain intact without significant deformation after being subjected to a tsunami overflow. The additional geogrid layer above the core prevented further scouring from

secondary armour layer rubbles during the tsunami, as shown in Figure 6.8. Thus, the GGRM III was considered the most efficient in resisting damage caused by tsunamis on RM breakwaters.

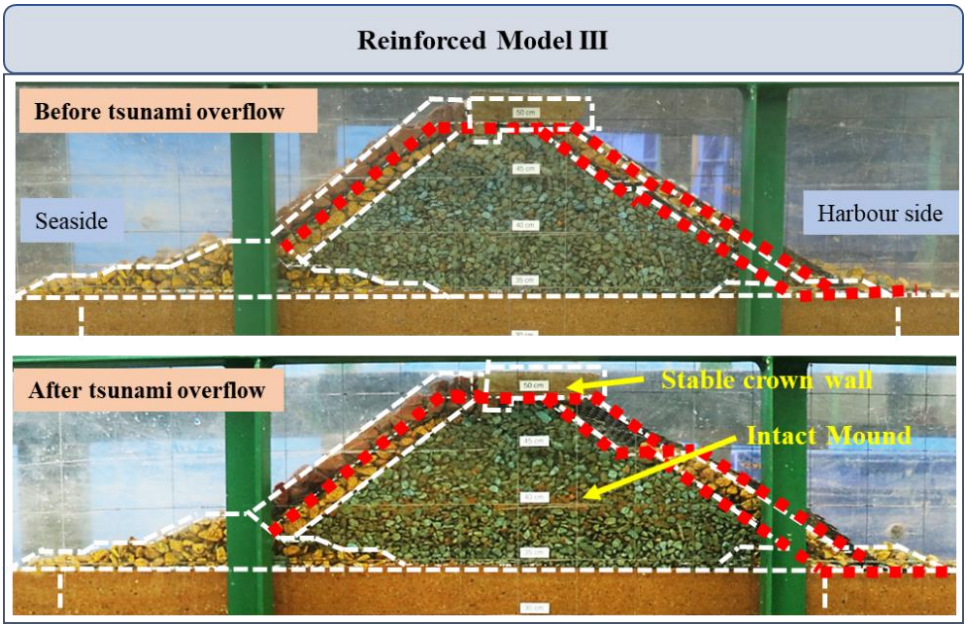

Figure 6.8 Deformations in the GGRM III model when subjected to tsunami overflow

Figure 6.9 shows a comparison of the deformation of the RM breakwater for each of the models after tsunami overflow. The emerged portion of the conventional RM breakwater was scoured away during the tsunami overflow. However, the effect of the tsunami was feeble below the MSL. The portion below the sea level was unaffected due to the extra stability offered by the hydrostatic forces from harbourside water, acting in the opposite direction to the tsunami. Additionally, the scoured rubbles from the crest were rolled down towards the harbourside seabed, effectively increasing the width of the breakwater towards the bottom. Thus, the scouring of RM occurred rapidly at the beginning of tsunami overflow and reached equilibrium, where further progression in scouring was not observed. In GGRMs I and II, the crown wall settled during tsunami overflow. The dislocation of rubbles from the core layer beneath the crown wall was a primary reason behind the settling of the crown wall. Even though tilted, the crown wall was functional in protecting the crest region of RM. The provision of shear key beneath the crown wall has prevented its lateral displacement significantly in the reinforced models. GGRM III efficiently prevented tsunami-induced damages on the RM

breakwater without undergoing significant deformation. The crown wall unit in this model remained stable without displacements even after tsunami overflow. Further, the dislocation of rubbles from the core layer was entirely arrested by the geogrid layer over the core layer.

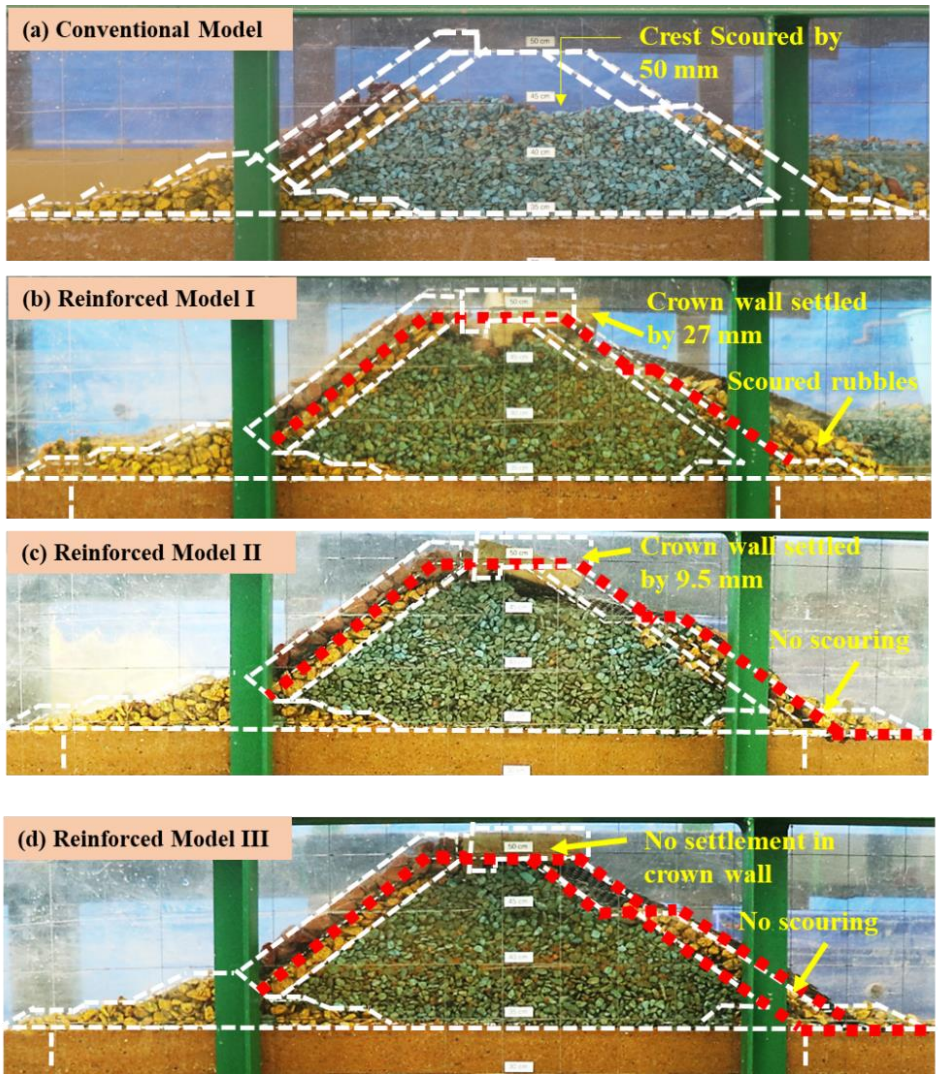

Figure 6.9 Comparison of conventional and GGRM models after tsunami overflow.

6.3 ANALYTICAL STUDY

Damage parameters were utilized to quantify the degree of damage that occurred on the breakwater before and after the tsunami. The two damage parameters considered in the present study are the relative displacement of armour units (Rd) and the relative eroded area (S).

6.3.1 Relative Displacement

The relative displacement of armour units can be described as a fraction of the total number of armour units. The secondary armour units along the harbourside slope (yellow rubbles) were accounted for when estimating this parameter. In the context of breakwater stability, a lower value of R_d indicates a more stable structure. The conventional breakwater experienced significant scouring, with nearly 86% of the total armour units being displaced during tsunami overflow, as demonstrated in Figure 6.10. The first reinforced model significantly reduced the value of R_d. Providing a geogrid layer on either side of the RM improved the stability of the breakwater. A notable reduction of 18% was observed in the GGRM I, where the geogrid layers on either side of the mound prevented armour rubble dislocation to an extent. However, some rubbles were scoured through the heel of the breakwater, leading to a settlement in the crest region. This erosion of rubbles was prevented by extending the geogrid beneath the heel of the RM breakwater. Therefore, the second GGRM showed more excellent stability, with a reduction of 40% in the displacement of armour units when compared to the conventional type. The third GGRM proved to be the most effective, with an impressive reduction of 86% in the displacement of armour units where the placement of a double layer of geogrid along the harbour side slope offered better stability to the mound.

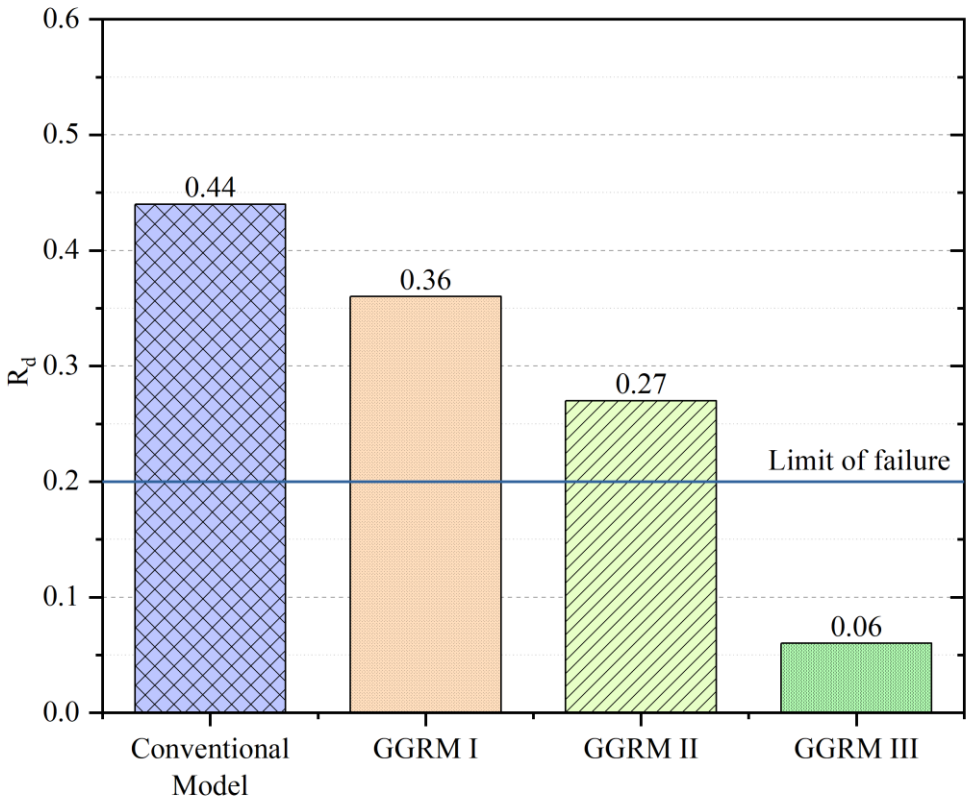

Figure 6.10 Relative displacements of armour units in conventional and GGRM models after the tsunami overflow

6.3.2 Relative Eroded Area

The relative eroded area (*S*) is a metric used to evaluate the damage to RM breakwaters. It is calculated by expressing the fraction of eroded armour area as a ratio of the average cross-sectional area of the eroded volume of the armour layer to the nominal size of an armour unit. The *S* values determined for both un-reinforced and reinforced breakwater models are depicted in Figure 6.11. The parameter was estimated by considering the displacement of secondary armour rubbles. It was observed that the conventional RM breakwater model was fully damaged after the tsunami overflow. However, the introduction of reinforcements reduced the *S* value. The first GGRM considerably reduces the *S* value due to the geogrid placement on the seaside and harbourside slopes. In the second GGRM, there was a significant reduction of 40% in the damage to the harbourside armour layer compared to the conventional model. GGRM III with double-layered geogrid has offered better resistance to tsunami-induced damages by

demonstrating an 86% reduction in *S* compared to its conventional counterpart. The *S* values estimated for all models except the third GGRM exceeded the threshold value of destruction. The threshold *S* value beyond which it represents destruction ranges between 12 and 18, depending on the inclination angle of the armour layer (Campos et al. 2020b). The third GGRM withstood the tsunami overflow without undergoing any deformations. Figure 6.11 demonstrates that the third GGRM is the most effective in resisting damage induced by tsunami overflow.

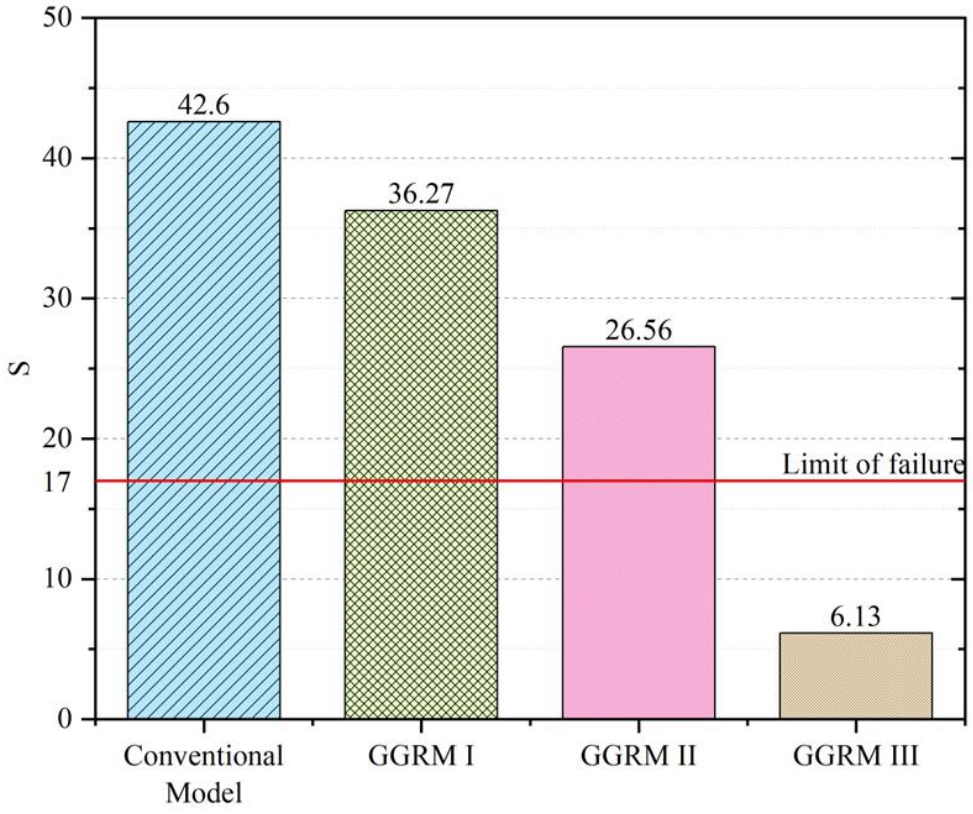

Figure 6.11 Relative eroded area of armour units in conventional and GGRM models after the tsunami overflow

6.4 PROFILE MAPPING

Figure 6.12 describes the results of scanning the profiles of RM breakwater models after being subjected to tsunami. The first GGRM reduced scouring volume by providing the geogrid layers on the seaside and harbourside. The estimated scouring volume in GGRM I was 0.0017 m^3 (1700 m^3 in the prototype). The extra stability

offered by extending the geogrid layer beneath the heel of RM in the second reinforced model further reduced the scouring volume to 0.0006 m^3 (600 m^3 in the prototype), which is less than half of the previous model. The third model was observed to be the most efficient, withstanding the tsunami impact without significant deformation and a significantly low scouring volume of 0.0001 m^3 (100 m^3 in the prototype). The data on scouring volume shows that the GGRM III is the most effective in mitigating damage to the RM breakwater caused by tsunamis.

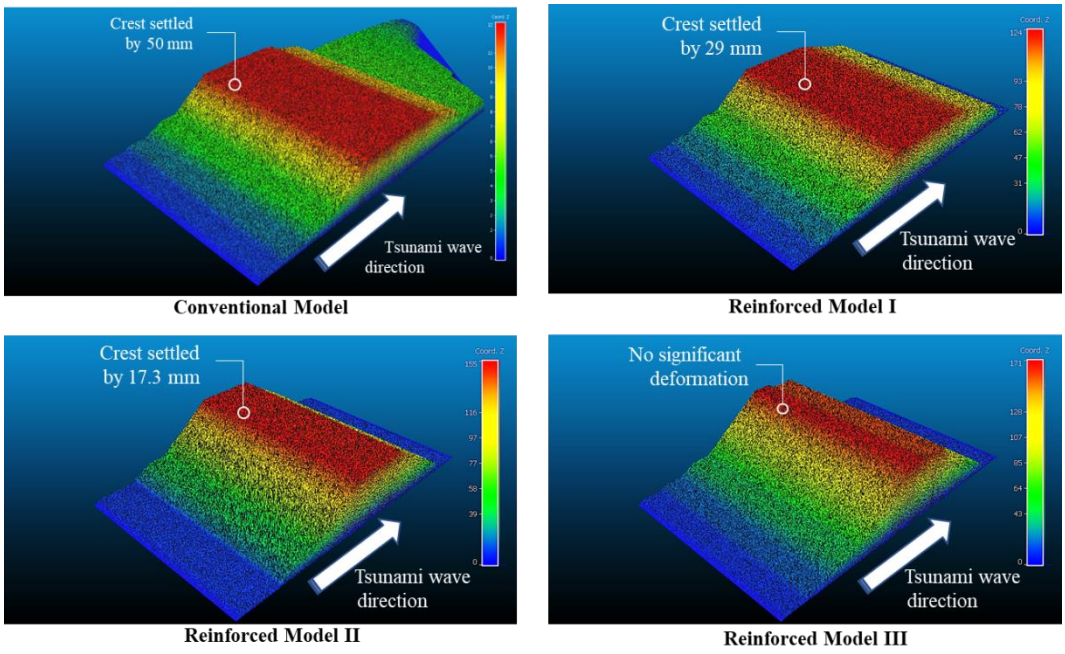

Figure 6.12 Profile of breakwater models after tsunami overflow

Figure 6.13 compares the scour depths of different RM breakwater models after being exposed to tsunamis. The relative depth of every point on the RM breakwater measured after the tsunami overflow concerning its initial position before the tsunami is depicted. It was evident from the scour depth profile that the crest of the RM breakwater was vulnerable to scouring during tsunami overflow. The blue band towards the harbour side represents the piling up of rolled-down rubbles on the harbour side of the breakwater. However, the geogrid layers used in GGRM I have reduced the rolling down of rubbles, as seen by the reduction in the width of the blue band.

The scour depth profile of GGRM II also follows a similar trend to GGRM I at the crest region. However, the scouring depth is reduced by 65% compared to the first reinforced model. Further, extending the geogrid below the heel of the RM has prevented erosion

of rubbles through the heel, as happened in the first reinforced model. It is evident from the disappearance of the blue band in the scour depth profile of the second GGRM. GGRM III has deformation limited to the crest region of the mound, with a noticeable 86% reduction in scour depth compared to the previous model, represented by the red band. It could be inferred that the third GGRM had no significant deformation along the slopes of the mound and had negligible settlement along the crest region, which is also evident from the thin red band in its scour depth profile.

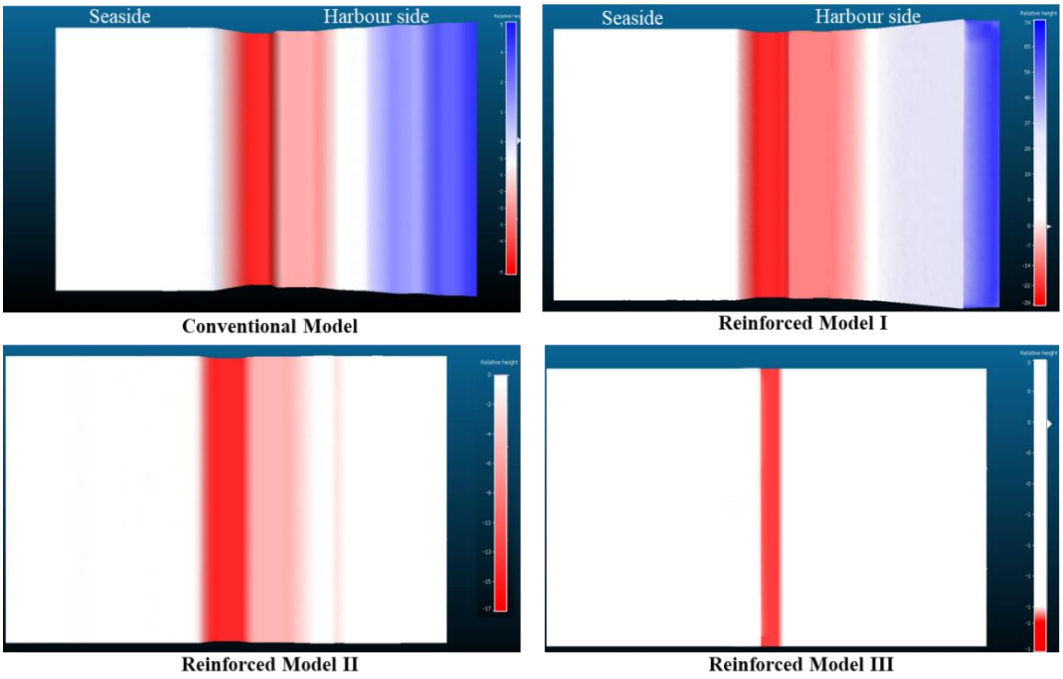

Figure 6.13 Scour depth profile of breakwater models (all dimensions are in mm)

6.5 NUMERICAL SIMULATION

The study uses PLAXIS 3D software to perform a numerical analysis of conventional and reinforced models. This analysis aimed to understand the reasons behind the failure of conventional RM breakwaters during tsunami overflow. Further, the effectiveness of reinforced RM breakwaters was also reconfirmed using numerical analysis. PLAXIS 3D's flow analysis module examines seepage flow and the resulting deformations. The geometric details of a scaled-down prototype were used to model the RM breakwater. The seabed was represented as a dense bottom layer and a top layer of loose sand. This representation is shown in Figure 6.14. The RM breakwater was modelled using constitutive soil models, which are mathematical models that describe the mechanical

behaviour of soils under different loading conditions. The use of constitutive soil models has been previously demonstrated to be a practical approach in modelling RM breakwaters by other researchers (Cihan et al. 2012; Cihan and Yuksel 2011, 2013). The results of this study provide further evidence of the effectiveness of this approach in understanding the failure mechanisms of RM breakwaters under tsunami overflow. The soil was modelled as 1.8 m long and 0.5 m wide with bottom and top layers of 0.15 m and 0.20 m in thickness, respectively. The geometry of the conventional model was discretized into finer meshes with 27,021 tetrahedral elements and 41,433 nodes. In the reinforced models, the sheet piles were modelled using six nodded plate elements, and geogrid layers were modelled using six nodded geogrid elements. The reinforced model was discretized into 26,060 elements and 42,747 nodes. The interaction of geogrid and sheet piles with surrounding soils was simulated by adding 12 nodded interface elements. The permeability of interfaces was assigned such that the sheet piles were impermeable to groundwater flow and geogrids were permeable to seepage.

Additionally, hydraulic boundary conditions that allow seepage were defined along the exposed surface of the mound and seabed soils. The tsunami overflow was defined as a water level of 150 mm above the seabed overflowing over the RM breakwater. The numerical model defined the water depth before tsunami overflow as 50 mm above the seabed level. The numerical model thus focused on simulating the tsunami induced seepage through breakwater and seabed, however, scouring of the breakwater was not simulated.

The geogrid layer was defined using geogrid elements on surfaces drawn over the seaside and harbourside slopes of the RM. Three sets of geogrid surfaces were created for the three different reinforced models. Each set of geogrid surfaces replicated a similar configuration to that used in physical model tests. However, Figure 6.14 represents only the first reinforced model. All three models have adopted the same reinforcing elements apart from the changes in geogrid layer configuration. The crown wall was modelled as a non-porous linear elastic material. The properties of materials to model the seabed soils, breakwater and geogrid layers pertains to the properties mentioned in Table 3.2, 3.4 and 3.5 respectively.

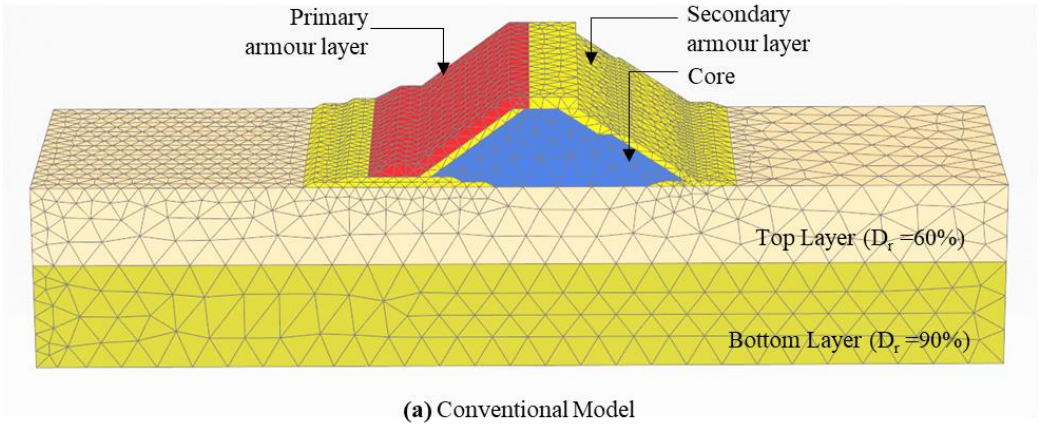

(a) Conventional Model

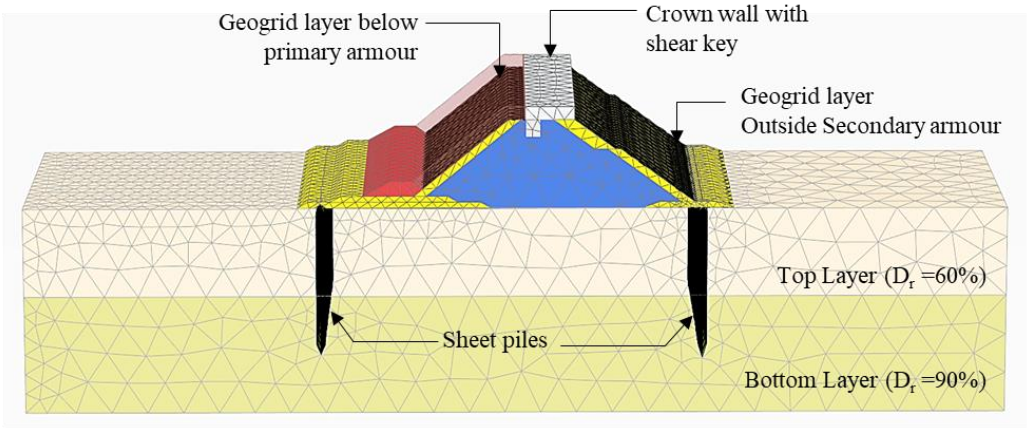

(b) Reinforced Models

Figure 6.14 Discretized geometry of numerical model (**a**) conventional (**b**) GGRM models.

6.5.1 Stability Analysis

The safety analysis calculation mode assessed the stability of both conventional and reinforced breakwater models. In this mode, the strength parameters, such as the angle of internal friction (ϕ), was reduced from the material input properties until failure occurred. Although erosion was not modelled, the factor of safety was evaluated to determine the initial stability of the intact breakwater for the specific condition when water level difference exist between the seaside and harbour side of the breakwater. The comparison between conventional and reinforced designs aimed to highlight the stability gains from reinforcement, providing essential insights for the initial phase. As a result, the displacement values obtained from the model in the safety analysis are unrealistic. On the other hand, the pattern of incremental displacements can give an

overview of the critical failure surfaces. Figure 6.15 displays the incremental displacement contours in the lateral direction for conventional and reinforced models during tsunami overflow. Although the displacement values in the model are not substantial, the pattern of contours indicates the failure surface. The colour bands represent the displacements, with the minor displacement denoted by blue and the most severe displacement by red. It can be concluded that adding reinforcements to the RM breakwater improved its stability. The improvement in the stability of the RM breakwater, when the seaside and harbourside geogrids were provided is evident from the reduction of red contours in GGRM I. However, as seen in GGRM I, the breakwater heel remains unstable, which was addressed by extending the geogrid beneath the heel at the harbourside. Among the reinforced models, GGRM III, with a double layer of geogrid placed along the harbourside slope, was found to be the most stable during tsunami overflow.

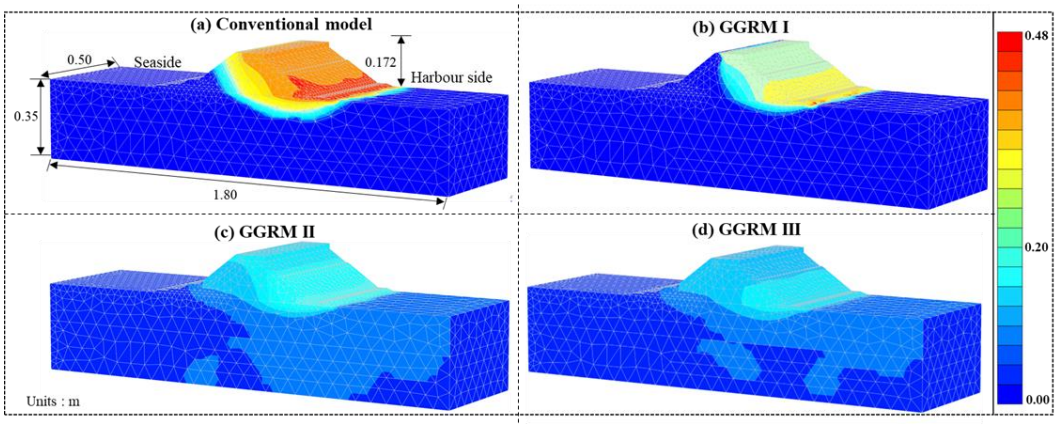

Figure 6.15 Stability analysis of conventional and GGRM models subjected to tsunami overflow

The global factor of safety for both the conventional and reinforced RM breakwaters was calculated for the tsunami overflow condition. This calculation was performed using the strength reduction approach. The cumulative sum (ΣM_{sf}) represents the factor of safety at any stage. Figure 6.16 displays the safety factor estimated for the conventional and reinforced RM breakwater models. As the factor of safety was calculated using the strength reduction method, it can be seen that the available strength of the conventional model was insufficient to withstand even a slight reduction in c and φ values during a tsunami overflow. It was evidenced by the near-to-unity ΣM_{sf} values

in the first column of the graph. The GGRM I could withstand the tsunami overflow more effectively than the conventional model, which experienced immediate failure. However, the safety factor for the first GGRM remained below 1.5. GGRMs II and III demonstrated significant stability during tsunami overflow conditions. The third GGRM, which featured two layers of geogrid along the harbourside slopes, was observed to be the most effective countermeasure to mitigate tsunami-induced damage on RM breakwaters.

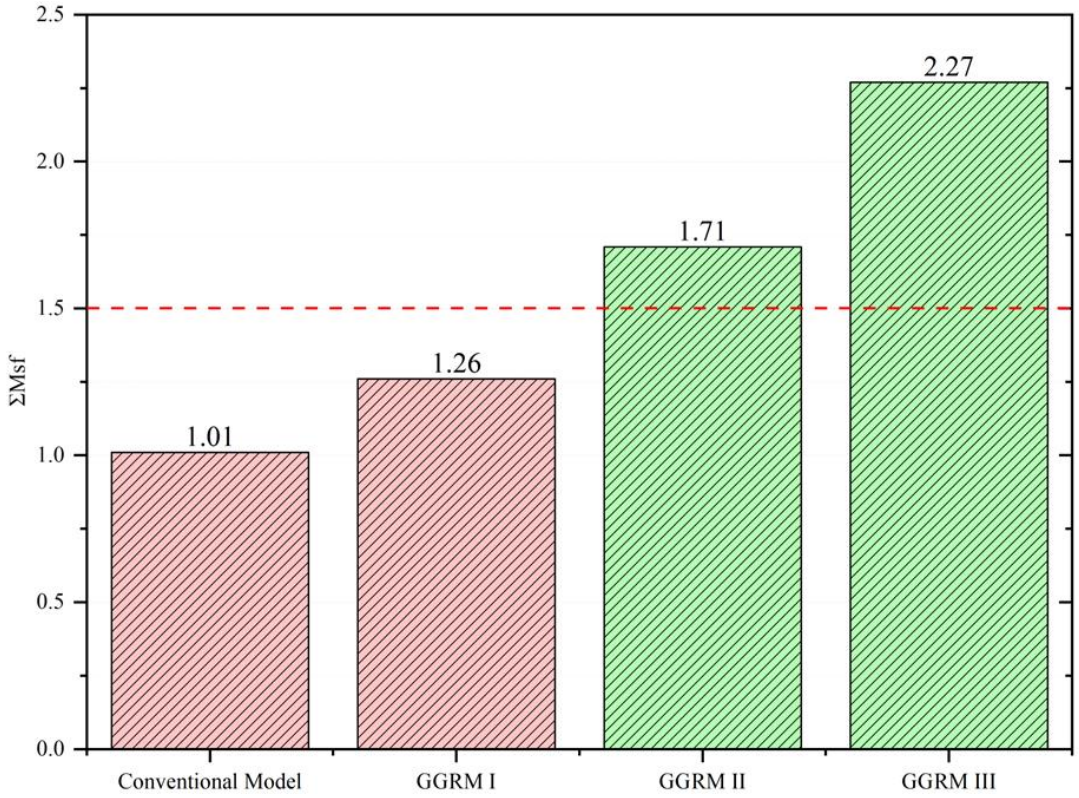

Figure 6.16 Factor of safety of conventional and GGRM models subjected to tsunami overflow

6.6 SUMMARY

The study proposed novel techniques to reinforce a conventional RM breakwater to mitigate tsunami-induced damages. A series of physical model tests have been conducted to understand the behaviour of a conventional RM breakwater when subjected to tsunami. Further, the proposed reinforced models were tested under the same conditions to ascertain the performance of the reinforced RM breakwaters under tsunami overflow. Three-dimensional numerical analysis was performed on all the

models to reconfirm the effectiveness of the proposed countermeasures. The following inferences were drawn from the comprehensive study:

a) The crest of conventional RM breakwater was scoured away by nearly 50 mm (5 m in prototype) when subjected to tsunami. The freeboard height of the prototype breakwater was 5.2 m. Consequently, most of the emerging portion of the breakwater was eroded by tsunami overflow.
b) With the addition of novel reinforcement techniques, the RM breakwater displayed better performance under tsunami overflow. The proposed reinforcements were geogrid layers on the sides of the mound, sheet piles in the seabed at either end and a crown wall (with a shear key) on top of the mound.
c) Three reinforced models were studied, focusing mainly on the effectiveness of the placement of the geogrid layer. Crown walls (with shear key) and sheet piles in seabed were used in all three models. The provision of geogrid layers laid on the harbourside and seaside slopes of the mound (GGRM I) was one of the crucial factors that improved breakwater stability. Further, extending the geogrid layer of harbourside slopes (GGRM II) improved the stability of the breakwater by preventing the erosion of rubbles through the heel. Finally, providing a double geogrid layer along harbourside slopes (GGRM III) was the most effective geogrid placement.
d) The GGRM III reduced the vertical settlement of the crest by 97.4% and arrested lateral displacement by 98.8%. The shear key embedded in the body of the breakwater offered better resistance to the crown wall against lateral forces exerted by the tsunami. The provision of sheet piles reduced the excess seepage through the seabed, thereby preventing any reduction in seabed soil strength beneath the RM breakwater. The IPWP measured beneath the breakwater models in the seabed was found to be reduced by 54.2% in the GGRM-reinforced models.
e) In the numerical analysis, the third GGRM was observed to have the highest stability (2.2 times the factor of safety of the conventional model) against the large destabilizing forces during tsunami overflow.

CHAPTER 7
WRAP-FACED GEOGRID REINFORCED RM BREAKWATER

7.1 INTRODUCTION

The proposed approach involves the strategic implementation of wrap-faced geogrids to reinforce the RM, the addition of a shear-keyed crown wall for enhanced breakwater crest protection, and the insertion of sheet piles to control seepage through the seabed. Extensive evaluations, including tsunami overflow tests, analytical assessments, and numerical simulations, were conducted to assess the effectiveness of these reinforcing elements thoroughly. The findings indicate that the proposed technique significantly fortifies RM breakwaters, enabling them to withstand level 1 tsunamis without experiencing significant damage. This research contributes essential insights to the development of resilient coastal defence systems, emphasising the importance of innovative design strategies in safeguarding coastal regions from the devastating impact of tsunamis.

7.2 PHYSICAL MODEL TEST

7.2.1 Settlement

The settlement of the breakwater crest is a critical factor that reduces the exposed height of the breakwater, allowing the incoming tsunami to access the harbour side more easily. The settlement analysis revealed that 39% of the total breakwater height was scoured during the tsunami overflow, as depicted in Figure 7.1. In the conventional breakwater, excess seepage through the breakwater body dislodged the armour rubbles, eventually exposing the core rubbles, which were then severely scoured. In contrast, the WGRM model demonstrated improved stability against seepage forces. The interlocking of geogrid and rubbles, combined with the lateral confinement of the slopes by the wrapped face of the geogrid layers, enhanced the breakwater's stability. With a substantial 97.5% reduction in the settlement, the seaside and harbour slopes of the RM remained intact within the wrapped geogrids throughout the prolonged tsunami overflow, markedly improving the stability of the crest.

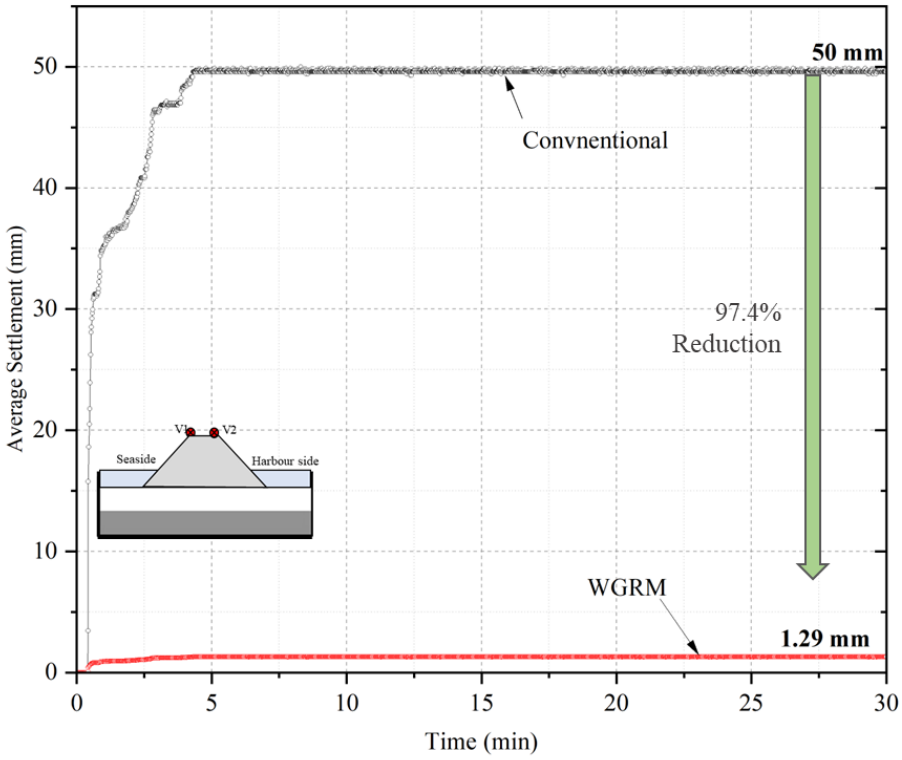

Figure 7.1 Settlement of the crest for conventional and WGRM models during tsunami

7.2.2 Lateral Displacement

The displacement of the breakwater crest was meticulously monitored and quantified using the measured lateral displacement from the crest of the RM breakwater. Notably, the average displacement between either end on the crest (was significantly more prominent in the conventional breakwater. The total width of the conventional breakwater crest was scoured away, indicated by a value exceeding unity in Figure 7.2. Tsunami-induced damages on conventional breakwaters manifested abruptly, with a significant portion of the breakwater exposed above sea level being scoured off within the initial 5-minute duration of the tsunami overflow.

In contrast, the WGRM model effectively mitigated the shift in the crest region. The presence of the crown wall with shear key contributed to enhanced resistance against tsunami forces, safeguarding the core layer rubbles from exposure to the drag forces of the overflowing tsunami. A remarkable reduction of more than 99.15 % in the lateral displacement highlights the success of the proposed WGRM model in withstanding

prolonged tsunami overflow without undergoing deformation. This addresses a critical mechanism behind the failure of tsunami breakwaters, exemplified by the past failure of structures like the Kamaishi breakwater.

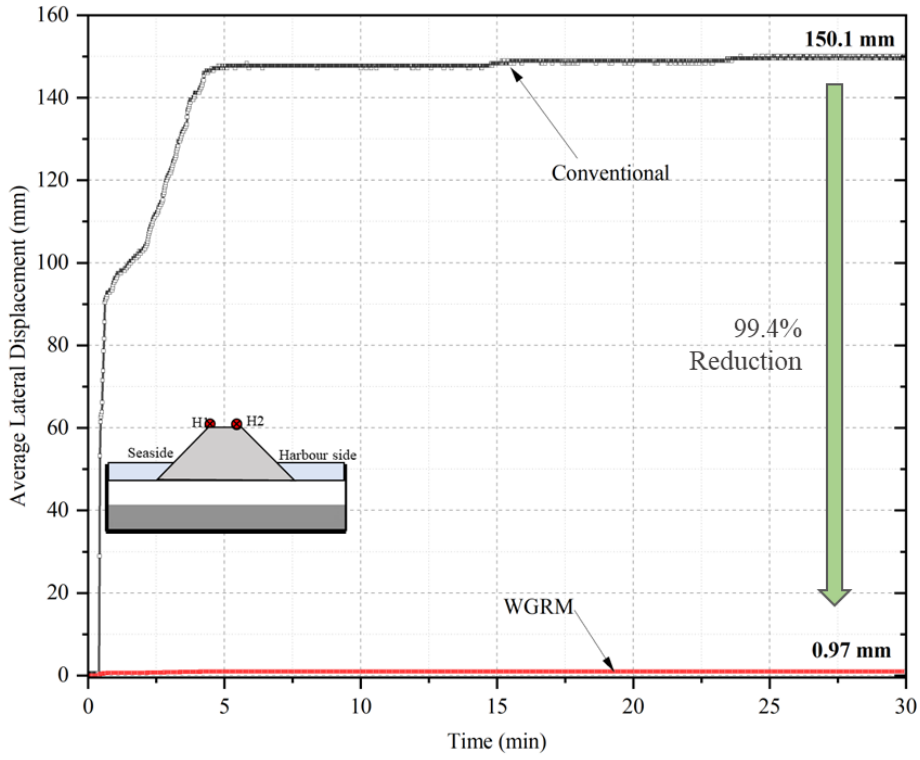

Figure 7.2 Lateral displacement of the crest for conventional and WGRM models

7.2.3 Incremental pore water pressure

The incoming crest of the tsunami rapidly elevates the sea level on the seaside side of the breakwater, creating a substantial water head differential between the seaside and harbour sides. This differential induces excess seepage through both the breakwater and seabed soils. In conventional breakwaters, this phenomenon leads to higher pore water pressure (IPWP) in the seabed soils, as depicted in the measured IPWP plotted in **Figure 7.3**. The excess pressure in the seabed soils, caused by steep gradients between water pressure on the harbour side and the sea sides of the breakwater, can dislodge soil grains, resulting in piping failure of the foundation.

High tsunami heads on the seaside resulted in elevated IPWP on both the sea and harbour sides in both conventional and reinforced models. However, the WGRM

model, incorporating sheet piles, effectively curtailed seepage through the loose seabed beneath the mound. In the pressure gauge P2, positioned below the mound, a significant 42.37 % reduction in PWP was observed. This reduction in the steep gradient between the two sides indicates lower seepage through the seabed soils in the WGRM model. The proposed insertion of sheet piles at either end of the breakwater proved efficient in mitigating seepage under prolonged tsunami overflow—a critical failure mechanism observed in the past failures of tsunami breakwaters.

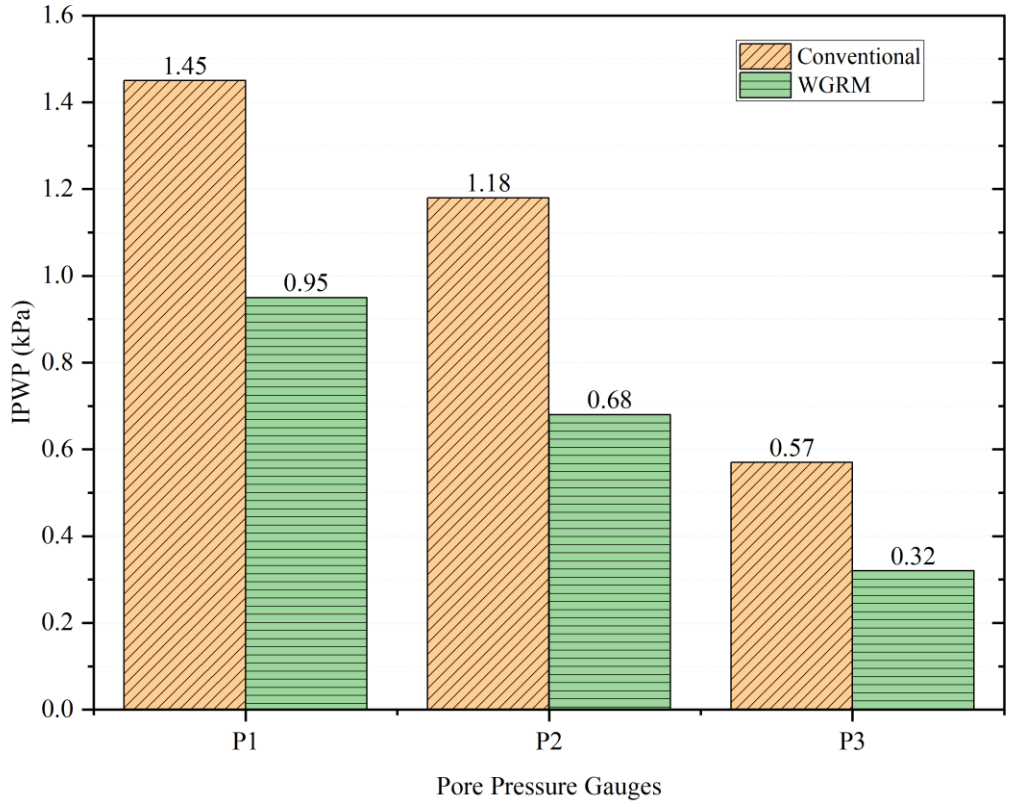

Figure 7.3 IPWP measured during the tsunami overflow for conventional and WGRM III models

7.2.4 Deformations of the Breakwater

The conventional model faced severe destruction due to the overwhelming impact of the overflowing tsunami. Approximately 40.9% of the exposed breakwater height was entirely scoured during the tsunami overflow. The dislodged rubbles were not only scoured but also rolled down and upheaved in the harbour seabed floor, illustrated in

Figure 7.4. This upheaval of the rolled-down rubbles increased the effective width of the breakwater, subsequently reducing further scouring.

Observations reveal that nearly 0.05 m of the breakwater height was scoured after the tsunami overflow. Even the heavier primary armour stones (depicted in red) were forcefully dragged towards the harbour side, succumbing to the colossal drag forces exerted by the overflowing tsunami.

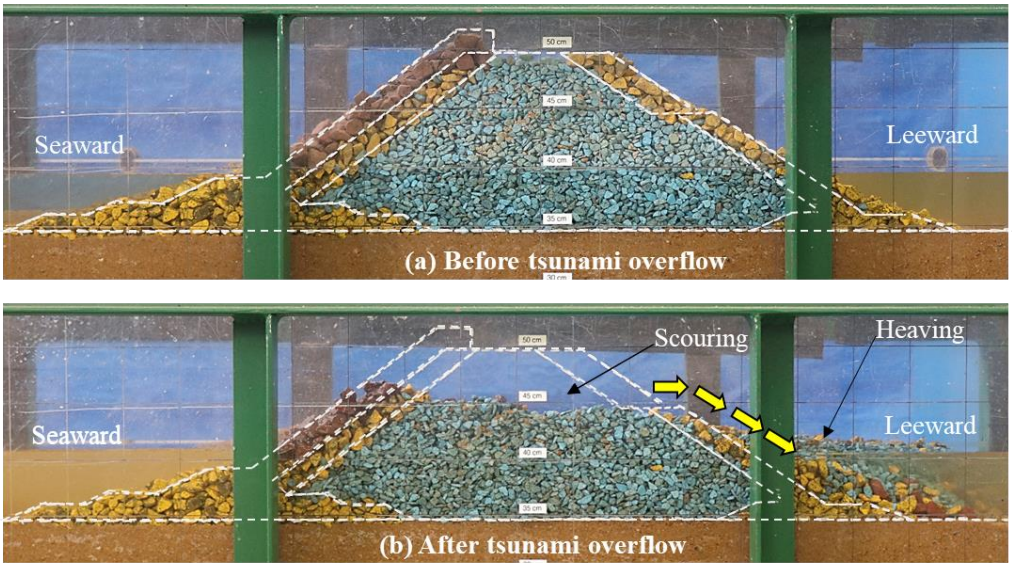

Figure 7.4 Deformations in the conventional model when subjected to tsunami overflow

In contrast, the WGRM model exhibited remarkable resilience throughout the tsunami overflow tests. The wrapped geogrid layers shielded the armour layer of the RM in the WGRM model, ensuring protection and stability. Despite the reduction in the total width of the breakwater by omitting the primary armour layer, the added stability provided by the geogrid reinforcements maintained the RM's integrity, as depicted in **Figure 7.5**.

Moreover, the shear key incorporated into the crown walls effectively withstood the lateral thrust exerted by the tsunami, preventing deformation. The impact of the overflowing tsunami bore on the harbour slopes of the mound caused the displacement of armour units in the conventional model. However, in the reinforced model, the confinement of armour units inside the geogrid wraps, with an aperture size smaller

than that of the core rubbles, prevented their dislocation. The synergistic effect of these reinforcements successfully preserved the structural integrity of the RM against potential failure mechanisms induced by the overflowing tsunami.

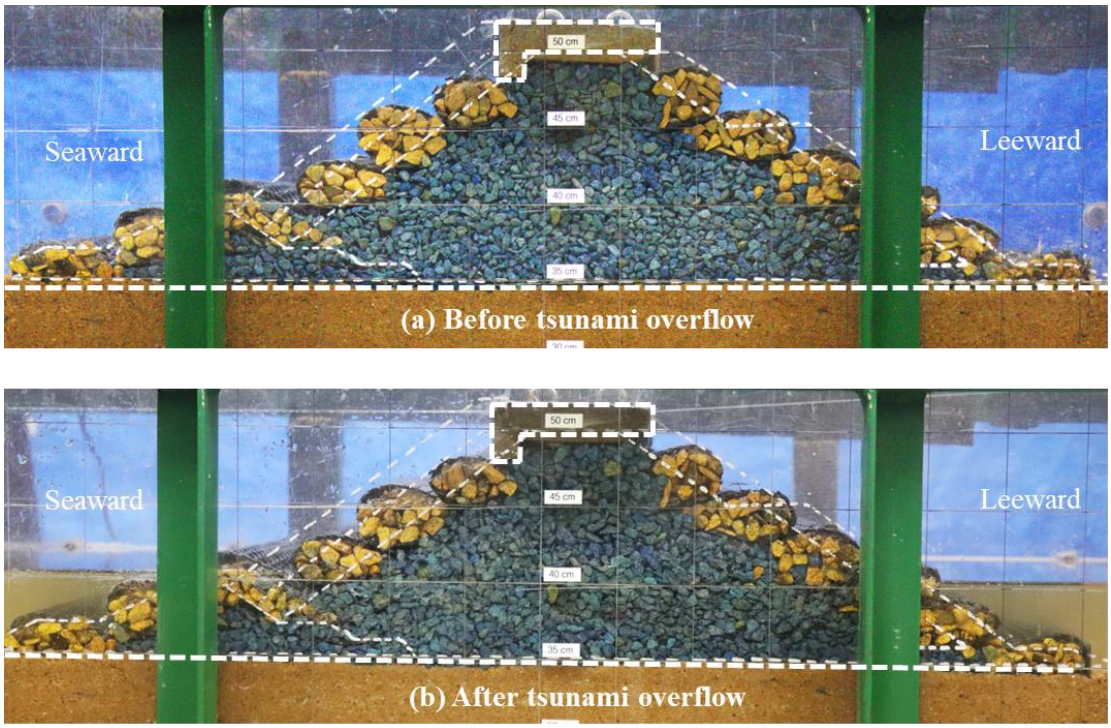

Figure 7.5 Deformations in the WGRM model when subjected to tsunami overflow

7.3 ANALYTICAL STUDY

7.3.1 Relative Displacement

Quantifying the damage on RM breakwaters involves assessing various damage descriptors, including relative eroded area and relative displacement. According to recommendations from previous studies, a value above 17 indicates total failure of the RM breakwater (Campos et al. 2020b).

Additionally, the relative displacement (R_d) gauges the degree of damage by considering the number of displaced armour units. In the conventional model, the relative displacement was 2.2 times higher than the failure threshold recommended by the Coastal Engineering Manual (United States Army Corps of Engineers 2002). In contrast, the WGRM model demonstrated remarkable stability, with the armour rubbles

interlocked within the wrap-faced geogrids remaining stable after the tsunami overflow, as illustrated in Figure 7.6. The damage descriptors measured in the case of WGRM models tended towards zero, underscoring the efficiency of the WGRM model in tsunami-prone areas.

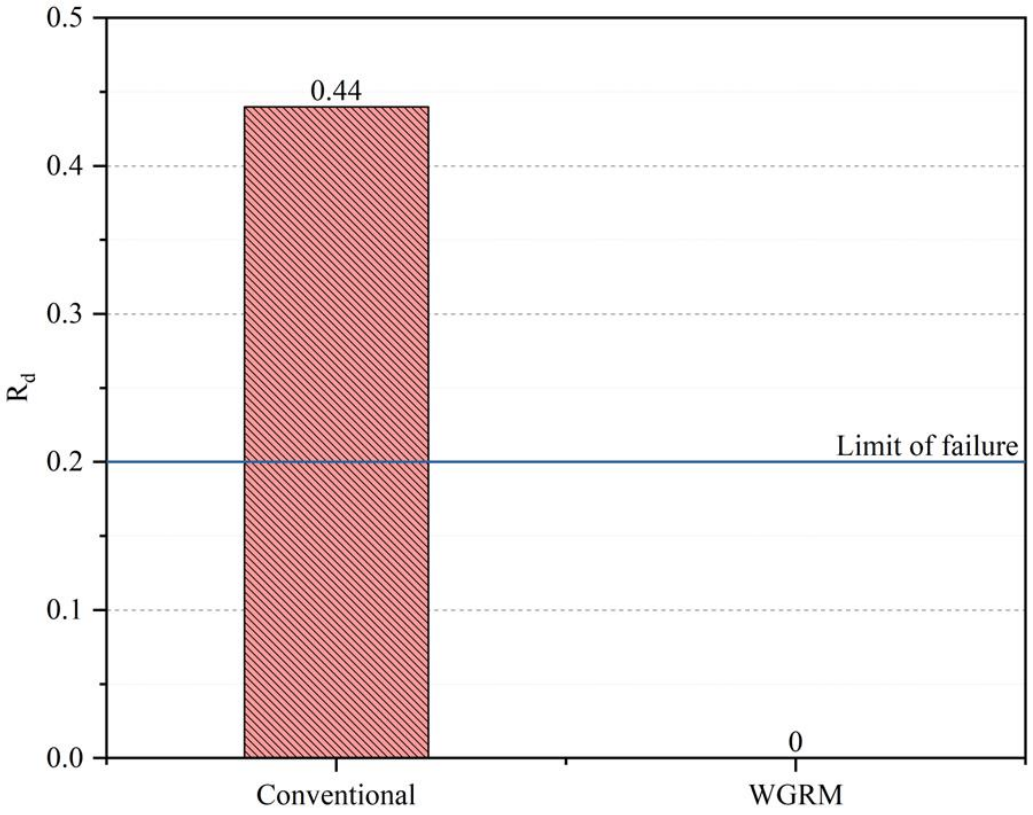

Figure 7.6 Relative displacement of armour units in conventional and WGRM models after the tsunami overflow

7.3.2 Relative Eroded Area

The Relative Eroded Area (S) indicates the average scoured area of the armour layer concerning the area of one face of an approximate cubic armour block (Vidal et al. 2004). A higher dimensionless parameter value signifies more extensive damage. In the conventional breakwater, the relative eroded area exceeded 2.5 times the threshold value, indicating a complete collapse of the breakwater, as illustrated in Figure 7.8. In cases involving WGRM models, the Relative Eroded Area consistently trended towards zero, indicating the remarkable efficacy of employing WGRM models in regions vulnerable to tsunamis.

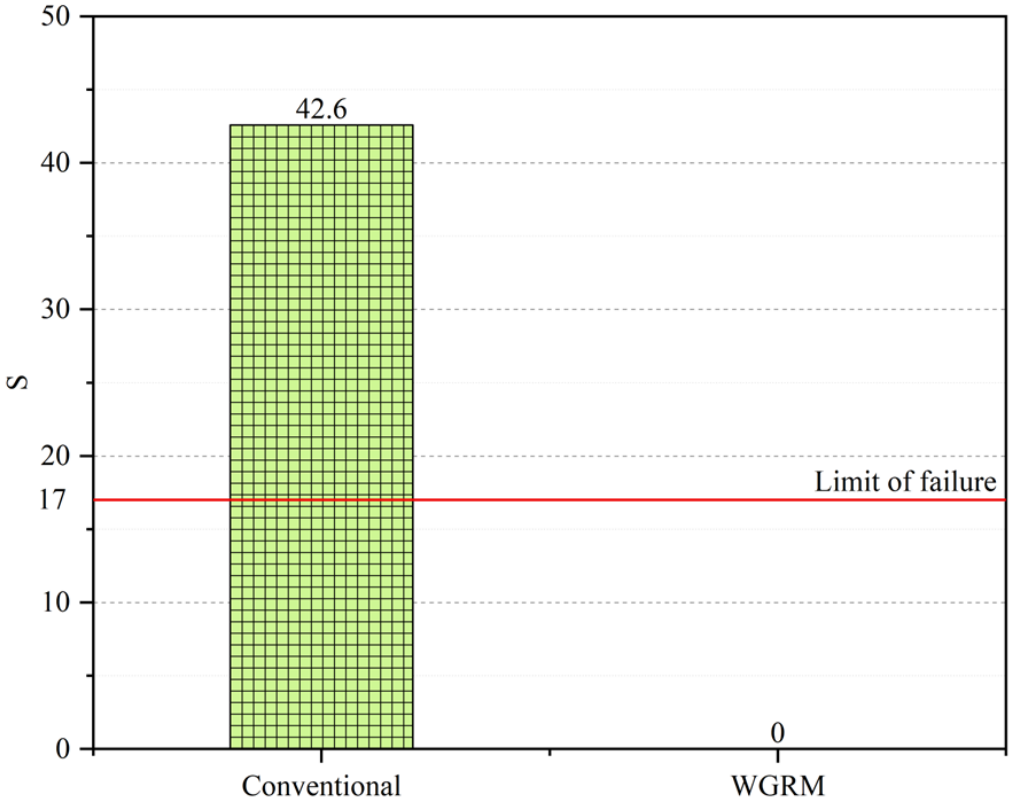

Figure 7.7 Relative eroded area of armour units in conventional and WGRM models after the tsunami overflow

7.4 PROFILE MAPPING

The damage descriptors used to assess the RM breakwater idealize the damage within a 2D plane, while actual damage is three-dimensional. To achieve a more accurate method of damage assessment, the author developed an automated profile mapper. This automated mapper generated 3D cloud points of the breakwater profile before the tsunami impact. The scanning process was then repeated on the deformed breakwater and seabed after the tsunami impact to obtain the 3D coordinates of the damaged profile. Comparative analysis between the two coordinate systems facilitated an adequate determination of the scouring on the conventional model and an assessment of the performance of the WGRM model.

The conventional model experienced a scouring volume of 4.5×10^{-3} $m^{3,}$ primarily at the crest region, as depicted in Figure 7.7. The scouring of the crest region resulted

from the combined effects of the rolling down of armour rubbles from the harbour slope and the displacement of exposed core rubbles from the crest. These two failure mechanisms were addressed to protect the crest of the WGRM breakwater model. Consequently, the comparative scoured profile for the WGRM model exhibited a flat surface.

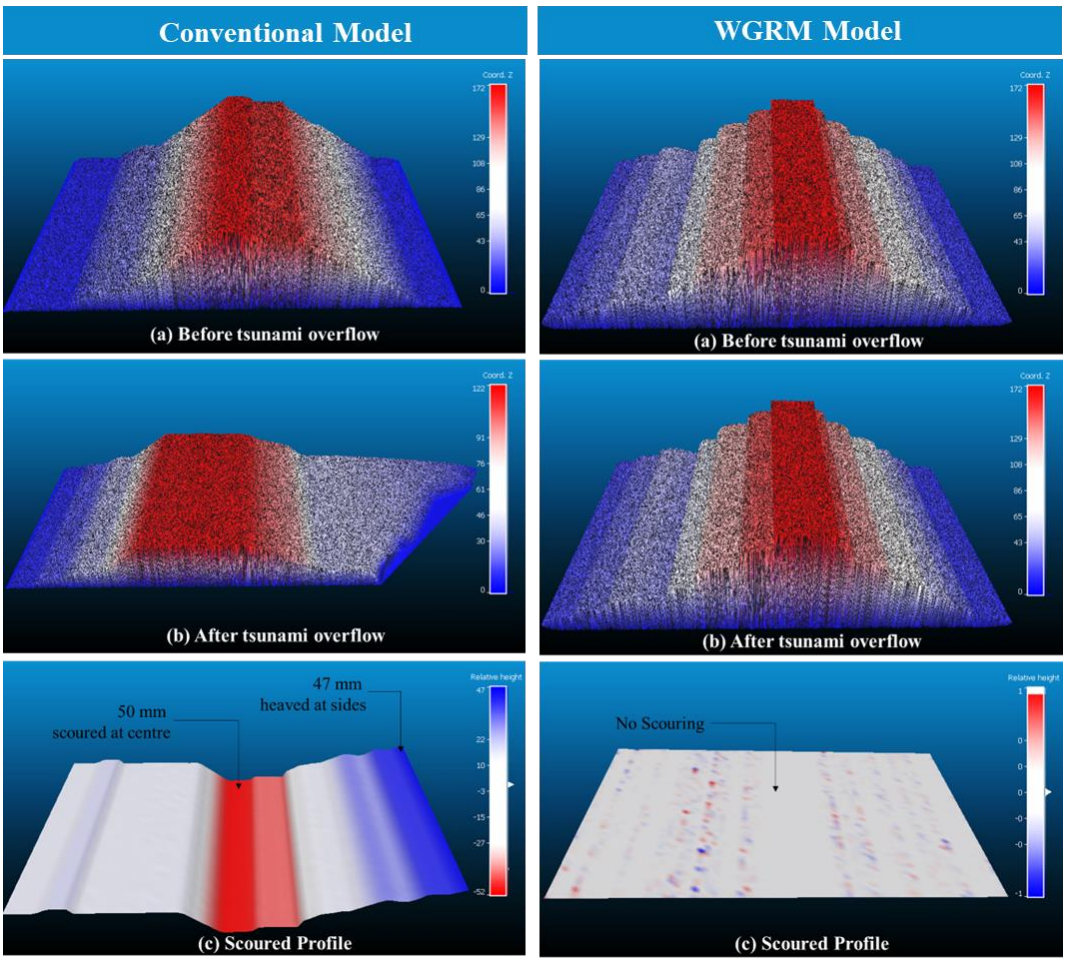

Figure 7.8 Damage assessment of the conventional and WGRM models during the tsunami overflow

7.5 NUMERICAL SIMULATION

The intricate geometry of the RM breakwater necessitates a comprehensive analysis under tsunami overflow conditions, which can be efficiently achieved through finite element software. In this study, PLAXIS 3D finite element software was employed to analyse the behaviour of both conventional and WGRM models during tsunami overflow. The RM breakwater and seabed soils were characterized by the elastoplastic

Mohr-Coulomb model with input parameters as defined in Table 3.2 and 3.4. This modelling approach, consistent with previous studies (Cihan et al. 2012; Cihan and Yuksel 2013; Sajan et al. 2024), has been validated against experimental observations.

Seabed and breakwater edges in contact with the sea level were defined with seepage hydraulic boundary conditions to simulate water seepage through the breakwater and foundation seabed during tsunami overflow. The static water surface before the tsunami's arrival was defined as sea level. In contrast, the rise and overflow of water from the seaside were represented using a head function that varied over time. This head function generated the rise and overflow of water over the breakwater model, simulating the physical model test. Thus, the numerical model focused on simulating the seepage effects on breakwater and seabed during the tsunami overflow. Howver, the study did not account erosion of the breakwater. Figure 7.9 illustrates the pore water pressure distribution in the breakwater and seabed soils during tsunami overflow. The excess pore water pressure at the locations of the pore pressure transducers, as highlighted in Figure 7.9 (b), was utilized to validate the numerical model.

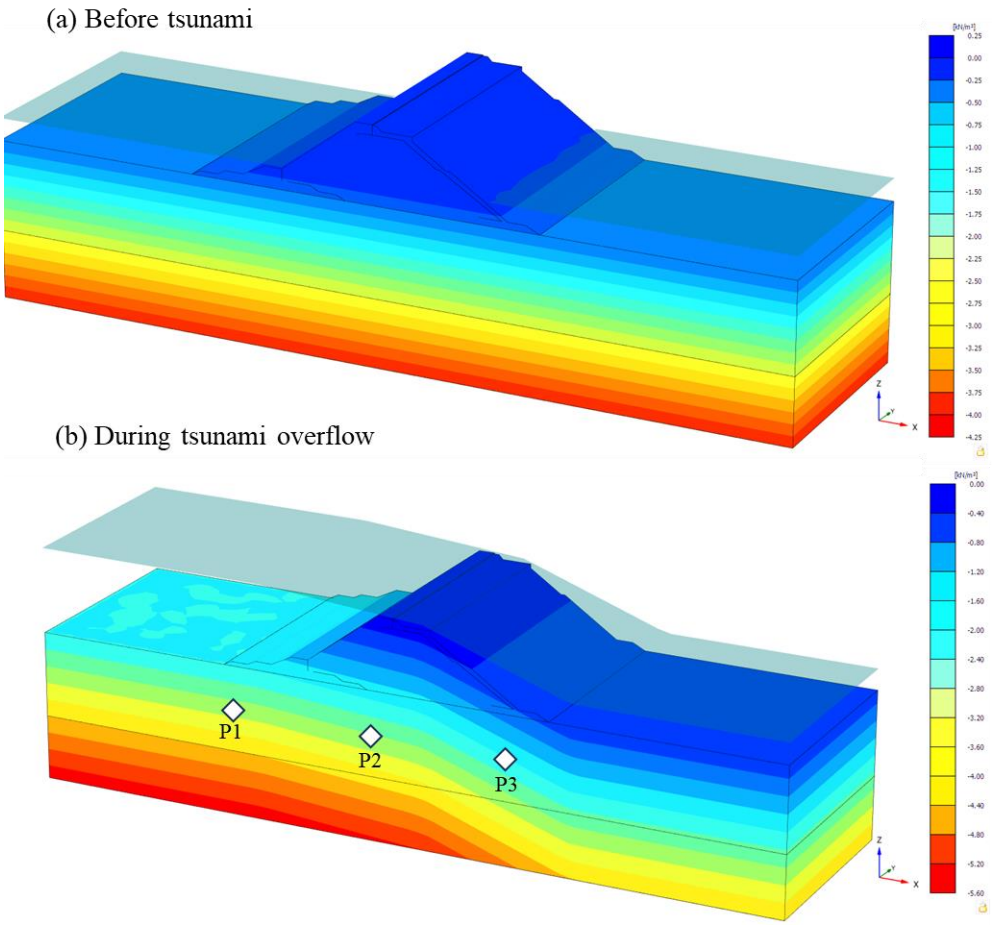

Figure 7.9 Pore water pressure contours during the tsunami overflow simulation

7.5.1 Effects of Shear Key

The effectiveness of the shear-keyed crown wall in mitigating lateral displacement of the crest in WGRM models was a notable observation. The shear key in the experiments was strategically placed on the sea side of the crown, reflecting the primary focus of the study, which did not encompass drawdown conditions. The present study placed the shear key solely on the sea side was driven by the specific objectives of the experiments, which were centred around understanding the breakwater response to tsunami overflow. While it is acknowledged that the shear key would also be necessary on the harbour side if drawdown conditions were considered, the exclusion of drawdown scenarios in this study justifies the placement of the shear key exclusively on the sea side in the physical model tests.

Therefore, the isolated impact of multiple shear keyed crown wall on a conventional breakwater model was not investigated in the physical model tests. Consequently,

numerical simulations were employed to analyze this specific aspect, along with an examination of the influence of varying the number of shear keys beneath the crown wall.

The findings revealed that the presence of a crown wall without a shear key had limited effectiveness in resisting tsunami overflow. Introducing a shear key beneath the seaside-facing side exhibited a reduction in the shift of crown walls in conventional models, as depicted in Figure 7.10. Furthermore, the addition of a second shear key at the harbour end significantly enhanced crown wall stability, leading to a further reduction in the lateral displacement. In regions prone to tsunamis, it is recommended to implement crown walls with shear keys at both ends. Nevertheless, incorporating an additional shear key at the middle of the crown wall did not yield a substantial reduction in the lateral displacement. Considering economic considerations, a single shear key was deemed optimal for minimizing crest displacement under tsunami overflow conditions.

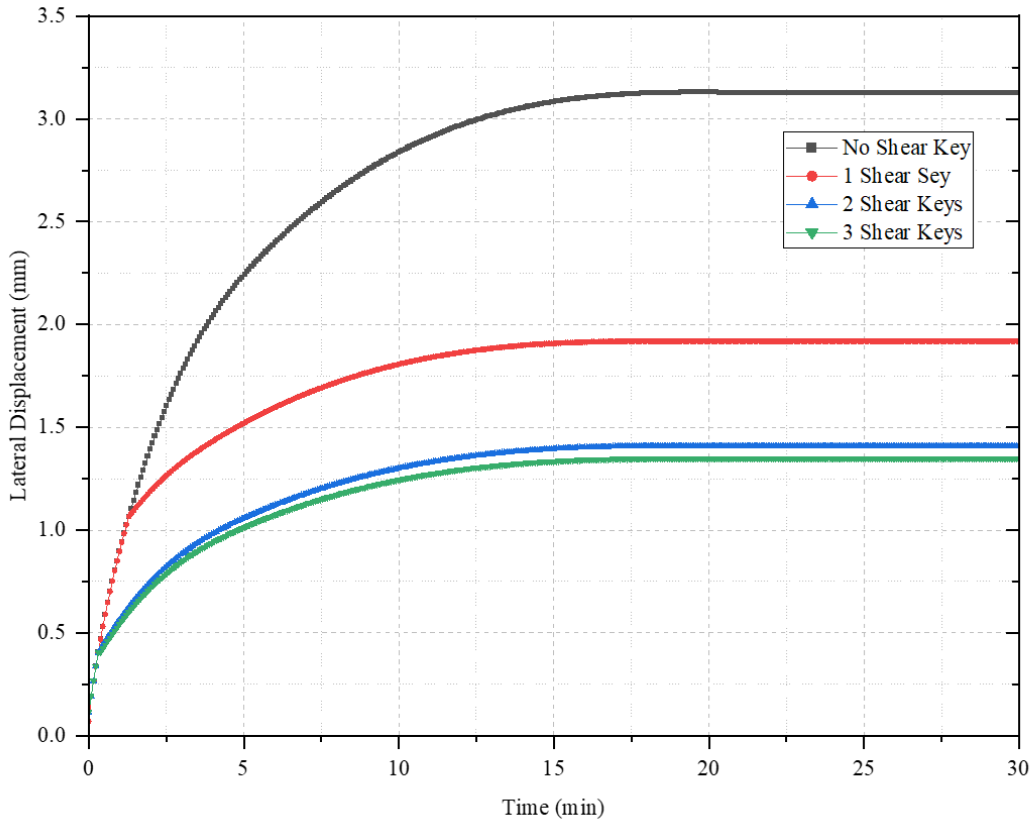

Figure 7.10 Effect of the number of shear keys in the crown wall during tsunami overflow

7.6 SUMMARY

Physical model tests were conducted, specifically focusing on the stability of the RM breakwater under continuous tsunami overflow in the tsunami flume. The findings from the studies on conventional RM breakwaters led to the proposal of mitigation techniques to enhance the resilience of breakwaters against tsunamis. The WGRM model, incorporating a wrap-faced geogrid breakwater, shear-keyed crown wall, and sheet piles, demonstrated remarkable resilience against level 1 tsunamis. After the overflow of the tsunami, the proposed breakwater remained stable enough to withstand further impacts, thereby providing enhanced protection to coastal regions. The critical inferences drawn from the present study highlight the effectiveness and resilience of the proposed WGRM model for RM breakwaters in the face of tsunamis.

- The conventional RM breakwater experienced severe damage during the tsunami overflow tests. Almost 40.9% of the exposed breakwater height was scoured, leading to the upheaval of rubbles and increased effective width. The primary armour stones were dragged toward the harbour side, illustrating the destructive impact of the overflowing tsunami. In contrast, the WGRM model demonstrated remarkable stability by reducing the settlement of the breakwater crest by 97.4%. The armour layer of the RM was protected by wrapped geogrid layers, preventing deformation.
- The lateral thrust exerted by the tsunami was effectively resisted by the shear key in the crown walls, reducing the lateral displacement of the crest by 99.4%. Further, the sheet piles reduced the IPWP developed beneath the breakwater by 42.4%, thereby prohibiting the chances of bearing capacity reduction.
- The WGRM model successfully withstood both continuous tsunami overflow tests, exhibiting remarkable resilience without undergoing significant deformation. The numerical parametric study indicated that the presence of two numbers of shear keys beneath the crown wall resists tsunami-induced forces more effectively.

CHAPTER 8
COMPARATIVE ANALYSIS

The four proposed reinforced models (GBRM, GRM, GGRM, and WGRM) were observed to be effective countermeasures against tsunami-induced damages to RM breakwaters. The effectiveness of the proposed countermeasure techniques was evident from the reduction in settlement, lateral displacement, IPWP and scouring of the breakwater during physical model tests. The results of the extensive study, which included physical model tests, analytical studies, profile mapping, and numerical simulations, are tabulated in Table 7.

Table 8.1 Comparison of results from tsunami overflow tests

Sl No	Parameters	Conventional Model	GBRM Model	GRM Model	GGRM 1 Model	GGRM 2 Model	GGRM 3 Model	WGRM Model
1	Settlement of the crest (mm)	50	4.9	0.25	27.49	9.51	1.29	1.29
2	Displacement of the crest (mm)	150	0.6	6	46	8.09	1.83	0.97
3	IPWP below breakwater (kPa)	1.18	0.87	0.75	0.54	0.54	0.54	0.68
4	Scoured Volume (m^3)	4.5×10^{-3}	0	0	1.7×10^{-3}	0.6×10^{-3}	0.1×10^{-3}	0
5	Relative Displacement	0.44	0	0	0.36	0.27	0.06	0
6	Relative Eroded Area	42.6	0	0	36.27	26.56	6.13	0

The cost-effectiveness of the proposed reinforced models was meticulously evaluated, and a comparison of the total cost of materials per running meter of the breakwater was estimated following the studies by Hauer et al. (1995). The results of the cost analysis are tabulated in Table 8. It was identified that the tsunami overflow totally scoured the emerged portion of the conventional rubble mound breakwater. Based on the scoured volume of the conventional breakwater, it was estimated that the repair cost of materials to rebuild the conventional breakwater was higher than the cost of adding the proposed reinforcing countermeasures to make tsunami-resilient RM breakwater.

In the case of GBRM models, the replacement of the primary and secondary armour layer entirely by cheaper substitutes such as the geobags and geogrids reduced the substantial cost involved in making the primary and secondary armour layers. Similarly, the replacement of the primary armour layer by gabions also reduced the cost involved in making concrete primary armour layer. However, since the gabions were made of rubbles, the required quantity of rubbles was higher, which contributed to a lower saving percentage. On the contrary, the application of geogrids along the slopes of the breakwater was the least expensive countermeasure technique. The method showcased the maximum savings against repairing the damaged RM breakwater. However, the required quantity of geogrid to construct the WGRM model was considerably higher, making the model the third most cost-effective solution for making tsunami-resilient RM breakwater.

Table 8.2 Cost analysis of RM breakwater models

Sl No	RM Breakwater Models	Reinforcing Cost (₹)	Repair Cost of Conventional Breakwater (₹)	Savings (%)
1	GBRM	3.66×10^5	32.54×10^5	89
2	GRM	19.82×10^5		39
3	GGRM	2.96×10^5		91
4	WGRM	13.03×10^5		60

CHAPTER 9
CONCLUSIONS

The RM breakwater stands as a vital defence against the devastating forces of tsunamis, crucially protecting coastal regions and their inhabitants. However, past catastrophes, such as the 2004 Indian Ocean tsunami and the 2011 Great East Japan tsunami, have starkly revealed the vulnerabilities of conventional RM breakwaters. In response, this thesis embarked on a comprehensive exploration aimed at fortifying RM breakwaters against tsunamis through innovative reinforcement techniques as countermeasures. Through a meticulous series of physical model tests, analytical studies, profile mapping, and numerical simulations, the conventional behaviour and the performance of reinforced RM breakwaters under tsunami overflow were scrutinized. The investigation encompassed a range of reinforcement methodologies, including the application of gabions and geosynthetics to make the GBRM, GRM, GGRM, and WGRM models. The key findings of this study, as listed below, underscore the critical vulnerabilities inherent in conventional RM breakwaters when subjected to tsunami overflow. In contrast, reinforced models exhibited significantly enhanced resilience, effectively withstanding the tsunami without deformation or failure;

a) The crest of conventional RM breakwater was scoured away by nearly 50 mm (5 m in prototype) when subjected to tsunami. The freeboard height of the prototype breakwater was 5.2 m. Consequently, most of the emerging portion of the breakwater was eroded by tsunami overflow. It was observed in the physical model test on the conventional RM breakwater that the breakwater crossed the damage threshold limit of destruction during the tsunami overflow test. The sudden upraise in the water on the seaside had not only induced high seepage through the body of the breakwater but also upward buoyancy forces on the rubbles, which resulted in deep scouring and rolling down of the rubbles. The combined effects of all these forces led to the failure of the conventional model.
b) The replacement of armour layers with geobag and geogrid, insertion of sheet piles in the seabed soils and placement of crown wall (with shear key) on the crest imparted high resiliency to the GBRM model against tsunami. The

reinforced RM was observed to withstand the severe tsunami overflow without any damage. An impressive 90.2% reduced the settlement of the breakwater crest, while lateral displacement was mitigated by 99.6%. Additionally, the incorporation of sheet piles in seabed soils demonstrated a marked 26.3% reduction in IPWP developed beneath the breakwater, enhancing the stability and integrity of the reinforced breakwaters. The stability analysis in numerical simulation reconfirmed that the stability of the reinforced model was improved by 2.2 times when compared with the conventional model. It was also identified from the stability analysis that when the height of the tsunami exceeds 1.8 times the initial sea level, the tsunami can dislodge even the heavier primary armour layer.

c) Similarly, the GRM model displayed exceptional resilience, with a remarkable reduction of 99.5% in crest settlement and 96% in lateral displacement. The comparative heaviness of the gabion units, along with its larger contact area, crown walls with shear key, and sheet piles, proved instrumental in fortifying the breakwater against the destructive forces of tsunami overflow. The placement of sheet piles in the seabed soils reduced IPWP by 36.4% in the reinforced model. The effectiveness of sheet piles in reducing seepage was reconfirmed in the numerical simulation as well.

d) In the GGRM reinforced models, three geogrid placement configurations were attempted. Among the three configurations, the placement of geogrid as a double layer on the harbour side (GGRM III) was observed to be the most efficient. In the GGRM III model, the settlement of the breakwater crest was reduced by 97.4% and lateral displacements by 98.8%. The model also reduced IPWP in the seabed below the mound by 54.2%, thereby evidently arresting excess seepage through the foundation seabed. The stability analysis performed in the finite element software also reconfirmed the improved stability of the GGRM III model, which was 2.2 times higher than that of the conventional model.

e) The WGRM demonstrated an unprecedented ability to withstand continuous tsunami overflow, withstanding the forces exerted by level 1 tsunamis. The incorporation of wrap-faced geogrid layers proved instrumental in enhancing

the structural integrity of the breakwater. Notably, the WGRM model exhibited a reduction of 97.4% in crest settlement and 99.4% in lateral displacement, underscoring its ability to resist the destructive forces of overflowing tsunamis. It was also noted that the IPWP was reduced by 42.4% by the sheet piles that acted as cutoff walls in the foundation seabed that prevented seepage. Furthermore, the numerical parametric studies reaffirmed the stability of the WGRM, highlighting the optimum efficacy of two shear keys below the crown wall in dissipating tsunami-induced forces.

f) The meticulous evaluation of cost-effectiveness revealed that the proposed reinforced models offer significant savings compared to the repair cost of conventional rubble mound breakwaters. Through the replacement of primary and secondary armour layers with more affordable substitutes such as geobags, gabions, and geogrids, substantial reductions in material costs were achieved across the reinforced models. Particularly noteworthy is the GBRM model, which demonstrated an impressive 89% saving against repair costs, emphasizing the economic viability of implementing reinforcing countermeasures. Since the GGRM models incorporated only geogrid along the slopes, the cost of reinforcement materials was the lowest compared to other models. Although the WGRM model required a higher quantity of geogrid materials, it still presented a considerable 60% saving, further highlighting the cost-effectiveness of adopting these innovative reinforcement techniques to create tsunami-resilient RM breakwaters.

The findings of this study underscore the importance of proactive measures in fortifying coastal infrastructure, thereby safeguarding lives and livelihoods against the ravages of natural disasters. Moving forward, the insights gleaned from this research offer invaluable guidance for policymakers, engineers, and coastal communities in bolstering their defences against future tsunamis and ensuring the sustainable development of coastal regions worldwide. The developed novel techniques of replacing armour blocks with gabions or geobag-geogrid systems can be adopted to mitigate tsunami-induced damages on breakwaters. The replacement of concrete armour units with gabions, geogrids, geobag-geogrid systems, or wrap-faced geogrids is a sustainable approach which depletes the carbon footprint of cement used to make precast armour blocks.

9.1 Recommendations and Scope of Future Research

To implement the novel countermeasure techniques proposed in this study for tsunami-resilient RM breakwaters, the following recommendations are suggested;

- **Site-Specific Adaptation and Optimization:** The dimensions, material types, and installation methods of reinforcement techniques, such as gabions, geobags, and geogrids, can be customized based on the specific requirements of each location.
- **Feasibility Studies:** Cost-benefit analyses to compare the long-term benefits of enhanced tsunami resilience with the upfront costs of implementing the reinforcement techniques can be performed.
- **Full-Scale Field Testing:** Pilot projects can be conducted at selected breakwater sites, particularly in tsunami-prone areas and monitor the performance of reinforced breakwaters by collecting data on the durability, stability, and effectiveness of the reinforcement techniques over time.
- **Environmental Impact Assessments:** Environmental impact assessments (EIAs) can be performed to evaluate the potential effects of reinforced breakwaters on coastal ecosystems, such as coral reefs, mangroves, and fish habitats.
- **Development of Engineering Guidelines:** Standardized engineering guidelines can be developed by collaborating with professional bodies for the application of the novel countermeasures. These guidelines should incorporate design parameters, installation methods, and maintenance practices

The possible extension of the present work can be done in the following ways,

- The efficacy of the proposed reinforcing techniques to make tsunami-resilient RM breakwaters can be estimated by conducting centrifuge experiments.
- The numerical modelling by Smoothed Particle Hydrodynamics (SPH) could be implemented in future studies to more accurately model erosion processes.
- The physical model tests and numerical analysis can be performed on different reinforcing techniques that include a combination of various types of reinforcing elements, such as gabions made of geogrids.
- The analytical method can be implemented with the aid of profile mapper in determining the scoured area.

REFERENCES

1. Alvarez, I. E., Rubio, R., and Ricalde, H. (2007). “Beach restoration with geotextile tubes as submerged breakwaters in Yucatan, Mexico.” *Geotextiles and Geomembranes*, 25(4–5), 233–241.
2. Aniel-Quiroga, Í., Vidal, C., Lara, J. L., and González, M. (2019). “Pressures on a rubble-mound breakwater crown-wall for tsunami impact.” *Coastal Engineering*, 152(January), 103522.
3. Aniel-Quiroga, Í., Vidal, C., Lara, J. L., González, M., and Sainz, Á. (2018). “Stability of rubble-mound breakwaters under tsunami first impact and overflow based on laboratory experiments.” *Coastal Engineering*, 135(February), 39–54.
4. Arikawa, T., Sato, M., Shimosako, K., Hasegawa, I., Yeom, G.-S., and Tomita, T. (2012). “Failure mechanism of Kamaishi breakwaters due to the Great East Japan Earthquake tsunami.” *Coastal Engineering Proceedings*, (33), 16.
5. Asian Consulting Engineers Private Limited. (2014). *Environmental Impact Assessment for Proposed Additional Coal Berths CB 3 (9 MTPA) and CB 4 (9 MTPA), Ennore Port, Tamil Nadu*.
6. Bayesteh, H., and Mansouriboroujeni, R. (2020). “Mechanisms of settlement of a rubble mound breakwater on a soft soil in tidal flats.” *Marine Georesources and Geotechnology*, 38(10), 1163–1176.
7. Bricker, J. D., Francis, M., and Nakayama, A. (2012). “Scour depths near coastal structures due to the 2011 Tohoku Tsunami.” *Journal of Hydraulic Research*, 50(6), 637–641.
8. Bricker, J. D., Nakayama, A., Takagi, H., Mitsui, J., and Miki, T. (2015). “Mechanisms of damage to coastal structures due to the 2011 Great East Japan Tsunami.” *Handbook of Coastal Disaster Mitigation for Engineers and Planners*, Elsevier Inc., 385–415.
9. Broderick, L. (1984). “Riprap stability versus monochromatic and irregular waves.” *George Washington University*, George Washington University.
10. Bruck, H. A., McNeill, S. R., Sutton, M. A., and Peters, W. H. (1989). “Digital image correlation using Newton-Raphson method of partial differential

correction.” *Experimental Mechanics*, 29(3), 261–267.

11. Campos, Á., Castillo, C., and Molina-Sanchez, R. (2020a). “Damage in Rubble Mound Breakwaters. Part I: Historical Review of Damage Models.” *Journal of Marine Science and Engineering*.
12. Campos, Á., Molina-Sanchez, R., and Castillo, C. (2020b). “Damage in rubble mound breakwaters. Part II: Review of the definition, parameterization, and measurement of damage.” *Journal of Marine Science and Engineering*, 8(306).
13. Celli, D., Li, Y., Chen, M., and Di, M. (2019). “The role of submerged berms on the momentary liquefaction around conventional rubble mound breakwaters.” *Applied Ocean Research*, 85(January), 1–11.
14. Celli, D., Pasquali, D., Girolamo, P. De, and Risio, M. Di. (2018). “Effects of submerged berms on the stability of conventional rubble mound breakwaters.” *Coastal Engineering*, 136(February), 16–25.
15. Chaudhary, B., and Hazarika, H. (2018). “Centrifuge modelling for stability evaluation of a breakwater foundation subjected to an earthquake and a tsunami.” *Ocean Engineering*, 148, 169–181.
16. Chaudhary, B., Hazarika, H., Ishibashi, I., and Abdullah, A. (2017a). “Sliding and overturning stability of breakwater under combined effect of earthquake and tsunami.” *Ocean Engineering*, 136(April 2016), 106–116.
17. Chaudhary, B., Hazarika, H., and Manafi Khajeh Pasha, S. (2018a). “Countermeasures for breakwater foundation subjected to foreshocks and main shock of earthquake loading.” *Marine Georesources and Geotechnology*, 36(3), 308–322.
18. Chaudhary, B., Hazarika, H., Murakami, A., and Fujisawa, K. (2017b). “Mitigation of earthquake induced damage of breakwater by geogrid reinforced foundation.” *Marine Georesources & Geotechnology*, (October).
19. Chaudhary, B., Hazarika, H., Murakami, A., and Fujisawa, K. (2018b). “Countermeasures for enhancing the stability of composite breakwater under earthquake and subsequent tsunami.” *Acta Geotechnica*, 13(4), 997–1017.
20. Chaudhary, B., Hazarika, H., Murakami, A., and Fujisawa, K. (2018c). “Geosynthetic-sheet pile reinforced foundation for mitigation of earthquake and tsunami induced damage of breakwater.” *Geotextiles and Geomembranes*,

46(5), 597–610.

21. Chaudhary, B., Hazarika, H., Murakami, A., and Fujisawa, K. (2019). “Development of Resilient Breakwater against Earthquake and Tsunami.” *International Journal of Geomechanics*, 19(1), 1–17.
22. Chaudhary, B., Hazarika, H., and Nishimura, K. (2017c). “Effects of reinforcement on the performance of breakwater foundation subjected to earthquake loadings.” *International Journal of Geotechnical Engineering*, 11(2), 186–197.
23. Chaudhary, B., Hazarika, H., and Nishimura, K. (2017d). “Effects of duration and acceleration level of earthquake ground motion on the behavior of unreinforced and reinforced breakwater foundation.” *Soil Dynamics and Earthquake Engineering*, 98(March), 24–37.
24. Cihan, K., and Yuksel, Y. (2011). “Deformation of rubble-mound breakwaters under cyclic loads.” *Coastal Engineering*, 58(6), 528–539.
25. Cihan, K., and Yuksel, Y. (2013). “Deformation of breakwater armoured artificial units under cyclic loading.” *Applied Ocean Research*, 42, 79–86.
26. Cihan, K., Yuksel, Y., Berilgen, M., and Cevik, E. O. (2012). “Behavior of homogenous rubble mound breakwaters materials under cyclic loads.” *Soil Dynamics and Earthquake Engineering*, 34(1), 1–10.
27. Contestabile, P., Iuppa, C., Lauro, E. Di, Cavallaro, L., Andersen, T. L., and Vicinanza, D. (2017). “Wave loadings acting on innovative rubble mound breakwater for overtopping wave energy conversion.” *Coastal Engineering*, 122(January), 60–74.
28. Dassanayake, D. T., and Oumeraci, H. (2012). “Hydraulic stability of coastal structures made of Geotextile Sand Containers (GSCS): Effect of engineering properties of GSCS.” *Coastal Engineering Proceedings*, 1(33), structures.55.
29. Dave, T., and Murty, D. (2012). “Assessment of portable traveling pluviator to prepare reconstituted sand specimens.” *Geomechanics and Engineering*, 4.
30. Dentale, F., Reale, F., Leo, A. Di, and Carratelli, E. P. (2018). “A CFD approach to rubble mound breakwater design.” *International Journal of Naval Architecture and Ocean Engineering*, 10(5), 644–650.
31. Esteban, M., Jayaratne, R., Mikami, T., Morikubo, I., Shibayama, T., Thao, N.

D., Ohira, K., Ohtani, A., Mizuno, Y., Kinoshita, M., and Matsuba, S. (2014). "Stability of Breakwater Armor Units against Tsunami Attacks." *Journal of Waterway, Port, Coastal, and Ocean Engineering*, 140(2), 188–198.

32. Esteban, M., Thao, N. D., Takagi, H., Jayaratne, R., Mikami, T., and Shibayama, T. (2015). "Stability of Breakwaters Against Tsunami Attack." *Handbook of Coastal Disaster Mitigation for Engineers and Planners*, Miguel Esteban, H. Takagi, and T. Shibayama, eds., Oxford, UK: Butterworth-Heinemann, 293–323.
33. Franco, L., Geeraerts, J., Briganti, R., Willems, M., Bellotti, G., and Rouck, J. De. (2009). "Prototype measurements and small-scale model tests of wave overtopping at shallow rubble-mound breakwaters: the Ostia-Rome yacht harbour case." *Coastal Engineering*, 56(2), 154–165.
34. Fredsøe, J., and Sumer, B. M. (1997). "Scour at the round head of a rubble-mound breakwater." *Coastal Engineering*, 29(3–4), 231–262.
35. Fujisawa, K., and Murakami, A. (2014). "A Theory for Predicting Velocities of Soil Particles and Seepage Flow During Upward Seepage Failure." *Japanese Geotechnical Journal*, 9(4), 511–520.
36. Fujisawa, K., Murakami, A., Nishimura, S., and Shuku, T. (2012). "Relation between seepage force and velocity of sand particles during sand boiling." *Geotechnical Engineering*, 44(2), 9–17.
37. Gent, M. R. A. van. (2013). "Rock stability of rubble mound breakwaters with a berm." *Coastal Engineering*, 78, 35–45.
38. Gent, M. R. A. Van, and Werf, I. M. van der. (2014). "Rock toe stability of rubble mound breakwaters." *Coastal Engineering*, 83, 166–176.
39. Gent, M. R. A. Van, and Werf, I. M. Van Der. (2019). "Influence of oblique wave attack on wave overtopping and forces on rubble mound breakwater crest walls." *Coastal Engineering*, 151(March), 78–96.
40. Ghazi, H., Shahir, H., and Ghalandarzadeh, A. (2022). "Effect of basal reinforcement on sinking and deformation of rubble mounds on a soft seabed." *International Journal of Geotechnical Engineering*, 16(8), 1032–1048.
41. Goseberg, N., Wurpts, A., and Schlurmann, T. (2013). "Laboratory-scale generation of tsunami and long waves." *Coastal Engineering*, 79, 57–74.

42. Guler, H. G., Arikawa, T., Oei, T., and Yalciner, A. C. (2015). “Performance of rubble mound breakwaters under tsunami attack , a case study : Haydarpasa Port , Istanbul , Turkey.” *Coastal Engineering*, 104, 43–53.
43. Guler, H. G., Baykal, C., Arikawa, T., and Yalciner, A. C. (2018). “Numerical assessment of tsunami attack on a rubble mound breakwater using OpenFOAM®.” *Applied Ocean Research*, 72, 76–91.
44. Gupta, G. V. M., Murthy, M. V. R., and Subramanian, B. R. (2005). *Preliminary assessment of impact of Tsunami in selected coastal areas of India*.
45. Harbitz, C. B., Nakamura, Y., Arikawa, T., Baykal, C., Dogan, G. G., Frauenfelder, R., Glimsdal, S., Guler, H. G., Issler, D., Kaiser, G., Kânoğlu, U., Kisacik, D., Kortenhaus, A., Løvholt, F., Maruyama, Y., Sassa, S., Sharghivand, N., Strusinska-Correia, A., Tarakcioglu, G. O., and Yalciner, A. C. (2016). “Risk Assessment and Design of Prevention Structures for Enhanced Tsunami Disaster Resilience (RAPSODI)/Euro-Japan collaboration.” *Coastal Engineering Journal*, 58(4), 1–37.
46. Hauer, M., Op Den Velde, W., Vrijling, J. K., and D’Angremond, K. (1995). “Comparison construction costs conventional rubble mound breakwaters / berm breakwater.” *Permanent International Association of Navigation Congresses:Proceedings of the third Seminar on Ports and Inland Waterways*, Brussels, Belgium: PIANC, 1–15.
47. Hazarika, H., Nishimura, K., and Chaudhary, B. (2015). “Model testing on resilient solution for breakwater protection against tsunami.” *Japanese Geotechnical Society Special Publication*, 3(2), 40–44.
48. Hudson, R. Y. (1959). “Laboratory Investigation of Rubble-Mound Breakwaters.” *Transactions of the American Society of Civil Engineers*, 126(4), 610–659.
49. Hur, D. S., Nakamura, T., and Mizutani, N. (2007). “Sand suction mechanism in artificial beach composed of rubble mound breakwater and reclaimed sand area.” *Ocean Engineering*, 34(8–9), 1104–1119.
50. Jayaratne, M. P. R., Premaratne, B., Adewale, A., Mikami, T., Matsuba, S., Shibayama, T., Esteban, M., and Nistor, I. (2016). “Failure mechanisms and local scour at coastal structures induced by Tsunami.” *Coastal Engineering*

Journal, 58(4), 1–38.

51. Jeng, D. S., and Ye, J. H. (2012). "Three-dimensional consolidation of a porous unsaturated seabed under rubble mound breakwater." *Ocean Engineering*, 53, 48–59.
52. Kasama, K., Zen, K., Nakagawa, Y., and Furukawa, Z. (2020). "Instability evaluation of rubble mound for breakwaters subjected to tsunami-induced overflow and seepage flow." *Soils and Foundations*, 60(6), 1532–1545.
53. Kato, F., Suwa, Y., Watanabe, K., and Hatogai, S. (2012). "Mechanisms Of Coastal Dike Failure Induced by The Great East Japan Earthquake Tsunami." *Coastal Engineering Proceedings*, 1(33), 40.
54. Kazama, M., and Noda, T. (2012). "Damage statistics (Summary of the 2011 off the Pacific Coast of Tohoku Earthquake damage)." *Soils and Foundations*, 52(5), 780–792.
55. Khattar, M. D. (2001). "Longest Breakwater in India." *Ports '01*, Reston, VA: American Society of Civil Engineers, 1–17.
56. Kikuchi, Y., Kawabe, S., Taenaka, S., and Moriyasu, S. (2015). "Horizontal loading experiments on reinforced gravity type breakwater with steel walls." *15th Asian Regional Conference on Soil Mechanics and Geotechnical Engineering, ARC 2015: New Innovations and Sustainability*, Japanese Geotechnical Society Special Publication, 1267–1272.
57. Kishida, T., Hoshino, F., Tasaki, K., Iwamae, N., Akiyama, Y., and Ikeya, T. (2013). "The experiment about the stability over the tsunami of the breakwater by friction-increasing asphalt mat." *Journal of Japan Society of Civil Engineers, Ser. B3 (Ocean Engineering)*, 69(2), I_467-I_472.
58. Knodel, P., Presti, D. Lo, Pedroni, S., and Crippa, V. (1992). "Maximum Dry Density of Cohesionless Soils by Pluviation and by ASTM D 4253-83: A Comparative Study." *Geotechnical Testing Journal*, 15, 180.
59. Koffler, A., Choura, M., Bendriss, A., and Zengerink, E. (2008). "Geosynthetics in protection against erosion for river and coastal banks and marine and hydraulic construction." *Journal of Coastal Conservation*, 12(1), 11–17.
60. Kozai, K., Kobayashi, E., Kubo, M., and Morita, K. (2005). "Tsunami disaster assessment of ports in India by using QuickBird images." *26th Asian*

Conference on Remote Sensing and 2nd Asian Space Conference, ACRS 2005, Tokyo, Japan: Asian Association on Remote Sensing, 59–63.

61. Lee, E. C., and Douglas, R. S. (2012). "Geotextile tubes as submerged dykes for shoreline management in Malaysia." *Geotextiles and Geomembranes*, 30, 8–15.
62. Losada, I. J., Lara, J. L., Guanche, R., and Gonzalez-Ondina, J. M. (2008). "Numerical analysis of wave overtopping of rubble mound breakwaters." *Coastal Engineering*, 55(1), 47–62.
63. Løvholt, F., Griffin, J., and Salgado-Gálvez, M. A. (2016). "Tsunami Hazard and Risk Assessment on the Global Scale BT - Encyclopedia of Complexity and Systems Science." R. A. Meyers, ed., Berlin, Heidelberg: Springer Berlin Heidelberg, 1–34.
64. Lykke Andersen, T., Burcharth, H. F., and Gironella, X. (2011). "Comparison of new large and small scale overtopping tests for rubble mound breakwaters." *Coastal Engineering*, 58(4), 351–373.
65. Mitsui, J., Matsumoto, A., Hanzawa, M., Koyama, H., Shinomura, Y., and Oike, N. (2013). "Effective methods for covering breakwater rubble mounds against tsunami using filter units." *Journal of Japan Society of Civil Engineers, Ser. B3 (Ocean Engineering)*, 69(2), I_479-I_484.
66. Mulders, P., Curto, V., Zanuttigh, B., Jan, H., and Uijttewaal, W. S. J. (2015). "Effects of gradation on the long-shore transport processes and reshaping of rubble mound breakwaters under construction exposed to head-on and oblique waves." *Coastal Engineering*, 106, 87–111.
67. Muttray, M. O., and Oumeraci, H. (2005). "Theoretical and experimental study on wave damping inside a rubble mound breakwater." *Coastal Engineering*, 52(8), 709–725.
68. Najma, A., and Ghalandarzadeh, A. (2019). "Experimental study on the seismic behavior of composite breakwaters located on liquefiable seabed." *Ocean Engineering*, 186(June), 106127.
69. Nørgaard, J. Q. H., Andersen, T. L., and Burcharth, H. F. (2013). "Wave loads on rubble mound breakwater crown walls in deep and shallow water wave conditions." *Coastal Engineering*, 80, 137–147.

70. Oumeraci, H., and Kortenhaus, A. (2011). “Core made of geotextile sand containers for rubble mound breakwaters and seawalls: Effect on armour stability and hydraulic performance.” *Ocean Engineering*, 38(1), 159–170.
71. Passalacqua, R. (1991). “A sand-spreader used for the reconstitution of granular soil models.” *Soils and Foundations*, 31(2), 175–180.
72. Puente, I., Sande, J., González-jorge, H., Peña-gonzález, E., Maciñeira, E., Martínez-sánchez, J., and Arias, P. (2014). “Novel image analysis approach to the terrestrial LiDAR monitoring of damage in rubble mound breakwaters.” *Ocean Engineering*, 91, 273–280.
73. Rajaratnam, N. (1981). “Erosion by plane turbulent jets.” *Journal of Hydraulic Research*, 19(4), 339–358.
74. Recio, J., and Oumeraci, H. (2008). “Hydraulic permeability of structures made of geotextile sand containers: Laboratory tests and conceptual model.” *Geotextiles and Geomembranes*, 26(6), 473–487.
75. Romano, A., Bellotti, G., Briganti, R., and Franco, L. (2015). “Uncertainties in the physical modelling of the wave overtopping over a rubble mound breakwater : The role of the seeding number and of the test duration.” *Coastal Engineering*, 103, 15–21.
76. Sajan, M. K., Chaudhary, B., Akarsh, P. K., and Kumar, S. (2024). “Geosynthetic reinforced rubble mound breakwater for mitigation of tsunami-induced damage.” *Geotextiles and Geomembranes*, 52(1), 72–94.
77. Sassa, S., Takahashi, H., Morikawa, Y., and Takano, D. (2016). “Effect of overflow and seepage coupling on tsunami-induced instability of caisson breakwaters.” *Coastal Engineering*, 117, 157–165.
78. Sheth, A., Sanyal, S., Jaiswal, A., and Gandhi, P. (2006). “Effects of the December 2004 Indian Ocean tsunami on the Indian mainland.” *Earthquake Spectra*, 22(SUPPL. 3).
79. Shin, E. C., and Oh, Y. I. (2007). “Coastal erosion prevention by geotextile tube technology.” *Geotextiles and Geomembranes*, 25(4–5), 264–277.
80. Sugano, T., Nozu, A., Kohama, E., Shimosako, K. I., and Kikuchi, Y. (2014). “Damage to coastal structures.” *Soils and Foundations*, 54(4), 883–901.
81. Sumer, B. M., and Fredsøe, J. (2000). “Experimental study of 2D scour and its

protection at a rubble-mound breakwater." *Coastal Engineering*, 40(1), 59–87.

82. Sutton, M., Wolters, W., Peters, W., Ranson, W., and McNeill, S. (1983). "Determination of displacements using an improved digital correlation method." *Image and Vision Computing*, 1(3), 133–139.
83. Suzuki, K., Zikuhara, S., Tatewaki, K., and Hosokawa, Y. (2018). "Clarifying the Stability of Armour Blocks behind the Caisson against Tsunami After Abrupt Change of Breakwater Width." *Coasts, Marine Structures and Breakwaters 2017*, ICE Publishing, 1131–1140.
84. Synolakis, C. E., and Kong, L. (2006). "Runup Measurements of the December 2004 Indian Ocean Tsunami." *Earthquake Spectra*, 22(3_suppl), 67–91.
85. Takahashi, H., Sassa, S., Morikawa, Y., Takano, D., Aoki, R., and Maruyama, K. (2014a). "Centrifuge tests on resistance force of breakwaters reinforced by embankment." *Journal of Japan Society of Civil Engineers, Ser. B3 (Ocean Engineering)*, 70(2), I_870-I_875.
86. Takahashi, H., Sassa, S., Morikawa, Y., Takano, D., and Maruyama, K. (2014b). "Stability of caisson-type breakwater foundation under tsunami-induced seepage." *Soils and Foundations*, 54(4), 789–805.
87. Takano, D., Lenoir, N., Otani, J., and Hall, S. A. (2015). "Localised deformation in a wide-grained sand under triaxial compression revealed by X-ray tomography and digital image correlation." *Soils and Foundations*, 55(4), 906–915.
88. Temel, A., and Dogan, M. (2021). "Time dependent investigation of the wave induced scour at the trunk section of a rubble mound breakwater." *Ocean Engineering*, 221(November 2020), 108564.
89. Tsujio, D., Yasuda, T., Mase, H., Mori, N., Maeda, K., and Yamaguchi, Y. (2013). "Experimental study on effects of reinforcement for caisson breakwaters against abnormal tsunami." *Journal of Japan Society of Civil Engineers, Ser. B3 (Ocean Engineering)*, 69, I_473-I_478.
90. Ulker, M. B. C., Tatlioglu, E., and Lav, M. A. (2018). "Dynamic response and liquefaction analysis of seabed-rubble mound breakwater system under waves." *Applied Ocean Research*, 78(June), 75–87.
91. United States Army Corps of Engineers. (2002). *Coastal Engineering Manual*,

EM 110-2-1100 (Part VI) Change 3 (28 September 2011). Coastal Engineering Manual, Washington, DC, USA,: USACE.

92. Vaid, Y. P., and Negussey, D. (1984). "Relative Density of Pluviated Sand Samples." *Soils and Foundations*, 24(2), 101–105.
93. Vicinanza, D., Contestabile, P., Quvang, J., Nørgaard, H., and Lykke, T. (2014). "Innovative rubble mound breakwaters for overtopping wave energy conversion." *Coastal Engineering*, 88, 154–170.
94. Vidal, C., Martin, F. L., Negro, V., Gironella, X., Madrigal, B., and García-Palacios, J. (2004). "Measurement of Armor Damage on Rubble Mound Structures: Comparison Between Different Methodologies." *Coastal Structures 2003*, Reston, VA: American Society of Civil Engineers, 189–200.
95. Xu, Z., Melville, B. W., Wotherspoon, L., and Nandasena, N. A. K. (2020). "Stability of Composite Breakwaters under Tsunami Attack." *Journal of Waterway, Port, Coastal, and Ocean Engineering*, 146(4).
96. Yan, S. W., and Chu, J. (2010). "Construction of an offshore dike using slurry filled geotextile mats." *Geotextiles and Geomembranes*, 28(5), 422–433.
97. Yu, Y., Zhang, B., and Zhang, J. M. (2005). "Action mechanism of geotextile-reinforced cushion under breakwater on soft ground." *Ocean Engineering*, 32(14–15), 1679–1708.
98. Zhao, H. Y., Liang, Z. D., Jeng, D. S., Zhu, J. F., Guo, Z., and Chen, W. Y. (2018). "Numerical investigation of dynamic soil response around a submerged rubble mound breakwater." *Ocean Engineering*, 156(February), 406–423.
99. Zhao, M., Zhang, G., Wang, P., Du, X., and Zhang, X. (2020). "An accurate frequency-domain model for seismic responses of breakwater-seawater-seabed-bedrock system." *Ocean Engineering*, 197(August 2019), 106843.

PUBLICATIONS

Journals:

1. **Sajan, M. K.,** Chaudhary, B., Akarsh, P. K., and Kumar, S. (2024). "Geosynthetic reinforced rubble mound breakwater for mitigation of tsunami-induced damage." ***Geotextiles and Geomembranes***, 52(1), 72–94. (**I.F 5.2**)
2. **Sajan, M. K.,** Chaudhary, B., Akarsh, P. K., Kumar, S., and Sah, B. (2024). "Novel Techniques for Reinforcing Rubble-Mound Breakwater against Tsunamis." ***Journal of Geotechnical and Geoenvironmental Engineering***, 150(3). (**I.F 4.7**)
3. **Sajan, M. K.,** Chaudhary, B., Akarsh, P. K., and Kumar, S. (2023). "Investigating the impact of tsunami waves on gabion material-reinforced coastal structures: A numerical analysis" *Materials Today: Proceedings*.
4. **Sajan, M. K.**, Chaudhary, B., Akarsh, P. K., Kumar, S., and Sah, B. (2024). Forthcoming. "Performance Assessment of Geosynthetic Reinforced Quays Under Concurrent Tsunami and Earthquake Aftershocks." ***Natural Hazards Review (ASCE)*.**
5. **Sajan, M. K.**, Chaudhary, B., Akarsh, P. K., and Sah, B. (2024). "Dam break analysis on developing tsunami resilient geogrid wrap-faced hybrid mound breakwaters." *Geosynthetics International*. *(Under review).*
6. **Sajan, M. K.**, Chaudhary, B., Akarsh, P. K., and Sah, B. (2024). "Investigations on the Development of Hybrid Mound Breakwaters for Tsunami Defense." *Applied Ocean Research*. *(Under review).*
7. **Sajan, M. K.**, Chaudhary, B., Akarsh, P. K., and Sah, B. (2024). "Experimental study on the effect of gabion configuration in modelling tsunami-resilient rubble mound breakwater." *Ocean Engineering*. *(Under review).*

Book Chapters (Scopus Indexed):

1. **Sajan, M K.,** and Chaudhary, B. (2021). "Stability of Reinforced Soil Quay Wall Subjected to Combined Action of Earthquake and Tsunami." *Advances in Sustainable Construction and Resource Management*, H. Hazarika, G. S. P. Madabhushi, K. Yasuhara, and D. T. Bergado, eds., Springer Nature, 349–359. **(Japan)**.

2. **Sajan, M. K.,** and Chaudhary, B. (2023). “Seepage Analysis of Resilient Rubble Mound Breakwater Under Tsunami Overflow: Numerical Analysis.” *Soil Dynamics, Earthquake and Computational Geotechnical Engineering*, K. Muthukkumaran, R. Ayothiraman, and S. Kolathayar, eds., Springer Nature, 23–30.
3. **Sajan, M. K.,** Chaudhary, B., Akarsh, P. K., and Kumar, S. (2024a). “Stability Analysis of Rubble Mound Breakwaters Under Tsunami Overflow.” *Geo-Sustainnovation for Resilient Society*, H. Hazarika, S. K. Haigh, B. Chaudhary, M. Murai, and S. Manandhar, eds., Springer Nature, 247–254. **(Japan).**
4. **Sajan, M. K.,** Chaudhary, B., Akarsh, P. K., Sah, B., and Kumar, S. (2024). “Mitigating Earthquake-Induced Damages on Foundation Structures Using Scrap Tire.” *Lecture Notes in Civil Engineering*., Springer Nature. *(Accepted)***.**
5. **Sajan, M. K.,** Chaudhary, B., Akarsh, P. K., Sah, B., and Kumar, S. (2024). “Dynamic Analysis on the Seismic Resilience of Rubble Mound Breakwaters.” 8ICRAGEE 2024. *Lecture Notes in Civil Engineering*., Springer Nature. *(Accepted)***.**
6. **Sajan, M. K.,** Chaudhary, B., Akarsh, P. K., Sah, B., and Kumar, S. (2024). “Numerical Analysis on Geogrid Reinforced Coastal Structures under Tsunami.” DFI 2024. *Lecture Notes in Civil Engineering*., Springer Nature. *(Accepted)*

BIODATA

Manu K Sajan

Address: Kochupurackel, 63rd Mile, Wallardie North, Periyar, Kerala, India -685533

Email: manuksajan@gmail.com

Phone: +91-9496856674

Education

July 2019- March 2024	Ph.D. National Institute of Technology Karnataka, Geotechnical Engineering CGPA - 9.31/10
August 2017- June 2019	Master of Technology APJ Abdul Kalam Technological University, Geotechnical Engineering CGPA - 8.5/10
September 2008- May 2012	Bachelor of Technology University of Kerala, Thiruvananthapuram, Civil Engineering CGPA - 7.15/10

Work Experience

July 2012 - September 2016	Project Engineer Al Adrak Trading & Contracting LLC, Oman Skills: *Construction Monitoring, Project Management, Quality Control, Technical Reports, Team Collaboration, Land Surveying, Ground Investigation*

Research Interests

Geotechnical Engineering, Physical Model Tests, Numerical Modelling, Offshore Geotechnics, Marine Geosynthetics, Geo-disaster Mitigation, Geotechnical Earthquake Engineering, IoT.